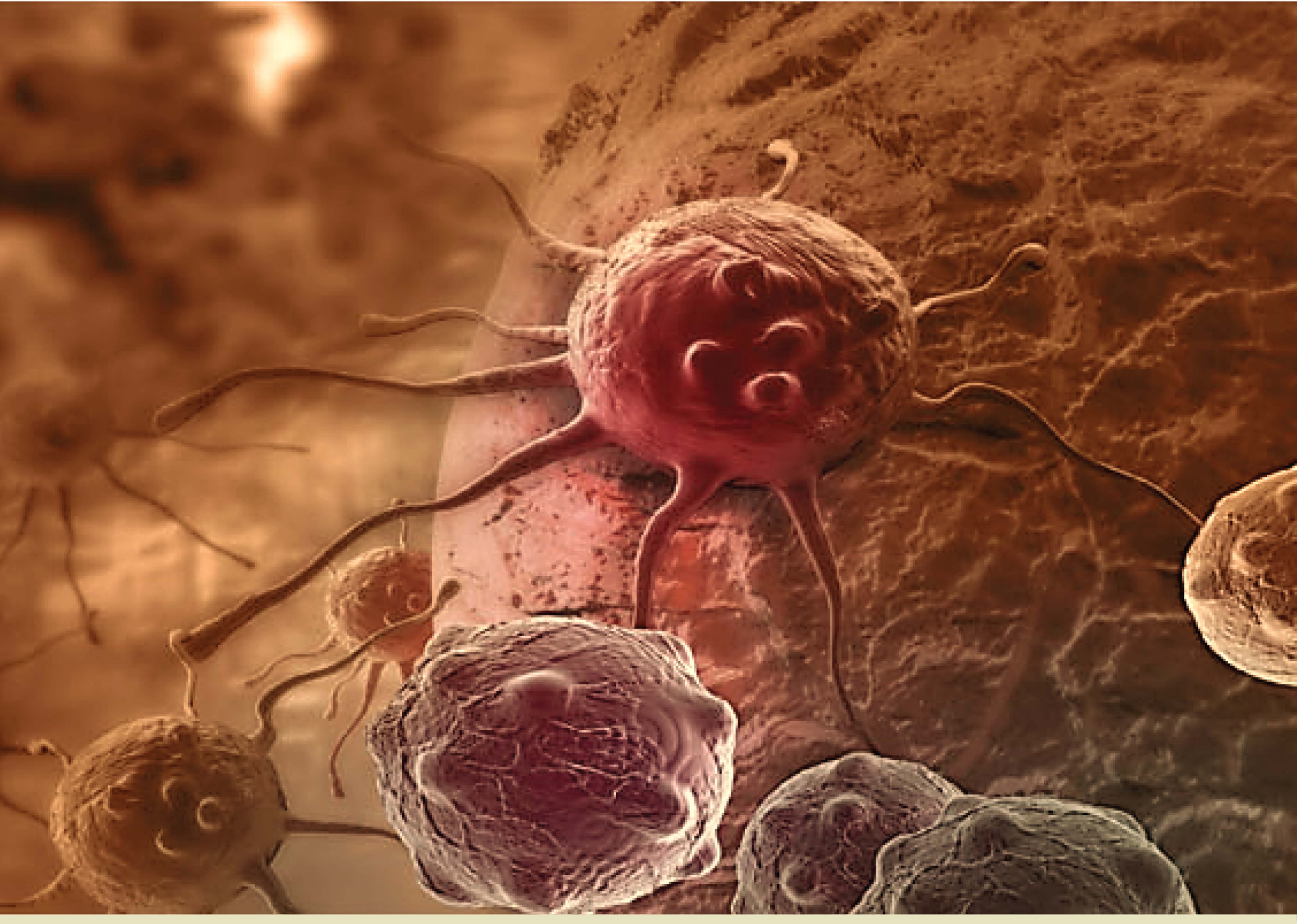

Madalena Guilherme Sousa

MIRNA-BASED METABOLIC MODULATION IN GLIOBLASTOMA CELLS: A STRATEGY TO SURPASS TUMOR CHEMORESISTANCE

Dissertação de Mestrado em Biologia Celular e Molecular, orientada pela Doutora Ana Maria Sequeira Cardoso e pela Professora Doutora Maria Amália da Silva Jurado e apresentada ao Departamento de Ciências da Vida da Faculdade de Ciências e Tecnologia da Universidade de Coimbra.

Julho de 2016

· U C ·

UNIVERSIDADE DE COIMBRA

Madalena Guilherme Sousa

MIRNA-BASED METABOLIC MODULATION IN GLIOBLASTOMA CELLS: A STRATEGY TO SURPASS TUMOR CHEMORESISTANCE

Dissertação apresentada à Universidade de Coimbra para cumprimento dos requisitos necessários à obtenção do grau de Mestre em Biologia Celular e Molecular, realizada sob orientação da Doutora Ana Maria Sequeira Cardoso (Centro de Neurociências e Biologia Celular e Molecular, Universidade de Coimbra) e da Professora Doutora Maria Amália da Silva Jurado (Departamento de Ciências da Vida, Universidade de Coimbra)

Julho de 2016

UNIVERSIDADE DE COIMBRA

O trabalho aqui apresentado foi realizado no Grupo de Vectores e Terapia Génica do Centro de Neurociências e Biologia Celular (Universidade de Coimbra, Portugal), liderado pela Professora Doutora Conceição Pedroso de Lima.

O trabalho foi co-financiado pela FEDER pelo Programa Operacional Factores de Competitividade – COMPETE e pela Fundação para a Ciência e Tecnologia (FCT) através do projecto UID/NEU/04539/2013.

The present work was performed in the Neuroendocrinology and Aging group of the Center for Neuroscience and Cell Biology (University of Coimbra, Portugal), headed by Professor Conceição Pedroso de Lima.

The present work was funded by FEDER funds through the Operational Programme Competitiveness Factors - COMPETE and national funds by FCT - Foundation for Science and Technology under the strategic project UID/NEU/04539/2013.

“Our greatest weakness lies in giving up. The most certain way to succeed is always to try just one more time.”

Thomas A. Edison

AGRADECIMENTOS

Gostaria de começar por agradecer à Doutora Conceição Pedroso de Lima e à Doutora Amália Jurado, não só pela oportunidade de poder realizar a Tese de Mestrado no seu laboratório, mas também por todo o saber transmitido, rigor cientifico e disponibilidade que prontamente demonstraram ao longo deste ano, fatores esses essenciais para a realização desta Tese. A ambas demonstro o meu profundo agradecimento.

À Doutora Ana Maria Cardoso, minha orientadora, quero deixar um agradecimento muito especial. Além de todos os ensinamentos, planeamento e conselhos, gostaria de agradecer-te por toda a tua disponibilidade para me ajudar em tudo o que fosse preciso. Obrigada por todas as chamadas de atenção e correções que contribuíram imenso para o meu crescimento tanto profissional como pessoal.

Gostaria também de mostrar o meu agradecimento à Doutora Ana Luísa Cardoso por todo o seu apoio nos mais variados aspetos, desde os ensinamentos sobre a realização de inúmeras técnicas e pelo positivismo transmitido ao longo deste ano.

À Catarina Morais e ao Pedro Cunha por todo seu apoio diário no laboratório, reflexões e discussões sobre as mais variadas técnicas e também pelos momentos de brain storm total.

À Doutora Luísa Cortes e Doutora Margarida Caldeira da Unidade de Microscopia (MIC) por toda a paciência e auxilio na realização das técnicas de análise bioenergética e quimiotaxia.

À Doutora Joana Guedes e Gladys Caldeira gostaria de demonstrar o meu agradecimento por toda a disponibilidade e ajuda apesar do resultado menos positivo da respetiva parte do projeto.

Gostaria de agradecer à Ana Rafaela Oliveira, amiga e colega, por toda a amizade, apoio e companheirismo no laboratório! Posso com certeza afirmar que sem ti este caminho teria sido mais longo e difícil, principalmente toda a saga das clonagens falhadas.

Não posso deixar de agradecer a todas as pessoas da Salinha dos Mestrados por todos os momentos de boa disposição, descontração e entreajuda que foram fundamentais durante todo este processo.

A todos os amigos que fui fazendo ao longo destes cinco anos e que permaneceram na minha vida. Aos amigos de BCM, nomeadamente as princesas Andreia, Ana Rafaela, Beatriz, Joana, Marta, Laetitia, Raquel e Rafaela obrigada por todo o vosso apoio que foi precioso ao longo destes dois anos. Aos amigos que apesar de longe fazem questão de estar presentes nem que seja com um telefonema e que ajudam a espairecer a mente, Ana André, Beatriz, Marta

e Joana. Por fim, gostaria de agradecer profundamente à Carina e Inês por todas as conversas e partilhas que foram fundamentais para a manutenção da minha sanidade mental durante os dois anos de Mestrado e onde a entreajuda, apoio incondicional e sofrimento coletivo foram uma constante. Serão sempre especiais para mim e nunca serei capaz de vos agradecer o suficiente por estes cinco anos de amizade verdadeira.

Gostaria de fazer um agradecimento muito especial a toda a minha família, acima de tudo pela compreensão do motivo que resultou na minha ausência da rotina familiar durante estes cinco anos longe de casa e por todo o apoio que como por milagre ia chegando quando mais precisava.

Ao meu irmão João, um agradecimento muito especial, por nunca se queixar de toda a atenção que fui "roubando" aos nossos pais durante estes cinco anos com telefonemas que no meu mundo eram mais importantes do que qualquer coisa que ele poderia querer dizer. Obrigado por todos os sacrifícios que tiveste de fazer para eu estar aqui, sim, porque quando eu decidi cometer esta loucura, toda a família teve de fazer sacrifícios, incluindo tu.

Para finalizar gostaria de agradecer aos responsáveis por me proporcionarem toda esta experiência fantástica, os meus pais. Vocês sabem o quanto significam para mim e o quanto isto teria sido uma experiência falhada sem a vossa constante motivação. Vocês são o meu exemplo e só espero um dia poder retribuir todo o apoio que me deram. Vocês eram as primeiras pessoas a quem ligava quando o dia não corria bem, quando me sentia desmotivada, quanto sentia saudades e nunca, mas nunca, se fartaram, mesmo quando já era tarde, quando também vocês não tinham tido um dia bom, colocando sempre a minha felicidade antes da vossa. Obrigado por todo carinho, orgulho e apoio incondicional. Sou uma sortuda e nunca me tinha apercebido.

TABLE OF CONTENTS

ABBREVIATIONS

α-KG - alfa-ketoglutarate

2-DG – 2-Deoxy-D-glucose

2-HG – 2 hydroxyglutarate

3'UTR - 3'untranslated region

A

AGO- Argonaute protein

AML - Acute myeloid leukaemia

AKT – Protein kinase b

AMPK- AMP-activated protein kinase

ATP - Adenosine thriphosphate

B

BER - Base excision repair

BSA – Bovine serum albumin

C

CDKNA - Cyclin-dependent kinase inhibitor 2A

CLL - Chronic lymphocytic leukemia

C-MET- C-methionine

CNS - Central nervous system

CSF - Cerebellar spinal fluid

D

DBS - Double strands breaks

DCA - Dichloroacetate

E

EGF – Epidermal growth factor

EGFR - Epidermal growth factor receptor

ETC - Electron transport chain

ENTPD5 - Ectonucleoside triphosphate diphosphohydrolase 5

F

FAD - Flavin adenine dinucleotide

FCCP- Carbonyl cyanide-4-(trifluoromethoxy)phenylhydrazone

FDG - deoxy-2-(18F) fluoro-D-glucose

FBS – Fetal Bovine Serum

FH - Fumarate hydratase

FoxO - Forkhead box subfamily O

G

GBM - Glioblastoma

GLUT- Glucose transporter

GCV - Ganciclovir

H

HIF-1α - Hypoxia inducible factor alfa

HK2 - Hexokinase 2

HPRT1 - Hypoxanthine phosphoribosyltransferase 1

HSV-TK- Herpex Simplex Virus Thymidine-kinase

I

IDH - isocitrate dehydrogenase

L

LDHA - Lactate dehydrogenase A

LKB1 - Liver kinase B1

M

MET - mesenchymal-epithelial transition

MGMT - Methylguanine-DNA methyltransferase

miRNA – micro RNA

miRNP - miRNA-containing ribonucleoprotein complex

N

NES - Nestin

NKX2-2 - NK2 homeobox 2

NADH - Nicotinamide adenine dinucleotide phosphate

NF1 – Neurofibromin 1

O

O6-MeG - O6- methylguanine

OLIG2 - Oligodendrocyte lineage transcription factor 2

OXPHOS - Oxidative phosphorylation

P

PBS – Phosphate-buffered saline

PDGFR-A - Platelet-derived growth receptor A

PDH - Pyruvate dehydrogenase

PDK - Pyruvate dehydrogenase kinase

PEP - Phosphoenolpyruvate

PFKFB3 - Phosphofructokinase 2

PHD - Proxyl hydroxylase

PI3K - Phosphatidylinositol 3-kinase

PK - Pyruvate kinase

PPP - Pentose phosphate pathway

PTEN - Phosphatase and tensin homolog

R

RISC - RNA-induced silencing complex

S

SDH - Succinate dehydrogenase

siRNA - small interfering double-stranded RNA

shRNA - short-hairpin RNA

T

TCA – Tricarboxylic acid cycle

TET - ten-eleven translocation family

TIGAR - TP53induced glycolysis and apoptosis regulator

TMZ - Temozolomide

TRBP - RNA-binding protein TAR

TRK - Tyrosine kinase receptors

TSC1 - Tuberous sclerosis complex protein 1

V

VHL - von Hippel-Lindau

ABSTRACT

Glioblastoma (GBM) is the most aggressive and common form of primary brain tumour characterized by fast proliferation, high invasion, and resistance to current standard treatment. The average survival rate post-diagnosis is only of 14.6 months, despite the aggressive standard post-surgery treatment approaches of radiotherapy concomitant with chemotherapy with temozolomide (TMZ). Currently, efforts are being endowed to develop a new and more efficient therapeutic approach capable to overcome chemoresistance, and to inhibit tumour progression and improve overall patient survival rate. Abnormal microRNA (miRNA) expression levels have been correlated with chemoresistance, proliferation and resistance to apoptosis, which result from their master regulatory role of molecular pathways important for these tumoral features. Additionally, altered cell metabolism, favouring glycolysis, has been identified as an emerging cancer hallmark and has been intensively described in GBM, thus offering a new target for new GBM therapies. In this work, we hypothesized that gene therapy based on modulation of miRNAs with aberrant expression in GBM and predicted to target crucial metabolic enzymes might promote a shift of GBM cell metabolism, decreasing the glycolytic dependence of tumor cells and contributing to their sensitization to chemotherapeutic agents. We have found that the transient increase of hsa-miR-200-3p and hsa-miR-144-3p levels, shown to be underexpressed in U87 and DBTRG human GBM cell lines, promoted the downregulation of mRNA of enzymes involved in bioenergetic pathways, with consequent alterations in cell metabolism. In this context, both miRNAs showed to be effective in inhibiting glycolysis in U87 cells, whereas in DBTRG cells hsa-miR-144 inhibited mitochondrial respiration and hsa-miR-200c-3p inhibited both mitochondrial respiration and glycolysis. Furthermore, modulation of both miRNAs impaired the migratory capacity of DBTRG cells, which, *per se*, indicates the potential therapeutic value of these miRNAs. Additionally, the ability of miRNA modulation to sensitize U87 and DBTRG cells to the chemotherapeutic drugs dichloroacetate (DCA) and TMZ was evaluated. Although no differences in U87 cell viability were found between cells treated with either drug and those submitted to the drug treatment combined with miRNA mimics, DBTRG cells became more sensitive to DCA and TMZ after hsa-miR-200c-3p modulation. Overall, our results show that the bioenergetic pathways constitute a promising therapeutic target of miRNA modulation to overcome chemoresistance mechanisms in GBM cells.

Key-words: Glioblastoma, miRNAs, energy metabolism, glycolysis, mitochondrial respiration, dichloroacetate, temozolomide, combined therapy

RESUMO

O glioblastoma (GBM) é o tipo mais agressivo e comum de tumor cerebral primário, caracterizado por uma rápida proliferação, elevada capacidade invasiva e resistência à terapia convencional. A taxa média de sobrevivência após diagnóstico é de apenas 14.6 meses, após uma terapia agressiva pós-cirúrgica, consistindo em radioterapia e quimioterapia com temozolamide (TMZ). Atualmente, têm sido desenvolvidos esforços no sentido de encontrar novas terapias, mais eficientes e capazes de obviar a quimio-resistência, inibir a progressão do tumor e aumentar a taxa de sobrevivência dos doentes. Em virtude do papel dos microRNAs (miRNAs) como reguladores de mecanismos moleculares envolvidos no desenvolvimento de GBM, a expressão anómala destas moléculas tem-se revelado responsável pelas características de extrema agressividade deste tumor. Alterações metabólicas que favorecem a dependência energética da glicólise, amplamente descritas em GBM, foram recentemente identificadas como características típicas das células cancerígenas, constituindo desse modo novos alvos terapêuticos para GBM. Neste trabalho, concebeu-se uma estratégia de terapia génica para GBM, baseada na regulação de miRNAs, cujos níveis se encontram alterados neste tumor e cujos alvos previstos incluem enzimas metabólicas. Esta abordagem resultaria numa alteração do metabolismo das células de GBM, diminuindo a sua dependência da via glicolítica e contribuindo para a sua sensibilização a agentes quimioterapêuticos. Demonstrou-se que o aumento transiente dos níveis de expressão dos miRNAs hsa-miR-200c-3p e hsa-miR-144-3p, em linhas celulares humanas de GBM (U87 e DBTRG), promoveu uma diminuição da expressão dos seus alvos envolvidos nas vias do metabolismo bioenergético, com consequentes alterações no metabolismo celular. Neste contexto, ambos os miRNAs inibiram a via glicolítica em células U87, ao passo que em células DBTRG o hsa-miR-144-3p demonstrou ser efetivo na inibição da glicólise e o hsa-miR-200c-3p inibiu a respiração mitocondrial e a glicólise. Adicionalmente, o aumento dos níveis de ambos os miRNAs resultou na diminuição da capacidade migratória das células DBTRG, o que aponta para um potencial terapêutico destes miRNAs. Além disso, avaliou-se o efeito da terapia combinada, consistindo no aumento dos níveis de miRNAs, seguido de incubação com os fármacos dicloroacetato (DCA) e TMZ, na viabilidade de células U87 e DBTRG. Apesar de não terem sido encontradas diferenças entre células U87 incubadas com cada um dos fármacos e com o tratamento combinado, em células DBTRG o aumento dos níveis do hsa—miR-200c-3p resultou num maior efeito tanto do DCA como do TMZ. O conjunto dos nossos resultados demonstra que as vias do metabolismo bioenergético são alvos promissores da ação de miRNAs, que, em combinação com quimioterapia, poderá constituir uma abordagem promissora no tratamento de GBM.

Palavras-chave: Glioblastoma, miRNAs, metabolismo energético, glicólise, respiração mitocondrial, dicloroacetato, temozolomide, terapia combinada

1 INTRODUCTION

1.1 CANCER: A MULTIFACTORIAL DISEASE

Cancer is the major cause of morbidity and mortality worldwide, with approximately 14 million new cases and 8.2 million cancer related deaths in 2012[1]. Based on GLOBOCAN 2008, about 12.7 million cancer cases and 7.6 million cancer deaths are estimated to have occurred in 2008, from which, 56% of the cases and 64% of the deaths occurred in the economically developed countries[2]. The continuous increase in cancer incidence and mortality is mainly due to the increase of life expectancy and growth of the world population, alongside with adoption of behaviors shown to have an active role in cancer development, such as diet, lack of exercise, obesity, exposure to infectious agents, and consumption of alcohol and tobacco. Due to its high prevalence and the different features of each type of cancer, it is essential to understand the biology of cancer and efforts should be made towards the discovery and development of effective and targeted anti-cancer therapeutic approaches.

Despite cancer heterogeneity, Hanahan and Weinberg (2000)[3] identified and described the six hallmarks of cancer cells that allow tumor growth and metastatic dissemination: ability to sustain the proliferative signaling pathways, resistance to death, capacity to replicate indefinitely, to stimulate invasion and metastasis and to evade growth suppressors, as well as to induce angiogenesis. More recently, after several years of research, the same authors[4] proposed the addition of two features to those previously associated with cancer pathogenesis – cellular energy metabolism reprogramming and ability to evade the immune system. Furthermore, Hanahan and Weinberg established that inflammation mediated by immune cells and genomic instability would be necessary for the acquisition of features leading to tumor growth and invasion[3]. It is widely accepted that cancer originates from cells carrying genomic alterations, translating into phenotypic heterogeneity within the tumor itself. Thus, it is possible to distinguish multiple cell populations, in a tumor, which constitute the main obstacle to the discovery and progress of anti-cancer therapeutics[5].

1.2 GLIOBLASTOMA CHARACTERIZATION

Glioma clinical classification. Glioma is the most common type of brain tumour in adults, accounting for 42% of all primary brain and central nervous system (CNS) tumours, and 77% of malignant tumours (USA statistics)[6]. Originated from glial cells, gliomas can be differently classified based on morphology and histology into astrocytomas, oligodendrogliomas, oligoastrocyomas (a mixture of the previous two), ependymomas and glioblastomas[6,7].

According to the 2007 WHO classification of CNS tumours, gliomas can be divided into four different histological grades based on their malignancy and invasiveness, from grade I to grade IV[8]. Grade I and grade II tumours, also denominated low grade tumours, share histological resemblance with the normal brain tissue and present low proliferative capacity, the possibility of their treatment with surgical resection being hence high. However, some types of grade II and grade III brain tumours, or anaplastic astrocytomas, usually exhibit histological evidences of malignancy, including nuclear atypia and brisk mitotic activity - anaplastic features- and high vessel density and proliferation ratio, thus demanding a more aggressive treatment with adjuvant chemotherapy and/or radiotherapy. Grade IV glioma, commonly denominated glioblastoma (GBM), usually located in the cerebral hemispheres, with a predisposition for the white matter of the *centrum semiovale* and *corpus callosum*[9], is the most frequent malignant primary brain tumour, accounting for more than 50% of all gliomas[8]. GBM displays the most malignant and aggressive phenotype of all gliomas, characterized by high levels of cellular heterogeneity, with both differentiated and non-differentiated cancer cells and small areas of necrotizing tissue being present, resistance to apoptosis, neoangiogenesis, vascular thrombosis[8,10] and rapid proliferation. Therefore, the infiltration into the surrounding normal brain tissue and possible extension into the ventricular wall or meninges can culminate in the release of cancer cells into the cerebellar spinal fluid (CSF) and, consequently, dissemination to the spinal cord. However, despite the distinctive infiltrating feature, the presence of metastasis beyond CNS is extremely rare, which has been assigned to a number of phenomenon, namely the filtration capacity of the blood brain barrier and the short life span of patients with GBM[9]. Due to the severe malignancy of this type of glioma, 50% of the patients with GBM have a median survival time of only 12 to 15 months following diagnosis.

GBM genesis and clinical subtypes. GBM can be originated *de novo*, in the absence of a precursor lesion (primary GBM), or through progression of a lower grade glioma (WHO grades II and III), being designated secondary GBM[8,11]. These two subtypes of GBM present different genetic alterations and consequently distinct altered molecular pathways, which are responsible for differences in age onset, survival rates and overall outcome. In elderly patients with a mean age of 62 years, the majority of GBMs, nearly 90%, develops *de novo* within 3-6 months. In contrast, secondary GBMs manifest themselves in younger patients (mean age of 42 years) and are associated with a lower degree of necrotic tissue, showing a better outcome[10,12]. Despite the similar histology, primary and secondary GBM can be distinguished by their genetic and epigenetic profiles. More specifically, the presence of mutations p53 (*TP53*) and in isocitrate dehydrogenase (*IDH1*) genes characterizes secondary GBM, IDH1 gene mutations being a decisive genetic marker, associated with a hypermethylation phenotype[16]. Additionally, secondary GBM has an increased expression of platelet-derived growth receptor A (*PDGFR-A*), whereas primary GBM often displays an amplified and mutated form of epidermal growth factor receptor (*EGFR*), known as *EGFRvIII*. Both types of mutations (*PDGFR-A* and *EGFRvIII*) result in increased activity of tyrosine kinase receptors (TRK), involved in numerous signalling pathways, such as RAS, PI3K and MAPK, which represent three crucial pathways in tumour development and proliferation[15].

GBM molecular subtypes. As a way to improve the knowledge about the molecular and genetic specificities of GBM, The Cancer Genome Atlas (TCGA), through an intense study on human GBM and normal brain samples, identified four GBM molecular subtypes: classical, mesenchymal, proneural and neural, differing in gene expression profile and genetic alterations, which are correlated with distinct clinical features and survival rates. Tumours from the classical subtype display amplified EGFR expression, astrocytic-related gene expression, alongside with deletion of cyclin-dependent kinase inhibitor 2A (*CDKNA*) loci, expression of neural precursor and stem cell marker *NES*, and increased Notch and Sonic hedgehog signalling pathways crucial for cell differentiation. On the other hand, the deletion of chromosome region containing neurofibromin (*NF1*) and phosphatase and tensin homolog (PTEN) genes, concomitant with increased expression of MET, a mesenchymal marker, and genes of the tumour necrosis super family and NF-ƙB pathways, characterize the mesenchymal subtype. GBMs presenting *IDH1*, *PDGRF-A* and *TP53* mutations along with higher expression of oligodendrocytic developmental genes, NK2 homeobox 2 (*NKX2-2*) and oligodendrocyte lineage transcription factor 2 (*OLIG2*), both associated with increased cell proliferation,

are included in the proneural subtype and related with an early GBM onset. Tumours comprised in the neural subtype are characterized by a normal brain tissue expression profile, along with astrocyte and oligodendrocyte gene markers[15–17]. Considering the heterogeneity among GBM tumours, and having in mind that the efficacy of the treatment can be influenced by the molecular features of each GBM subtype, a detailed molecular characterization of these tumours can facilitate a more personalized treatment approach, in order to achieve better results and, consequently, increase patient survival rate after diagnosis.

Epidemiology. GBM is classified as a rare tumour, with an annual incidence of 2-3 cases per 100,000 individuals in Europe and North America, resulting, however, in a death rate of almost 50% of the diagnosed patients within a year and 90% within 3 years[18]. Epidemiologic studies have demonstrated that incidence of GBM in European descendants is twice higher than in African, American or Asian descendants[10,19]. Commonly, GBM occurs in the elderly, with a median age of 64. Nonetheless, GBM can appear at any age, being extremely rare in children[19]. A slight preponderance of GBM was observed in males, with an incidence rate 1.3 times higher than in females[19], and in white individuals, being the incidence twice higher than in black individuals[15]. In the last 20 years, the number of identified cases of GBM has increased due to improved radiologic diagnosis, especially in aged patients, and particularly in developed countries as compared with under-developed ones, as a consequence of a more facilitated access to health care[12].

Etiology. Despite the increasingly large number of GBM cases worldwide, the predisposing factors are still under study and poorly understood, and the etiology of GBM remains mainly unidentified[10,19]. To date, the only validated environmental risk factors associated with gliomas are exposure to ionizing radiation, such as that involved in leukaemia treatment, and the presence of rare genetic tumour syndromes, observed in 5% of gliomas, such as Li–Fraumeni syndrome, Cowden's disease, tuberous sclerosis, retinoblastoma 1, Turcot's syndrome and neurofibromatosis 1 and 2[10,12,15,20,21]. Other environmental factors may contribute to GBM malignancy, such as exposure to rubber manufacturing, petroleum production, and several pollutants, such as vinyl chloride, and pesticides, as well as to tobacco. Furthermore, increasing evidences have shown a possible connection between the exposure to residential electromagnetic fields,

formaldehyde, diagnostic irradiation and cell phones. In fact, a meta-analysis published in 2007 demonstrated an increased incidence among people who used cell phones for at least 10 years and especially those who had mostly unilateral exposure[15,22].

Symptomology. As a result of its highly proliferative and invasiveness features, GBM can affect diverse areas of the cerebrum. Therefore, depending on the affected area and the tumour size, patients will manifest varied symptoms, the most common being nausea, headache, seizures, mood and personality changes and progressive focal neurologic deficits, such as aphasia, paresthesia, hemiparesis and visual disturbances[10,15].

Clinical diagnosis and standard treatment. When neurological symptoms as the ones mentioned previously are manifested, computed tomography (CT), magnetic resonance imaging (MRI) - the imaging technique of first choice - and positron-emission tomography (PET) scans are performed, with subsequent stereotactic biopsy or craniotomy for tumour resection and confirmation, through histological and genetic analysis. Alongside, and for a deeper knowledge about the tumour, advanced MRI modalities can be performed, such as perfusion imaging and magnetic resonance spectroscopy, allowing the visualization of vascular abnormalities, altered tumour blood flow and metabolic characterization of the tissue, by determining the concentration of several metabolites[9,19]. However, new continuing update in PET has been vital. In fact, and having in mind the metabolic alterations that take place in cancer cells, including in GBM cells, with an increase in glucose uptake and consumption, the predominantly conversion of glucose into lactate and alanine can be determinant to distinguish GBM tumour from the surrounding healthy tissues[23]. Additionally, the distinct ability to uptake the glucose analog deoxy-2-(18F)fluoro-D-glucose (FDG) by high-grade gliomas, and its negative correlation with patient survival, could offer an important new diagnostic tool[24,25]. However, despite all the pros for the use of FDG, the elevated glucose uptake by normal brain cells constitutes a problem for the application of conventional MRI based on the uptake of this compound, C-methionine (C-MET), a radiolabelled amino acid, showing advantages over FDG[26].

Currently, the standard treatment strategy for GBM begins with the maximum surgical resection of tumour tissue. However, taking into account the GBM infiltrative capacity, it is nearly impossible to remove the totality of tumour cells, the treatment

including also radiotherapy with concomitant or adjuvant temozolomide (TMZ) administration as chemotherapy, along with symptomatic treatment[15].

1.3 CANCER METABOLISM: AN OVERVIEW

Cancer cells are characterized by high levels of proliferation through sustained proliferative signalling, evasion from growth suppressors and high resistance to apoptosis. Malignant cells also acquire the ability to induce angiogenesis and promote the invasion/metastasis process. The acquisition of such fundamental features appears to be a consequence of random mutations, originated by genomic instability and repair defects, the inflammatory state of premalignant lesions having also shown to contribute for tumour development. Together, these enabling characteristics are instrumental for cancer cell survival, proliferation and dissemination. More recently, an update of cancer hallmarks showed that two novel hallmarks should be proposed: (1) evasion from the immune system and (2) reprogramming of energy metabolism to maintain cell growth and proliferation[4].

In non-malignant mammalian cells, proliferation is stimulated by growth factors, whose bioavailability is highly regulated, and the uptake of nutrients from the environment is, hence, under strict control. However, cancer cells, as a result of genetic mutations that functionally alter signalling pathways, show no dependence on growth factors to promote the uptake and metabolism of nutrients, which sustain cell growth, thereby fuelling tumourigenesis. Moreover, evidence over the years has demonstrated that the signalling pathways altered in cancer cells, besides contributing to the most studied cancer hallmarks, converge to play a crucial role in shifting the cell metabolism, in order to respond to demanding energy requirements and promote cell proliferation by potentiating macromolecule's biosynthesis, rapidly generating ATP and conserving cell redox status[27].

1.3.1 The Warburg Effect

One of the best described processes by which cancer cells reprogram their metabolism, in order to fulfil the high energy demands for cell proliferation, is the Warburg effect, which consists of altering the pathway cell uses for ATP generation, glycolysis being preferred over oxidative phosphorylation (OXPHOS)[28]. In 1930, Otto Warburg observed that even in the presence of oxygen, cancer cells restricted their energy metabolism mainly to glycolysis, a

state denominated "aerobic glycolysis", with consequent abundant production of lactate[28]. This contrasts with what happens in normal proliferative cells under aerobic conditions, which use the pyruvate originated from glucose via glycolysis to produce ATP through mitochondrial OXPHOS, a process that is much more efficient than glycolysis in energetic terms. The puzzling preference of cancer cells for a less efficient metabolism motivated many studies. A proposed explanation for this phenomenon is that tumour hypoxia has constituted the pressure for the natural selection of cells dependent on anaerobic metabolism[29]. However, cancer cells employ glycolysis even when not exposed to hypoxic conditions. As an example, leukemic cells, although residing within the bloodstream with high oxygen levels, are highly glycolytic[30]. Therefore, although tumour hypoxia state is instrumental for some cancer biological characteristics, it does not appear to be a major element in triggering cancer cell aerobic glycolysis switch. Since energy is less efficiently produced by aerobic glycolysis as compared with OXPHOS, Warburg hypothesized that cancer cells used the former process because, during cancer formation and progression, the cells would acquire mitochondrial defects, resulting in impaired mitochondrial respiration, the cells being thus pushed to a glycolytic metabolism[28]. However, later studies demonstrated that most cancer cells display a normal mitochondrial function and, when in the presence of mitochondrial defects, these are not necessarily the Warburg Effect onset. In fact, the concept that cancer cells do not need functional mitochondria is not correct, since mitochondrial enzymes are used in the synthesis of macromolecule precursors, as it is the case of the carbon flux from glucose to the biosynthetic pathways, which requires mitochondrial metabolism[31]. Therefore, the question of why a less efficient metabolism, in terms of ATP production, is preferentially selected by cancer cells remained to be answered. Nowadays, the hypothesis most accepted in the scientific community proposes that the metabolic switch to aerobic glycolysis in proliferating cells aims at obtaining glycolytic intermediates, which fuel the biosynthesis of macromolecules required to the assembly of new cells, by enforcing a massive production of nucleotides, amino acids and lipids (**Fig.1**).

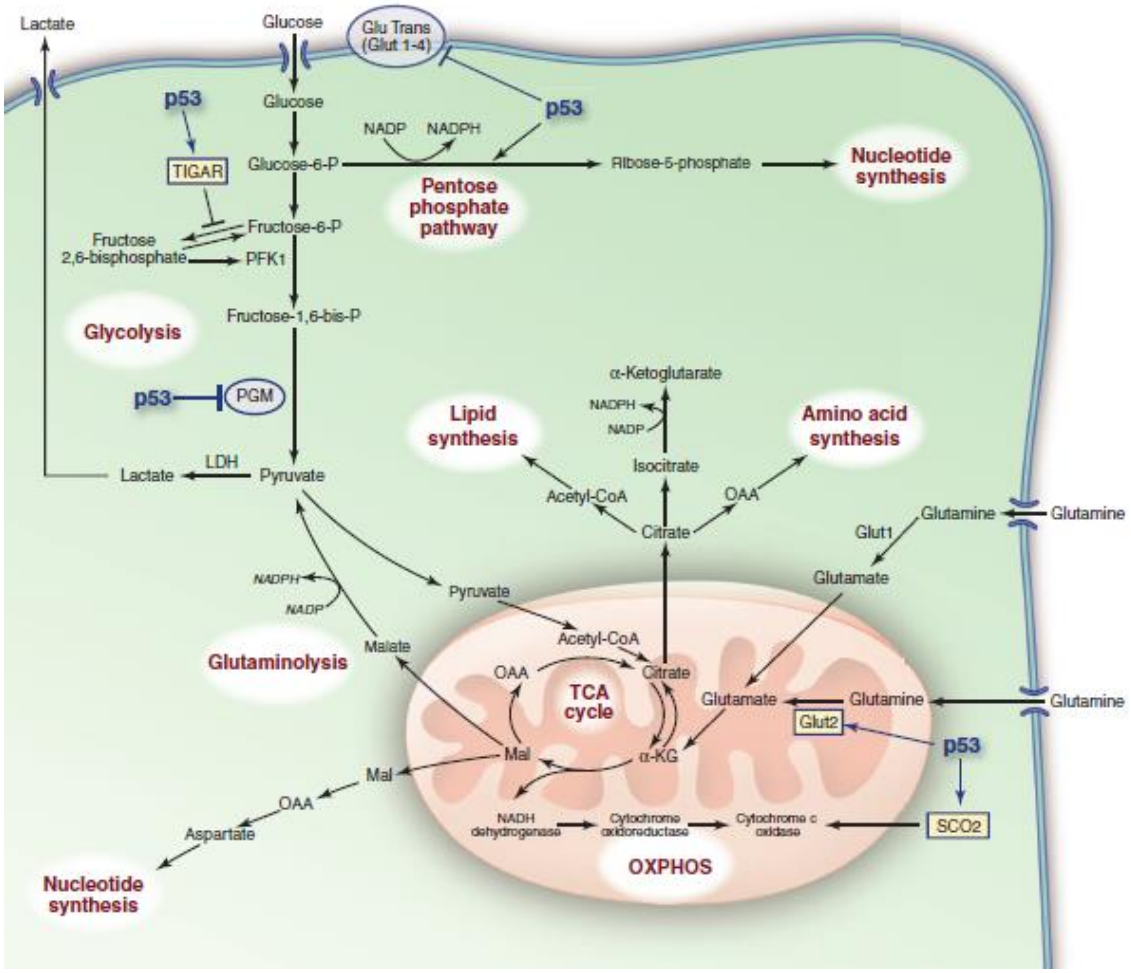

Figure 1. Signalling pathways involved in metabolic remodelling in proliferating cells. Besides glycolysis, glucose can be processed in PPP pathway, originating ribose 5'-phosphate and NADPH, or enter into TCA cycle, localized in the mitochondria. The citrate originated in the TCA cycle will be utilized to form Acetyl-CoA and OAA, crucial for lipid and amino acid synthesis, respectively. Adapted from Levine *et al.*[32]

1.3.2 Regulation of the Warburg Effect in GBM

PI3K/AKT pathway. The proteins phosphatidylinositol 3-kinase (PI3K) and v-akt murine thymoma viral oncogene homolog 1 (AKT/PKB) regulate one of the most commonly altered signalling pathways in human cancer, which is essential for cell proliferation, migration and, consequently, for tumourigenesis and tumour dissemination[33]. Mutations in tumour suppressor genes in GBM, such as PTEN, and the aberrant expression of PDGFRα and tyrosine kinase receptors (TRK), like EGFR, mainly present in primary GBM, result in PI3K/AKT pathway activation, through PI3K phosphorylation of PIP2 with production of PIP3 activating serine/threonine [33,34]. Subsequently, AKT, by mTOR activation that

promotes expression of its downstream targets, is able to stimulate glycolysis, since (1) increases the expression and membrane translocation of glucose transporters; (2) phosphorylates key glycolytic enzymes, such as hexokinase and phosphofructokinase 2 (PFKFB3)[36]; (3) activates ectonucleoside triphosphate diphosphohydrolase 5 (ENTPD5), creating an ATP hydrolysis cycle[37]. Additionally, and contributing to a higher glycolytic capacity, AKT inhibits forkhead box subfamily O (FoxO) transcription factors by triggering nuclear exclusion and proteasomal degradation[38]. The mechanism by which FoxO inhibition influences glycolysis is not yet fully understood for all the family members (FoxO1, FoxO4 and FoxO6). Lastly, inactivation of mTOR inhibitor stimulates both protein and lipid biosynthesis by directly promoting mRNA translation and at the metabolic level activates HIF-1α, even under normoxic conditions[39].

HIF-1α and MYC. HIF1 and HIF2 transcription factor complexes are heterodimers, composed of the constitutively expressed HIF1β subunit, and either HIF1α or the HIF2α subunits. In normal cells, the expression of HIF1α subunits is downregulated mainly through post-translational processes, like oxygen-dependent hydroxylation of specific proline residues, Pro02 and Pro564 in human HIF-1 sequence, through proxyl hydroxylases (PHDs), ultimately resulting in subunit degradation and low activity levels[40]. However, under hypoxic conditions, the enzymatic activity of PHDs is downregulated, resulting in higher activities of HIF-1 and HIF-2, through HIF subunit stabilization. Similar to what happens in PI3K/AKT pathway, loss of function mutations in PTEN, EGFR, VHL, succinate dehydrogenase (SDH) and fumarate hydratase (FH), which occur frequently in GBM, can promote HIF stabilization even in the presence of normal oxygen levels[41–45]. Once activated, HIF-1 and HIF-2 targets play essential roles in processes such as erythropoiesis, angiogenesis and glycolysis, the latter being mediated by transcription of genes encoding glucose transporters and glycolytic enzymes[46]. Besides glycolysis activation, HIF-1 reduces pyruvate flux into TCA cycle, decreasing both OXPHOS and oxygen consumption rate by promoting transcription of pyruvate dehydrogenase kinases (PDKs), which inactivate the mitochondrial pyruvate dehydrogenase complex (PDC) through phosphorylation of pyruvate dehydrogenase (PDH), the enzyme responsible for pyruvate decarboxylation and reductive acetylation of lipoic acid[47]. Growing evidences have demonstrated that MYC, a well-studied oncogene, despite its role in mitochondrial biogenesis and function, collaborates with HIF in the activation of glucose transporters and glycolytic enzymes, along with triggering the expression of PDK1, lactate dehydrogenase A (LDHA), hexokinase 2 (HK2) and pyruvate kinase M2 (PKM2)[48,49].

p53. The cellular tumour antigen p53 (p53) is a well-known tumour-suppressor protein due to its important role in DNA damage response (DDR) and cellular stress, inducing cell cycle arrest and apoptosis, with consequent inhibition of tumour development. In GBM, as in various human malignancies, the gene loci of p53 (*TP53*) is found to be mutated. In fact, p53 mutations seem to play a substantial role in secondary GBM, originated from low-grade diffuse astrocytomas, since they are present in ~65% of precursor lesions[33]. Moreover, one of the key functions of p53 is to activate gene expression, acting as a transcription factor. More specifically, p53 has been found to activate the expression of, among other genes, the hexokinase 2 (HK2) gene and TP53-induced glycolysis and apoptosis regulator (TIGAR) gene, demonstrating its importance for metabolic reprogramming[50,51]. HK2 converts the uptaken glucose to glucose-6-phosphate (G6P), which then either participates in glycolysis with subsequent production of ATP, or contributes to macromolecular biosynthesis of nucleotides, amino acids and fatty acids through the pentose phosphate pathway (PPP)-mediated production of ribose 5-phosphate, erythrose 4-phosphate, and reducing equivalents (NADPH), respectively[52]. TIGAR, otherwise known as fructose-2,6-bisphosphatase, acts as a regulator of HK2 activity, by dephosphorylating the glycolytic activator fructose-2,6-biphosphate, thus inhibiting its action[50,52].

AMP-activated protein kinase. AMP-activated protein kinase (AMPK) is a member of a protein kinase family and functions as an energy sensor, playing a major role in cell metabolism, including glucose regulation and lipid and protein metabolism, in response to various cell stimuli, such as ATP levels, oxidative stress, heat shock and hormones. AMPK is a heterodimer composed of one catalytic (α1 or α2), one regulatory (β1 or β2) and one AMP/ATP-binding (γ1, γ 2 or γ 3) subunit[53,54]. In normal cells, liver kinase B1 (LKB1) phosphorylates and, consequently, activates AMPK, in response to energetic stress characterized by increased levels of AMP/ATP ratio, shifting cell metabolism towards OXPHOS and inhibition of cell proliferation[53,54]. Additionally, AMPK counteracts the effects of AKT1 pathway, either by direct activation of TSC2 resulting in mTORC1 suppression, or by p53 phosphorylation with impact on apoptosis[56]. Therefore, in order to survive and proliferate, tumour cells must overcome AMPK signalling pathway (**Fig. 2**). In fact, as it was previously mentioned, cancer cells may display alterations in almost all the intervenient of AMPK pathway[54]. For instance, TSC2 and p53 mutations and serine/threonine kinase 11 (STK11) deficiency, results in imperfect AMPK activation and consequent activation of mTOR and HIF-1α, which trigger the shift to a glycolytic metabolism[54,55]. However, despite

these observations, high levels of pAMPK in tumours, such as GBM, were observed, which seem to contribute to cell growth and survival[53,56]. Hence, the role of AMPK in cancer mechanisms, cell proliferation, survival and metabolism is still far from being understood.

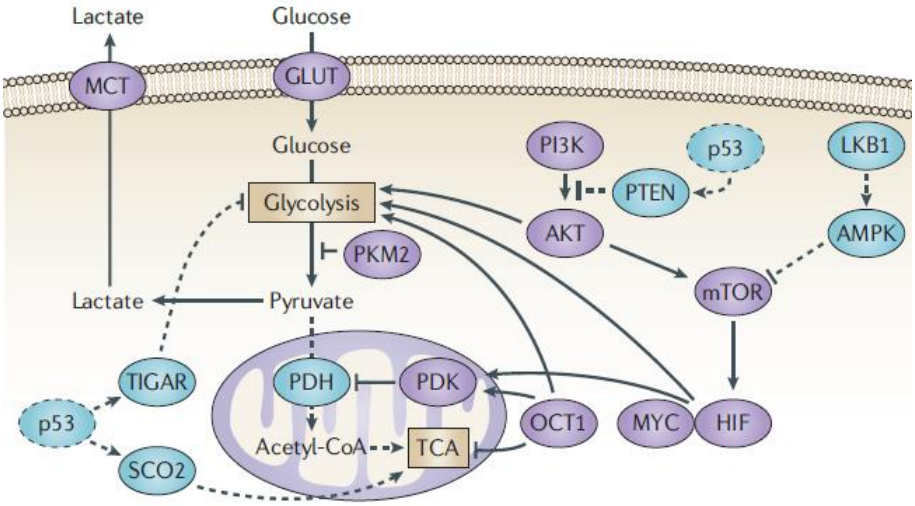

Figure 2. Signalling pathways altered in cancer cells. Glycolysis is stimulated by PI3K activation of AKT and mTOR activation of HIF-1α, ultimately regulating the expression of glycolytic enzymes, glucose transporters and pyruvate dehydrogenase kinase isoenzyme 1 In normal cells, LKB1 tumour suppressor, through AMPK opposes the glycolytic phenotype by mTOR inhibition. However, in proliferating cells, LKB1 has been shown to be the target of several mutations, resulting in its inhibition, therefore the sub sequential steps from this pathway are changed towards favouring HIF-1α expression and transcriptional regulation of glycolytic enzymes. Adapted from Cairns et al[52].

Pyruvate Kinase. Pyruvate kinase (PK) catalyses the rate-limiting and ATP-generating last step of glycolysis, by transferring the high-energy phosphate from phosphoenolpyruvate (PEP) to ADP to produce ATP and pyruvate[57]. Subsequently, pyruvate is reduced to lactate by LDH in the cytosol or metabolized to acetyl CoA by pyruvate dehydrogenase in mitochondria[57]. Multiple PK isoforms can be found in mammals, namely (1) type L, which is mostly found in liver and kidneys; (2) type R, with higher expression in erythrocytes; (3) type M1, found in tissues with higher energy demand such as skeletal muscle, heart, and brain in adults, and (4) type M2, expressed in most cells and predominantly present in fetal tissues, self-renewing cells like embryonic and adult stem cells, being subsequently substituted by the remaining isoforms[57,58]. PKs are encoded by the *PKLR* (1q22) and *PKM2* (15q23) genes, *PKLR* giving rise to the L (PKL) and R (PKR) isoforms, while *PKM2* generates the M1 (PKM1) and M2 (PKM2) isoforms[58]. *PKM2* is the dominant M isoform in most adult tissues, and, interestingly, is the one most expressed in cancer cells. Whereas PKL, PKR and PKM1 form stable tetramers, PKM2 exists in dimmers and tetramers. Contrary to what was accepted for decades in the scientific community, PKM2, in its dimeric form, has a low

affinity for PEP, slowing glycolysis and redirecting glucose-derived carbons towards biosynthesis, necessary for cell proliferation and tumour growth, and also acts indirectly in Warburg effect regulation through pyruvate kinase dependent gene expression, a process that involves a protein kinase (PK) activity of this enzyme[58,59]. More specifically in GBM, reduced levels of PKM1 expression were observed, accompanied with reduced PK activity in comparison with normal brain. On the other hand, GBM showed 3 up to 5-fold increase of both PKM2 mRNA and protein levels, independently of their genesis, in comparison with low-grade gliomas[59].

Despite of what was mentioned above concerning the absence of mitochondrial defects in cancer cells, several studies over the years have demonstrated that cancer metabolic phenotype is strictly associated with homoplasmic mitochondrial genome mutations, which have been found in primary tumours and related with tumour initiation, growth and metastatic process[60–62]. The contribution of ntDNA mutations was also acknowledged in tricarboxylic acid (TCA) cycle genes, such as fumarate hydratase (FH), succinate dehydrogenase (SDH), isocitrate dehydrogenase 1 and 2 (IDH1 and IDH2) in cancer, including GBM[14,63–67].

SDH and FH mutations. SDH, a TCA cycle enzyme embedded in the inner mitochondrial membrane, is responsible for the conversion of succinate into fumarate, with concomitant reduction of flavin adenine dinucleotide (FAD) to $FADH_2$. SDH plays a singular role in connecting the TCA cycle to the mitochondrial electron-transport chain, due to its function as the respiratory complex II[31], which is oxidized by coenzymeQ. A correlation was observed between the presence of inactivating mutations of several SDH subunits and various types of hereditary and sporadic human malignancies, including paraganglioma, renal carcinoma, breast cancer, among others[68–70]. Additionally, FH, which catalyses the reversible conversion of fumarate to malate, has been identified, similarly to SDH, as a mutated TCA cycle enzyme in cancer, such as in renal cell cancer and paraganglioma, associated with tumour migration[63,71,72]. In GBM, FH was found to be downregulated[73].

Recent studies have demonstrated that both SDH and FH may function as mitochondrial tumour suppressors[45], since the accumulation of succinate and fumarate in mitochondria, due to SDH and FH mutations and consequent inactivation, results in substrate leakage to cytosol and subsequent PHDs inhibition[44,45].Therefore, and having in mind that PHDs are crucial for HIF-1α degradation pathway, two possible outcomes for PHDs inhibition resulting from SHD and FH mutations were identified: (1) resistance to specific apoptotic signals, (2) and activation of a pseudohypoxic response. Regarding the

ability to surpass apoptosis, this characteristic seems to be acquired as a result of PHD3 specific inactivation, one of the targets of cellular succinate accumulation, although the exact PHD3 substrate responsible for the apoptotic pathway is still unclear[74]. The most studied and well characterized effect of SDH and FH mutations in cancer cells relies in the inhibition of PHDs, with subsequent HIF-1 α stabilization, and then increased levels of HIF-1 α and its targets, such as glycolytic and pro-angiogenesis genes, culminating in (1) hypoxic response[75], (2) glycolysis[76] and (3) angiogenesis stimulation[77] in cancer cells, under normoxic conditions, also denominated pseudohypoxic state.

IDH1 and IDH2 mutations. IDH1 and IDH2 are NADP-dependent homodimeric enzymes, located in the cytoplasm and mitochondrial matrix, respectively, which are responsible for providing cellular NADPH, through conversion of isocitrate into α-ketoglutarate (αKG). Besides IDH1 and IDH2, which are highly homologous, the NAD-dependent enzyme IDH3 is involved in the tricarboxylic acid cycle contributing with NADH production, necessary for the electron transport chain[78]. The presence of somatic mutations in *IDH* has long been identified as one of the mechanisms driving the tumourigenic process. In this regard, two independent cancer genome sequencing studies, Parsons *et al.*, (2008) and Mardis *et al.*, (2009), identified mutations in IDH enzyme in GBM and acute myeloid leukaemia (AML) respectively[79,80]. Further studies demonstrated an unique pattern in GBM, where 80% of the adult grades II and III gliomas and secondary GBMs displayed mutations in IDH1 and IDH2 enzymes[66]. Interestingly, IDH1 mutations are believed to be one of the earliest events in low-grade gliomas formation, preceding any well characterized mutations such as p53 gene mutations[14]. Moreover, somatic mutations in *IDH1* have been reported to be restricted to arginine residues leading to amino acid residue substitutions (p.R132H and p.R132S), while for *IDH2* the most common alterations take place at p.R172K. R132 is highly conserved and can be found in the IDH1 substrate binding site, important for hydrophilic interaction between R132 and α- and β- carboxylate of isocitrate[81]. The first studies proposed that the presence of *IDH1* and *IDH2* somatic mutations would result in alterations that could affect such hydrophilic interactions and subsequently modify enzyme activity, leading to a dominant-negative inhibition of IDH enzymes activity with repercussions on the decline of αKG concentration, a cofactor of prolyl hydroxylases responsible for the degradation of HIF1α, thus leading to HIF1α stabilization[82]. However, a different line of research demonstrated that, as opposed to wild-type IDH1, IDH1-R132 and IDH1-R172 mutants may also acquire a new enzymatic activity with the ability to convert α-ketoglutarate to (R)-2-hydroxyglutarate (2HG), an oncometabolite, with concomitant NADPH consumption(**Fig.3**). In support of this finding is the observation of lower levels of α-ketoglutarate accompanied

with higher levels of 2HG in human gliomas. Since the levels of 2HG can be detected through magnetic resonance, this oncometabolite can be considered as biomarker for IDH1 mutations[83]. Despite the modest knowledge about this metabolite, the number of studies on its role in cancer metabolism have increased, which identified 2-HG as an inhibitor of α-kG-dependent dioxygenases, such as Jmjc domain histone demethylases and ten-eleven translocation (TET) family of 5-methylcytosine hydroxylases, crucial for epigenetic regulation of gene expression, and, therefore, showing a correlation with the hypermethylation phenotype that characterizes gliomas and secondary GBM[84–86]. As a consequence of IDH1 mutation, the epigenetic alterations caused by 2-HG high levels in glioma tissues interfere with a series of cellular processes, like proliferation and differentiation. However, it remains to be determined if higher 2-HG levels are indeed responsible for IDH1 and IDH2 ability to drive tumourigenesis when mutated.

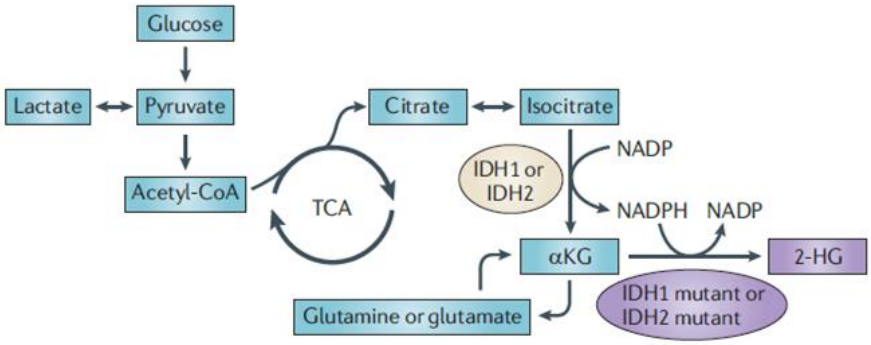

Figure 3. Mutations in IDH1 and IDH2 enzymes. Somatic mutations in crucial arginine residues, which are commonly observed in GBM, in isocitrate dehydrogenase 1 (cytoplasmic) and in isocitrate dehydrogenase 2 (mitochondrial) result in gain of function of a novel enzymatic activity, with instead of isocitrate conversion to α-ketoglutarate (α-KG), this metabolite is converted into 2-hydroxyglutarate (2-HG), with consequent accumulation in tumour cells, with a possible role in DNA methylation. Adapted from Cairns *et al.*[52]

1.4 miRNAs: REGULATORS OF GENE EXPRESSION

A large number of studies involving different scientific fields, such as transcriptomics, proteomics and bioinformatics, indicate that small single stranded RNA molecules are extremely important in the regulation of cellular gene expression and play a pivotal role in the most basic cellular processes, namely embryonic development, cell differentiation, metabolism, proliferation and cell death in a wide range of organisms, including humans[87].

Biogenesis and Mechanisms of Action. miRNA synthesis is a highly regulated process initiated in the nucleus and completed in the cytoplasm. MiRNAs are transcribed from the initial chromosome encryption as double stranded miRNA precursors, consisting of an imperfectly paired stem with a terminal loop, a 5'- cap and a 3'-polyadenylated tail denominated primary transcripts (pri-miRNAs)[87–89]. Afterwards, pri-miRNAs are cleaved by a microprocessor complex, that, among other proteins, contains the RNase III enzyme Drosha, giving rise to a 70-nucleotide hairpin-structure miRNA precursor (pre-miRNA) through excision of the stem loop[90] (**Fig.4**). However, a non-conventional mechanism for the production of pre-miRNAs was discovered, in which the pre-miRNAs are generated through splicing of short-hairpin introns (miRtrons) further processed by the spliceosome[91]. Via transporter exportin-5, the pre-miRNA is carried from the nucleus to the cytoplasm, where it undergoes a second cleavage process by a multiprotein complex, which comprises the endonuclease Dicer and the RNA-binding protein TAR (TRBP), originating a miRNA duplex with approximately 21-23 nucleotides. One of the strands of the miRNA duplex is selected as the mature miRNA (the guide) and integrated into an effector microRNA/complex, while the complementary strand is eliminated (the passenger), although some new biological functions have been attributed to this strand[88,92](**Fig.4**).

Mature miRNAs are incorporated into Argonaute (AGO) proteins, the core of the miRNA-containing ribonucleoprotein complex (miRNP), also known as miRISC. The miRNP complexes play an essential role in recognizing the miRNA strand selected as mature miRNA, pairing it with its target mRNA and preventing mRNA translation. Consequently, miRNA complexes are crucial in the miRNA-guided mRNA silencing pathway[87,93]. The posttranscriptional mRNA silencing mediated by miRNAs occurs through complementary binding of miRNA to the 3'untranslated region (3'UTR) of mRNA, resulting in mRNA cleavage, translational inhibition, or mRNA decay. The downstream result of miRNA-mediated mRNA silencing is determined by the level of complementarity between the miRNA and its target mRNA. In fact, an imperfect miRNA-mRNA pair match results in translational repression followed by mRNA deadenylation and decay[94], and a complete complementarity leads to complete mRNA silencing by AGO[95] (**Fig.4**). Consequently a decrease of the mRNA-encoded protein levels is observed, which can affect a cluster of cellular processes, such as proliferation, migration, differentiation, metabolism and apoptosis[90]. Nevertheless, studies have demonstrated that miRNAs can not only negatively regulate mRNA, but also act as transcriptional activators of target mRNA, by facilitating transcriptional machinery assembly and/or by increasing the mRNA half-life[96].

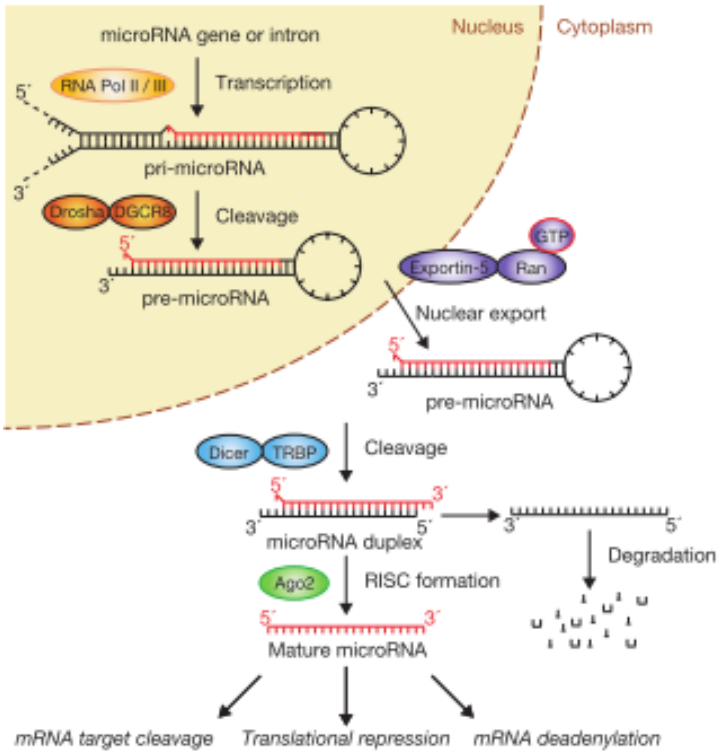

Figure 4. MicroRNAs biogenesis and mechanisms of action. A pre-miRNA, transcribed from specific sequences or originated from spliced sequences, is transported through exportin 5 to the cytoplasm where the maturation of the double-stranded pre-miRNA takes place, giving rise to a ~22 nucleotide single strand miRNA molecule, followed by assembly of RISC complex. Subsequently, the cleavage, translation repression or activation of the target mRNA occur. Adapted from Winter *et al.*[89]

1.4.1 MiRNAs and Cancer

In almost every type of human malignancies is possible to observe a dysregulation of miRNA expression levels, mainly caused by homozygous deletion of miRNA genes[97] and/or epigenetic modifications that directly modulate their 'host' genes[98]. However, the complex processing pathway and dysregulation of transcription factors that target specific miRNAs[87,99] can also be in the origin of miRNA dysregulated expression in human malignancies. In addition, dysregulated miRNAs seem to be not only responsible for tumour initiation, but also for tumour progression and formation of metastasis[100], due to their crucial participation in numerous molecular mechanisms, such as cell proliferation, metabolism, angiogenesis and apoptosis. The very first evidence supporting this concept was the finding that hsa-miR-15a and hsa-miR-16-1, located in a region of the 13q14 locus, were downregulated or deleted in most patients diagnosed with chronic lymphocytic leukemia (CLL)[101]. Afterwards, a large number of studies have identified miRNAs

dysregulated in breast, gastric cancer, leukemia and GBM[90,102–105]. Subsequently, functional studies performed in cancer cell lines and in cancer animal models have supported that numerous miRNAs could be involved in tumourigenesis[91], either by acting as tumour suppressors or as oncogenes[87].

MiRNAs dysregulated in GBM. Ciafre *et al* in 2005 were the first to acknowledge an aberrant miRNA expression in GBM[106], and since then many studies have been published establishing newly identified dysregulated miRNAs in GBM and their specific targets that could be involved in the onset of this disease, predominantly related with cancer hallmarks. More recently, a review on GBM-related miRNAs was published, collecting information from all the upregulated and downregulated miRNAs in GBM, when comparing normal brain tissue with GBM tumour samples and identifying the possible cellular processes where each miRNA could be involved[90]. Such data are summarized in **Tables 1** and **2**.

Table 1. Upregulated miRNAs, their targets and functional implication in GBM hallmarks. Adapted from Moller et al[90]

MiRNA	Target	Proliferation	Apoptosis	Angiogenesis	Invasion/Migration	Chemiosensitivity
hsa-miR-9	CAMTA1, PTCH	•		•		
hsa-miR-10b	HOXD10, CDKN1A	•			•	
hsa-miR-15b	CCNE1	•				
hsa-miR-17	TGFβ-RII, CTGF, CAMTA1, POLD2, PTEN	•	•	•		
hsa-miR-18a	SMAD4, CTGF	•	•	•		
hsa-miR-20a	TGFβ-RII, CTGF, TIMP2	•		•	•	
hsa-miR-21	RECK,MMP9 , TIMP3, PTEN, PDPD4	•	•		•	•
hsa-miR-25	MDM2, TSC1	•				
hsa-miR-26a	PTEN, PHB	•		•		
hsa-miR-30e	IκBα	•		•	•	
hsa-miR-92	CTGF	•				
hsa-miR-93	Integrin-β8	•		•		
hsa-miR-155	MX1, FOXO3	•	•			•
hsa-miR-221	P27, PTEN, PUMA, P57, PTPμ	•	•		•	
hsa-miR-381	LRRC4, NEFL	•				•

Table 2. Downregulated miRNAs their targets and functional implication in GBM hallmarks. Adapted from Moller et al[90]

MiRNA	Target	Proliferation	Apoptosis	Angiogenesis	Invasion/Migration	Chemosensitivity
hsa-miR-7	FAK, EGFR, IRS1/2	•	•		•	•
hsa-miR-29b	PDPN	•	•		•	
hsa-miR-34	CCND1, E2F1, MET, MSI1, NOTCH1/2, RICTOR	•	•		•	
hsa-miR-101	EZH2, MSI1	•	•	•	•	
hsa-miR-124	PTBP1,RB1, CDK4/6, PPP1R13L, SNAI2,RRAS NRAS,CLOCK	•			•	
hsa-hsa-miR-125a	PDPN				•	
hsa-hsa-miR-128	WEEI1,P70S6K1, MSI1, E2F3A, BMI1, SUZ12, EGFR, PDGFRA, EPHB2, SP1	•		•		
hsa-miR-135a	STAT6, SMAD5, BMPR2	•	•			
hsa-miR-137	CDK6, RB1, MSI1	•			•	
hsa-miR-181d	BCL2, KRAS	•	•			
hsa-miR-218	IKKβ, BMI1				•	
hsa-miR-326	SMO, NOTCH1/2	•	•		•	
hsa-miR-483	ERK1	•				
hsa-miR-491	MMP9				•	

1.4.2 MiRNAs and Cancer Metabolism

As previously mentioned, several molecular pathways involving oncogenes and tumour suppressor genes participate in the metabolic switch in cancer cells, and most of the participants of these pathways are miRNA targets. An example is PI3K which is targeted by hsa-miR-320, hsa-miR-123a, hsa-miR-422, hsa-miR-506 and hsa-miR-136. However this is not the only key protein involved in metabolism targeted by miRNAs[107]. In fact, growing evidences, such as those emerged from the study of Tibiche and Wang[108], as a result of

functional association analysis of miRNAs and metabolic pathways, uncover that miRNAs predominantly regulate central metabolic pathways, such as amino acid biosynthesis, and glucose and lipid metabolism (**Table 3**). The regulation of metabolic activity by miRNAs can be achieved in different ways: (1) directly, targeting key molecules, such as transporters, modulating their expression, and enzymes of metabolic processes, modulating their activity, or (2) by regulating multiple oncogenic signalling pathways, through influencing the expression levels of transcription factors and oncogenes or tumour suppressor genes, including p53, c-Myc, AMPK and AKT signalling pathways. Thus, the molecular mechanisms that give rise to Warburg Effect can in part serve as an example of the importance of miRNAs regulation in energy metabolism[107].

The first step in the glycolysis pathway is the uptake of glucose into the cell through glucose transporters (GLTUTs). Torens *et al.* [109] observed that the amount of the GLUT1, GLUT2, and GLUT3 transcripts were elevated, while mRNA levels of GLUT4 and GLUT5 were below detection in most cancer tissues. High GLUT levels increased glucose uptake in malignant cells, thus accelerating metabolism[109]. Two miRNAs, hsa-miR-133 and hsa-miR-195, showed to target GLUT3, affecting not only is translation, but also their expression in cellular membrane [110,111]. Other examples of the effects of miRNAs in GLUT expression and, consequently, glucose uptake include: (1) hsa-miR-133, which regulates the expression of GLUT4 by targeting KLF15 in animal models[112]; (2) downregulation of hsa-miR-199a, hsa-miR-138, hsa-miR-150 and hsa-miR-532-5p, in renal cell carcinoma, which was associated with higher expression of GLUT1, while upregulation hsa-miR-130b, hsa-miR-19a, hsa-miR-19b and hsa-miR-301a was responsible for lower expression of GLUT1[113].

Regarding PI3K/Akt pathway, extremely activated in cancer cells, several studies have shown an interplay between this pathway and miRNAs, such as the loss of hsa-miR-126 in colorectal, gastric lung and breast cancer, which in normal cells targets p85b subunit of PI3K decreasing mRNA levels, thereby inhibiting tumour cell growth. AKT can also be regulated by hsa-miR-21, which unlike hsa-miR-126, stimulates glycolysis by directly regulating glycolytic enzymes such as PFK1 and activating AKT downstream mammalian target of rapamycin (mTOR) activity[107,114–117].

Under hypoxic conditions, which are characteristic of solid tumours, the transcription factor HIF-1α accumulates in cells and contributes to the metabolic switch from OXPHOS to glycolysis. Chan *et al.* (2010) and Devlin *et al.* (2011) demonstrated that, besides the alterations in HK2, PK, enzymes expression, HIF-1α was also responsible for the expression of hsa-miR-210, the "master miRNA" of hypoxic response, which is upregulated in hypoxic environements[118,119]. In fact, recent studies show that transcriptional activation of hsa-miR-210 blocks mitochondrial respiration OXPHOS in lung cancer cell lines, and renal

cell carcinoma[120,121] Thus, by downregulating several elements of the mitochondrial metabolism, including the Electron Transport Chain (ETC) complexes, hsa-miR-210 contributes to cancer cell metabolic switch and activation of an aerobic glycolysis metabolism[122]. In addition, several other miRNAs contribute to either HIF-1α stabilization or inhibition. In CLL, hsa-miR-32-1 mediates the stabilization of HIF-1α under normoxia, by targeting the tumour suppressor VHL, which is the E3 ligase involved in HIF-1α degradation [123]. Concerning the inhibition of HIF-1α expression, a specific set of miRNAs seems to be involved, including hsa-miR-17-92 cluster, hsa-miR-107, hsa-miR-20b and hsa-miR-22, which modulate the expression of HIF-1α and consequently alter the tumour growth[124].However other studies, more recently showed that hsa-miR-519 and hsa-miR-138 also inhibit HIF-1α, resulting in suppression of tumour angiogenesis, growth and metastization process[125,126].

Table 3. Hsa- miRNAs involved in cell metabolism, their targets and corresponding metabolic activity ot pathway affected. Adapted from Hatziapostolou et al[127], and Chan et al[128].

miRNA	Target Genes	Metabolic Activity/Pathway	Cancer Types
hsa-miR-1, hsa-miR-206	G6PD, TKT, 6PGD, GPD2	TCA cycle, PPP	Lung and prostate cancer
hsa-miR-17	MnSOD, GPX2, TrxR2	Mitochondrial Antioxidant	Prostate cancer
hsa-miR-17-3p	LDH-2	Glycolysis	Prostate cancer
hsa-miR-17-92	E2F1	Redox State	Lung cancer
hsa-miR-21	SOD3 and TNF-α	Redox State	Bronchial Epithelial cancer
hsa-miR-23a	GLS2, PGC-1α, G6PC	c-Myc, Glutamine metabolism	Lymphoma and prostate cancer
hsa-miR-23b	ATG12, POX/PRODH	Autophagy, c-Myc, glutamine metabolism	Pancreatic, prostate cancer and Lymphoma
hsa-miR-26a	PDHX	Glucose Metabolism	Colorectal cancer
hsa-miR-34a	HK1, HK2, GP1, PDK1	P53, Glucose metabolism	Lung and colon cancer
hsa-miR-106a	SLC2A3	Glucose uptake	Glioblastoma
hsa-miR-122	SMARCD1, MAP3K, CAT-1, PKM2, Aldo	Mitochondrial Metabolism, Krebs Cycle, Glycolysis, Lipid Metabolism	Hepatocellular carcinoma, Leukeia and Liver Cancer
hsa-miR-124	SLC16A1	Aerobis Glycolysis	Medulloblastoma
hsa-miR-124	PKM2	Glycolysis	Colorectal cancer
hsa-miR-125	PKM1, HK2	Glucose Metabolism	Colorectal, hepatocellular cancer
hsa-miR-125b	PDK1, AKT2, HK2	Glucose, glutathione and lipid	Leukemia
hsa-miR-126	IRS1	Mitochondrial metabolism, AKT	Mesothelioma
hsa-miR-133a, hsa-miR-133b	PKM2	Glycolysis	Tongue squamous carcinoma
hsa-miR-143	HK2	Glycolysis, Glucose Metabolim	Lung Cancer and Glioblastoma
hsa-miR-155/hsa-miR-143	HK2	Aerobic Glycolysis	Breast cancer
hsa-miR-181a	PTEN	Glycolysis, PTEN/AKT	Colon cancer cells
hsa-miR-183	IDH2	TCA cycle, PPP	Glioma cells
hsa-miR-185, hsa-miR-342	SREBP-1, SREBP-2	SREBP-lipogenesis	Prostate cancer
hsa-miR-195	GLUT3	Glucose uptake	Bladder cancer
hsa-miR-200	PGI	Glycolysis	Breast cancer
hsa-miR-205	ACSL1	Lipid Metabolism	Hepatocellular carcinoma
hsa-miR-210	ISCU, COX10, SHD,NDUFA4	Hypoxia, Krebs Cycle, Glycolysis, ROS	Breast, colon, head, neck and esophageal cancer
hsa-miR-320	PFKm	Glycolysis	Lung Adenocarcinoma
hsa-miR-326	PKM2	AMPK	Glioblastoma
hsa-miR-375	LDHB	Anaerobc Glycolysis	Maxillary sqamous carcinoma
hsa-miR-378	ESRRG, GABPA, ERRγ	Metabolic Switch	Breast cancer
hsa-miR-451	CAB39	LKB1/AMPK	Glioblastoma
hsa-miR-520	PFKP	Glycolysis	Hepatocellular carcinoma
hsa-miR-1291	GLUT1, NMN, NMNT	Glucose Metabolism	Renal cell carcinoma, Pancreatic Cancer

1.5 THERAPEUTIC STRATEGIES FOR GBM

1.5.1 Current standard treatment

As previously mentioned, the standard treatment for newly diagnosed GBM patients relies in radiotherapy with adjuvant administration of TMZ after the surgical resection of the tumour, which confers a median survival time of 14.6 months. For a long time, GBM was classified as refractory for chemotherapy, indicating its resistance to early rounds of chemotherapy, and therefore, the usual treatment consisted in post-operative radiotherapy[129]. Moreover, before the development of TMZ, nitrosoureas, liposoluble drugs that cross the blood-brain barrier, were the most frequently used treatment for cerebral tumours. However, over the years, randomized studies failed to demonstrate the positive impact of nitrosoureas administration after surgery and radiotherapy in patient survival rates[129]. More recently, and through a randomized phase III trial conducted by the European Organisation for Research and Treatment of Cancer (EORTC)/National Cancer Institute of Canada (NCIC), a significant improvement in patient survival was achieved when the patients were submitted to tumour resection and treated with a combination of radiotherapy and concomitant TMZ, with 6 cycles of subsequent TMZ after a 4-week break[130]. TMZ is a small lipophilic molecule with an extensive tissue distribution, which crosses the blood–brain barrier and reaches the CNS. This drug is preferentially activated within tumour tissue since it requires a narrow alkaline pH window, and brain tumours possess a more alkaline pH compared with the surrounding healthy tissue[131]. TMZ, synthesized in the late 80s by Stevens and coworkers[132], belongs to the class of imidazotetrazine prodrugs and acts as an orally monofunctional DNA alkylating agent, transferring a methyl group to DNA purine bases O6-guanine, N7-guanine and N3-adenine. The most common TMZ-induced methylation takes place at N7-guanine (70%), however, the therapeutic value of this reaction is scarce due to the efficient base excision repair (BER) mechanism that can overcome the lesions[131]. The anti-cancer activity of TMZ is due to a small fraction of DNA methylation which takes place at O6-guanine (5%). This methylation results in mispair of O6-methyl-guanine (O6-MeG) with thymine in DNA replication, activating DNA mismatch repair (MIM) mechanism that is capable of removing thymine but not O6-MeG, thus initiating a continuous cycle of thymine insertion and excision, that ultimately results in persistent DNA double strands breaks (DBS)[133]. A series of events

promoted by TMZ, beginning in the replication fork collapsing as a consequence of DBS and cell cycle arrest at G2/M phase via ART/CHECK-1 dependent signalling, culminates in apoptosis[134]. Nonetheless, O6-MeG can be repaired by methylguanine-DNA methyltransferase (MGMT), a small protein present in cytoplasm and nucleus, which reverts the cytotoxic effect of TMZ by transferring the O6-MeG from a guanine residue to a cysteine residue. Mutations in *MGMT*, protein phosphorylation resulting in MGMT inactivation, and loss of chromosome 10, where the *MGMT* gene is located, were found in human cancers however, the loss of MGMT activity is commonly attributed to MGMT promoter methylation, a frequent epigenetic phenomenon in tumourigenesis. In fact, Stupp and co-workers observed that the patients that displayed methylation of the MGMT gene promoter methylation benefited more from the administration of TMZ, correlating with higher survival rates[130]. TMZ resistance by the GBM cells frequently results in tumour recurrence and a new tumour resection is performed, when possible, and a second line of treatment this time using bevacizumab, a VEGF monoclonal antibody already approved for other human cancers[135].

1.5.2 New approaches

Despite all the work developed over the years to achieve an effective treatment for GBM, translated in increasing median survival rates, the outcome remains dismal when using the current treatment. Therefore, there is a huge demand for new therapeutic approaches. In this regard, several different approaches are being developed, either based on the design of new and more sophisticated chemotherapeutic drugs targeting specific tumour characteristics or mechanisms, on the "education" of the immune system to induce tumour cell elimination by the organism, or on gene therapy strategies targeting key genes or regulatory elements of gene expression implicated in tumour malignancy.

1.5.2.1 Dichloroacetate (DCA)

Recent reports have described an inhibitor of the mitochondrial pyruvate dehydrogenase kinase (PDK), and, consequently, an activator of pyruvate dehydrogenase complex (PDC), dichloroacetate (DCA), as having a potential antitumor capacity in non-small cell lung cancer, GBM, breast, endometrial and prostate cancer[15]. DCA has caught the attention of oncology field due to its ability to target glycolytic tumours while sparing the surrounding oxidative healthy organs. In 2007, Michelakis and colleagues demonstrated the

anticancer therapeutic potential of DCA in human non-small cell lung cancer (A549) xenografts in rats, which showed significant toxicity, with induction of apoptosis and impaired tumour growth[136]. Additionally, this group reported that, after DCA treatment, tumour tissue from GBM patients displayed decreased expression levels of HIF-1α, reactivated mitochondrial function and modified cellular metabolism[137]. In 2014, the results regarding phase I trial of DCA in adults with recurrent malignant brain tumours were published, in which the authors concluded that DCA is a well-tolerated compound without toxicity problems for patients bearing recurrent malignant gliomas and other tumours metastatic to the brain[138].

1.5.2.2 Immunotherapy

Over the years, exciting results obtained in various forms of human malignancies using immunotherapy, have shown the potential of boosting the organism's natural defense to specifically target tumour cells, sparing the normal surrounding tissue and being capable of maintaining long term antitumour responses without inducing neurologic side effects. Currently, there are two immunotherapy strategies under tests in brain tumours: (1) the adoptive immunotherapy, or passive immunotherapy, where in vitro activated patient's immune cells or specific antibodies are introduced in the bloodstream, and (2) the active immunotherapy, which promotes patient's native immune response, acting as a vaccine, through the use of tumour antigens, which can be tumour cells' lysates, mRNA, intact tumour cells, and peptides obtained from tumour cells such as MHC class I molecules[139,140].

Due to GBM ability to acquire TMZ resistance through MGMT expression, immunotherapy can be used as a complement for standard treatment. Recently, Ardon and co-workers[141] reported a strategy of vaccination using autologous dendritic cells (DC) derived from patient's monocytes, which were previously stimulated with autologous tumour cells, and administered between the end of radio/chemotherapy and the beginning of adjuvant chemotherapy. This treatment ultimately translated into increased median overall survival for all 8 patients (24 months) with progression-free survival rate after 6 months of 75%[141]. In another phase I/II clinical trial using DC vaccination, it was demonstrated that DC was responsible for tumour shrinkage and increased concentration of tumour-infiltrating CD8(+) lymphocytes, translating into higher median survival of 525 days, as compared with 380 days for control patients (not submitted to immunotherapy) [142].

1.5.2.3 Gene Therapy

Gene therapy can be defined as the use of gene expression-modifying strategies to address the treatment of diseases with a genetic component. Depending on the specific therapeutic objective, different gene therapy approaches exist, namely 1) the introduction of a gene that is dysfunctional or absent; 2) the addition of a therapeutic gene; 3) the replacement of a non-functional gene and 4) the knockdown of an overexpressed gene. Due to the abnormal gene expression profile presented by cancers, this disease could be treated using gene therapy strategies. The gene therapy modality of introducing a therapeutic gene can be exemplified by the elegant approach of suicide gene therapy reported by Mohyeldin and co-workers, aiming at promoting GBM cell death. The strategy consisted in the delivery of a plasmid encoding the Herpex Simplex Virus Thymidine-kinase (HSV-TK), which was preferentially expressed in cancer cells expressing specific cancer cell markers, followed by administration of the prodrug ganciclovir (GCV). This prodrug is converted into a toxic metabolite denominated GCV-triphosphate, which inserts into the DNA, blocking its replication and, therefore, inducing cell cycle arrest with consequent apoptosis[143].

Two of the most promising gene therapy's active agents are small interfering double-stranded RNA (siRNA) and short-hairpin RNA (shRNA), which can be delivered into target cells and promote gene silencing. After delivery to the cell's cytoplasm, one of the strands of the siRNA has the ability to be incorporated into RNA-induced silencing complex (RISC) and, by base pairing with a complementary mRNA, mediates its degradation, decreasing both RNA function and protein synthesis. Recent studies have focused on silencing of genes related with various altered signalling pathways in cancer, including GBM, such as metabolic reprogramming. Sanzey and collaborators demonstrated, that shRNA-mediated reduction of glycolytic enzyme expression levels interfered with GBM growth in cellular models, and, importantly, the knockdown of glycolytic genes, such as PFKP and PDK1, in intracranial GBM xenografts, resulted in dramatic increase of survival of mice, confirming the importance of glycolytic pathway for GBM growth[144].

MiRNA modulation. MiRNA based therapeutic approaches have been explored over the years and successfully applied in pre-clinical models for several human malignancies, GBM being one of the most promising[7,18,87]. This strategy consists of the use of mimics or inhibitors of mature miRNAs, to achieve either gains or losses of normal miRNA function.

Overexpression of miRNAs downregulated in Cancer

In this approach, miRNA mimics can be delivered to the target cells as mature miRNAs, which consist of double-stranded RNA molecules, similar to the endogenous Dicer product.

Since miRNA mimics have unfavourable physicochemical features for in vivo administration, they are chemically modified to (1) increase protection from nuclease degradation, (2) decrease activation of innate immune system, and (3) reduce the incidence of nonspecific target effects. Another strategy is based on the delivery of shRNA or pri-miRNA mimics using a plasmid or viral construct, which results in more stable expression than the delivery of the mature miRNA mimics and allows the expression of several miRNAs[145]. As an example, the overexpression of hsa-miR-7, involved in the repression of the oncogenic AKT pathway, decreased the proliferation and invasion in GBM cells, whereas the overexpression of hsa-hsa-miR-128 was able to repress the proliferation of glioma cells by targeting a specific protein E2F transcription factor 3(E2F3)[146,147].

Silencing of miRNAs Overexpressed in Cancer

This approach relies on the ability of ssDNA and dsDNA or RNA analogues to inhibit the activity of selected single-stranded genetic sequences by base-pairing with complementary oligonucleotide sequences. The most efficient technology for controlling miRNA expression includes anti-miRNA oligonucleotides, complementary to the mature miRNA, and antisense oligonucleotides (ASOs) designed to block the function of miRNAs in the hsa-miRNP silencing complex. Additionally, synthetic polymers with similarities with DNA and RNA, peptide nucleic acids (PNAs), which consist of repeating units of N-(2-aminoethyl)-glycine linked by peptide bonds, have also been shown as worthy candidates for antisense therapies, since they are not easily recognized by nucleases or proteases and can be simply modified to increase miRNA targeting efficiency.

One practical example for this approach is the silencing of hsa-miR-21, which has been reported in several studies to be overexpressed in a wide range of human tumours such as GBM. In fact, oligonucleotide-mediated hsa-miR-21 silencing resulted in higher levels of tumour suppressors PTEN and PDCD4, activation of caspase 3/7, and decreased tumour cell proliferation[145]. However, an efficient in vivo delivery of nuclei acids to brain tumours needs to overcome some obstacles, the reason why the development of adequate targeted delivery systems has deserved higher attention by scientific community.

2 OBJECTIVES

As observed in a large number of human malignancies, GBM cells undergo a complex metabolic reprogramming in order to adapt and fulfil the energetic demands, for promoting tumour proliferation and resistance to apoptosis. Taking into consideration the high GBM chemoresistance to standard chemotherapeutics, there is an urgent need for new therapeutic approaches to tackle this disease. MiRNAs, constituting important modulators of metabolic key-signalling pathways with impact on tumour recurrence, emerge as promising molecular targets for a gene-based therapeutic intervention towards GBM. In this context, the ultimate goal of the present study is to design an effective therapy for GBM, based on the modulation of dysregulated miRNAs combined with a standard chemotherapeutic for GBM (temozolomide) or a drug (dicholoroacetate), known to target cell metabolism. To achieve our main objective, several tasks were performed with the following aims:

(1) Assessment and comparison of the expression levels of hsa-miRs, identified as crucial players in cancer metabolism, in normal human astrocytes and human GBM cells;

(2) Modulation of the expression of the selected hsa-miRs in GBM cells through delivery of synthetic hsa-miR mimics;

(3) Quantification of the expression levels of hsa-miRs and their potential targets after hsa-miR modulation;

(4) Evaluation of the effects of hsa-miR modulation on GBM cell viability, cell bioenergetics, cell migration and cell cycle;

(5) Assessment of the therapeutic potential of a combined strategy for GBM involving hsa-miR modulation and cell treatment with temozolomide or dichloroacetate.

3 Materials and Methods

3.1 Cell Lines and Culturing Conditions

The U-87 MG (U87) human glioma cell line, kindly provided by Dr. Peter Canoll (Columbia University, New York, NY), was maintained in Dulbecco modified Eagle's medium – high glucose (DMEM–HG; Sigma, D5648), supplemented with 10% (v/v) heat-inactivated fetal bovine serum (FBS) (Gibco, Paisley, Scotland), 100U/mL penicillin (Sigma-Aldrich), 100 μg/mL streptomycin (Sigma-Aldrich), 10 mmol/L HEPES and 12 mmol/L sodium bicarbonate. The DBTRG-05MG (DBTRG) human recurrent glioma cell line, established from a 59 years Caucasian female patient with GBM treated with local brain irradiation and multidrug chemotherapy and kindly provided by Dr. Massimiliano Salerno (Siena Biotech, Italy), was maintained in Roswell Park Memorial Institute 1640 (RPMI-1640) (Sigma-Aldrich, R4130), supplemented with 10% heat-inactivated FBS (Gibco, Paisley, Scotland), 100U/mL penicillin (Sigma-Aldrich), 100 μg/mL streptomycin (Sigma-Aldrich) and 12 mmol/L sodium bicarbonate. Human astrocytes (HA), kindly provided by Dr. Anne Régnier-Vi gouroux (Johannes Gutenberg Universität-Mainz), were maintained in DMEM (Sigma-Aldrich, D5648), supplemented with 2% heat-inactivated FBS (Gibco, Paisley, Scotland), 100 U/mL penicillin (Sigma-Aldrich), 100 μg/mL streptomycin (Sigma-Aldrich), 10 mmol/L sodium bicarbonate. HA medium was freshly supplemented with 1% N2 (Sigma-Aldrich) and 1% non-essential amino acids (Sigma-Aldrich). The cells were cultured at 37°C under a humidified atmosphere containing 5% of CO_2 and grown adherent, being detached upon addition of enzyme-free dissociation buffer. Cell suspensions were diluted 1:1 with Trypan blue and cells were counted using a hemocytometer.

3.2 Total RNA Extraction and cDNA Synthesis

Total RNA, including miRNAs, was extracted from cells using the miRCURY Isolation Kit (Exiqon), and total mRNA was similarly isolated using NucleoSpin (Macherey-Nagel), according to manufacturer's instructions for cultured cells. Regarding miRNA isolation, briefly, cells were lysed with a lysis solution containing 10 μl of B-mercaptoethanol per milliliter of lysis buffer, and then total RNA was bound to a silica matrix provided by the manufacturer and washed with the recommend buffer. A DNA digestion step was performed before the elution on columns with DNase I (Sigma-Aldrich) for maximal removal of DNA and according to manufacturer's recommendation. Finally, the RNA was eluted with 30 μl of elution buffer. The total RNA extracted was quantified using the NanoDrop 2000 Spectrophotometer (Thermo Scientific) and stored at -80°C. Concerning the total RNA isolation, the steps were similar to miRNA isolation with exception of the reagents used, which were recommended by the manufacturer. Complementary DNA (cDNA) synthesis for miRNA quantification was performed using the Universal cDNA Synthesis Kit (Exiqon).

cDNA was synthesized from 10 ng of total RNA in a 10 μL reaction, according to the following protocol: 60 min at 42°C, followed by reverse transcriptase heat-inactivation for 5 min at 95°C. The obtained cDNA was then diluted 1:40 with RNase-free water and stored at -20°C. For mRNA quantification, cDNA synthesis was performed using up to 500 ng of total RNA in a 10μL reaction, employing the NZY First-Strand cDNA Synthesis Kit (NZYtech, Lisbon, Portugal) and applying the following protocol: 10 min at 25°C, 30 min at 50°C and 5 min at 85°C for reverse transcriptase inactivation. Subsequently, the samples were incubated with NZY RNase H (E.coli) for 20 min at 37°C in order to degrade the RNA template in cDNA:RNA hybrids. The produced cDNA was diluted 20 times with RNase-free water and stored at -20°C.

3.3 Quantitative Real Time PCR (qPCR)

Quantitative PCR was performed in a StepOnePlus Thermocycler (Applied Biosystems) using 96-well microtiter plates. For miRNA quantification, the miRCURRY LNA TM Universal RT microRNA PCR system (Exiqon) was employed using SYBR Green Master Mix (Exiqon). The primers used were acquired from Exiqon, including the reference genes, non-coding small nuclear RNA (snRNA) U6(RNU6) and small nucleolar RNA, C/D box 44 (SNORD44) (**Table 4**). A master mix was prepared for each primer set, containing 5 μL of SYBR Green and 1 μL of primer mixture (corresponding to 1 μM each primer, FW and RV). For each reaction, 6 μL of master mix were added to 4 μL template cDNA. All reactions were performed in duplicate at a final volume of 10 μL per well. qPCR protocol consisted of polymerase activation and DNA denaturation at 95°C for 10 min, followed by 45 amplification cycles of 10 s at 95°C and 1 min at 60°Cat ramp-rate of 1.6°C/s. For mRNA quantification, the SsoAdvanced Universal SYBR Green Supermix (Bio-Rad) was used. The primers for the tested genes were designed using the bioinformatics primer designing tool Primer-BLAST, which relies on Primer3 to design PCR primers for a specific PCR target and BLAST and global alignment to select primer pairs, and purchased from Invitrogen. Hypoxanthine phosphoribosyltransferase 1 (HPRT1) was used as reference gene (**Table 5**). For each reaction, performed in duplicate, 4 μL of template cDNA were added to 6 μL of a master mix, composed of 5 μL of SYBR GREEN Supermix and 1 μL of the primer set to achieve a final concentration of 1μM for each primer pair. The reaction conditions consisted of enzyme activation at 95°C for 1 min and 30 s, followed by 45 cycles of 10 s at 95°C (denaturation), 30 s at 55-60°C (annealing temperature, depending on primer melting temperatures), and finally 30 s at 72°C (elongation phase).For both miRNA and mRNA quantifications, the melting curve acquisition protocol started immediately after amplification, which consisted of 1 min heating at 55°C followed by 0.5°C temperature

increments in 80 steps of 10s until a maximum of 95°C. The No Template Control (NTC) and the No Reverse Transcriptase Control (noRT) were assessed, for each primer set, in all experiments performed. The threshold value for threshold cycle determination (Ct) was defined as 10000 and the baselines adjusted for each sample. Fold changes of miRNAs and mRNA levels were determined according to the Pfaffl method using the levels of RNU6 and SNORD44 (miRNAs) and HPRT1 (mRNA) as internal controls, taking into consideration the different amplification efficiencies of each primer set (ranging from 80-120%) obtained from a standard curve generated by making serial dilutions. The amplification efficiency for each target or reference miRNA and mRNA was determined according to the formula: $E=10^{(-1/S)}-1$, where S is the slope of the obtained standard curve.

Table 4. Primer sequences used for hsa-miRNAs qPCR analysis and respective target sequences

MIRNA	TARGET SEQUENCE
hsa-miR-19a-3p	UUGCAAAUCUAUGCAAAACUGA
hsa-miR-183-5p	UAUGGCACUGGUAGAAAUUCACU
hsa-miR-155-5p	UUAAUGCUAAUCGUGAUAGGGGU
hsa-miR-23a-3p	AUCACAUUGCCAGGGAUUUCC
hsa-miR-144-3p	UACAGUAUAGAUGAUGUACU
hsa-miR-200c-3p	UAAUACUGCCGGGUAAUGAUGGA
U6	CACGAATTTGCGTGTCATCCTT

Table 5. Primer sequences used for qPCR analysis and respective amplicon sizes

GENE	PRIMER SEQUENCE (5'-3')		AMPLICON
HPRT1	Forward	CTGCGTAACTCCATCTGA	103 bp
	Reverse	ACCGTAATTGGCATCGT	
IDH1	Forward	ATGGTGACGTGCAGTCGG	76 bp
	Reverse	GGACAAACCAGCACGCT	
TIGAR	Forward	CTGACTGAAACTCGCTAAGG	105 bp
	Reverse	CAGAACTAGCAGAGGAGAGA	
IDH2	Forward	AGACCTCATCAGGTTTGCCCA	111 bp
	Reverse	TTCACATTGCTGAGGCCGT	
PDK1	Forward	GGCTATGAAAATGCTAGGCG	93 bp
	Reverse	CTGTCCTGGTGATTTTGCATT	
PDHA1	Forward	TGGAGTCAGTTACCGTACACGAG	107 bp
	Reverse	CCACACTGGCAAGATTGCTG	
STAT3	Forward	CCTGCAGCAATACCATTGAC	118 bp
	Reverse	GTGAGGGACTCAAACTGCC	

3.4 Lipoplex Preparation

The miRIDIAN hsa-miR-200c-3p and hsa-miR-144-3p mimics (Dharmacon) and the non-targeting control oligonucleotide (control ON) were resuspended in sterile water and stored in 20 μM aliquots at -20°C (**Table 6**). For cell transfection ONs were formulated into lipoplexes prepared from delivery liposomal system (DLS) liposomes, as described in Trabulo *et al.* 2010[148]. DLS stock solution was prepared by mixing 1mg of dioctadecylamidoglycylspermidine (DOGS) (Promega, Madison, WI) with 1 mg of dioleoylphosphatidylethanolamine (DOPE) (Sigma, Munich, Germany) and then dissolved in 40 μ of 90% ethanol, followed by a ten-fold dilution in sterile H_2O, to achieve a final lipid concentration of 5 mg/mL (2.5 mg of DOGS and 2.5 mg of DOPE). The mixture was homogenized by gentle vortexing and incubated for 30 min at room temperature, to allow liposome formation. DLS/ON lipoplexes were prepared in OPTIMEM freshly for every experiment. Briefly, 25 pmol of each ON were mixed with the appropriate volume of DLS

suspension to achieve the desired ratio of 95 μg DLS/10 μg ON. The complexes were let to incubate for 30 min at room temperature, to allow complex formation.

Table 6. Hsa-miRNA mimics and their respective sequences

	Sequence (5'-3')
Oligonucleotide control (ON)	UUCUCCGAACGUGUCACGUdTdT
hsa-miR-200c-3p mimic	UAAUACUGCCGGGUAAUGAUGGA
hsa-miR-144-3p mimic	UACAGUAUAGAUGAUGUACU

3.5 Cell Transfection

For flow cytometry experiments, qRT-PCR analysis and chemotaxis assay, cells were plated onto 12-well plates (Costar), at a density of $6x10^4$ cells/well in a final volume of 1 mL of culture medium (DMEM and RPMI supplemented with 10% serum for U87 and DBTRG cells, respectively). For density assay, U87 and DBTRG were seeded at a density of $6x10^3$ and $5x10^3$ cell per well, respectively, in 200 μl, onto 96-well plates (Costar), and the plate border wells were filled with 200 μl of sterile water. On the following day, the cell medium was replaced with OPTIMEM (Gibco) and the lipoplexes were added to the cells, at a final concentration of 25 nM per well, in a volume of 500 μL or 45 μLper well in 12-well and 96-well plates, respectively. After 4 h of incubation at 37°C, the transfection was stopped by replacing the OPTIMEM medium with the corresponding complete culture medium.

3.6 Drug Storage and Cell Incubation

Temozolomide (TMZ, Temodar, Merck) was acquired from Selleckchem and dichloroacetate (DCA) was acquired from Sigma (Sigma, Germany). Stock solutions of TMZ (20mM) and DCA (8 M) were prepared in DMSO (Sigma, Germany) and sterile water, respectively, and stored at -20°C and 4°C, respectively. Twenty-four hours after transfection of U87MG and DBTRG-05MG cells with miRNA mimics, cells were incubated with the drugs for 48 h at 37°C under a humidified atmosphere containing 5% CO_2.

3.7 Cellular Bioenergetics Analysis

GBM cellular bioenergetics was analyzed using the XF24 Extracellular Flux Analyser, which allows the measurement of mitochondrial oxygen consumption rate (OCR) and extracellular acidification rate (ECAR). While OCR is a measurement of electron flux through the mitochondrial respiratory system resulting in oxygen reduction to water, ECAR is an indirect measurement of the glycolytic capacity of the cells, leading to lactate production.

For OCR and ECAR measurements, U87 and DBTRG cells were seeded onto XF24 Cell Culture Microplates (Seahorse Bioscience) and incubated at 37 °C under a humidified atmosphere containing 5% CO_2. Transfection and drug incubation protocols were applied as described above for 96-well plates. Twenty-four hours before the assay, 1 ml of XF Calibrant Solution was placed into each well of the sensor hydration microplate and the sensor cartridge placed onto the microplate and incubated in a non-CO_2 incubator at 37 °C for ~12 h (overnight).

On the day of the experiment, 70 ml of XF Assay Medium, at 37 °C, was supplemented with glucose and glutamine to achieve the concentrations present in the normal cell growth media. For U87 cells, the XF Base Medium was supplemented with 25 mM glucose (Sigma) and 4 mM L-glutamine (Sigma), while for DBTRG cells the XF Base Medium was supplemented with 2 mM L-glutamine (Sigma). Media pH was adjusted at 7.35 ± 0.05 using 0.1 M NaOH. Cells were gently washed twice with 1 mL of XF assay medium at 37 °C without disturbing the cell monolayer and, then, incubated with 450 µL of XF assay medium at 37 °C for 1 hour in a non-CO_2 incubator.

Solutions of oligomycin (1 µM), FCCP (0.3 µM) and rotenone (1 µM) were prepared by dilution of DMSO stock solutions (10x concentrated) in the previously prepared XF Base Medium, as described by Moura *et al.* 2015[149]. A solution of 2-DG (1.2 M) was prepared freshly in XF Base Medium on the day of the experiment. Each compound was loaded in its respective cartridge, where different volumes were used to compensate for the dilution effect in the wells, and injected by the following order: 50 µL of oligomycin, 55 µL of FCCP, 60 µL of 2-DG and 65 µL of rotenone, respectively (**Fig. 5A and B**). ATP synthase inhibition was achieved by injection of oligomycin, resulting in decreased mitochondrial ATP production and, consequently, shifting the energy production to glycolysis with an increase in ECAR (**Fig. 5A and B**). FCCP acts by transporting protons across the mitochondrial membrane and allows the dissipation of the proton gradient, thus uncoupling the electron transport from ATP synthesis (**Fig. 6A**). Therefore, FCCP injection is expected to result in an increased OCR due to the effort of mitochondria to re-establish the proton gradient across the inner mitochondrial membrane (**Fig. 5A**). In turn, 2-DG is a glucose analogue, which has

a 2-hydroxy group replaced with hydrogen. This analogue prevents glycolysis progression by inhibiting glucose-6-phosphate production (**Fig. 6B**). Consequently, a decrease in ECAR (**Fig. 5B**). Rotenone by inhibiting electron transfer from iron-sulfur centers in complex I to ubiquinone, supresses mitochondrial respiration. Thus, adding rotenone enables the calculation of non-mitochondrial respiration, or residual oxygen consumption, driven by processes outside the mitochondria, such as that involving the NADPH oxidase complex.

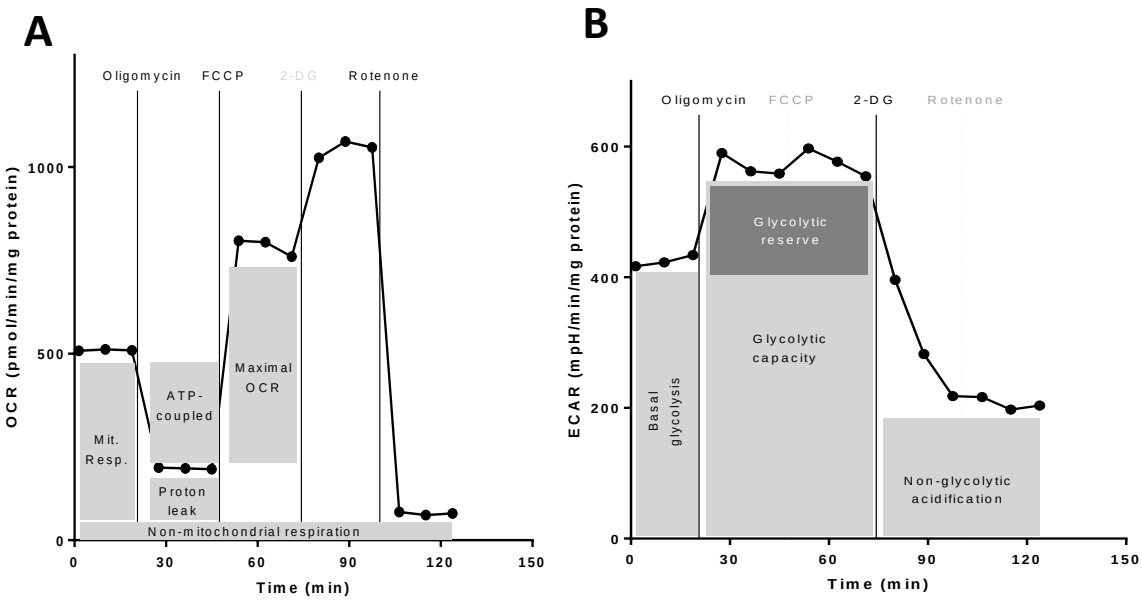

Figure 5. OCR (A) and ECAR (B) determination using the XFe Seahorse Bioanalyzer. Oligomycin, FCCP and Rotenone are sequentially injected for OCR measurements, whereas Oligomycin and 2-DG are used for ECAR measurements.

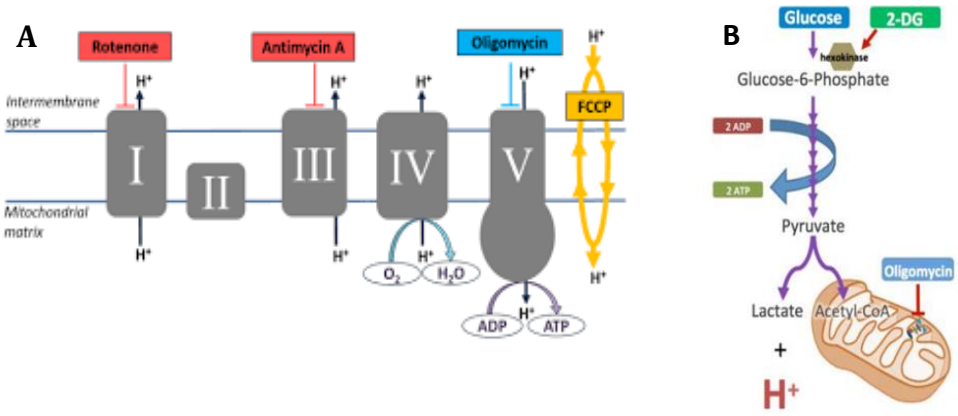

Figure 6. Compounds used for OCR and ECAR measurements and their effects on OXPHOS (A) and glycolysis (B). Rotenone inhibits electron transfer from iron-sulfur centers in complex I to ubiquinone; Antimycin A exerts its inhibitory effect at the levels of complex III; Oligomycin is a well-known inhibitor of ATP synthase (complex V) and 2-DG blocks glycolysis by inhibiting HK2. Adapted from Seahorse XFe Analyzer (Seahorse Biosciences).

Several parameters were calculated from bioenergetics analysis, namely, basal mitochondrial basal respiration, taken as the difference between OCR of resting cells cultured in medium containing glucose and OCR after rotenone injection; spare respiratory capacity which reflects the capacity of mitochondria to perform additional respiration when challenged with the decoupler FCCP; ATP-coupled respiration, determined as the difference between OCR of cells cultured in medium containing glucose and OCR after oligomycin injection; proton leak evaluated as the difference between OCR after oligomycin injection and rotenone injection. Non-mitochondrial respiration and FCCP-activated OCR were determined as the average of three measurements after rotenone injection and after FCCP injection, respectively. Additionally, Other parameters were determined from ECAR measurements including basal glycolysis, determined as the difference between ECAR of resting cells cultured in medium containing glucose and after 2-DG injection; glycolytic capacity, assessed as the difference between ECAR measurements after oligomycin stimulation and after 2-DG inhibition; glycolytic reserve representing the difference between ECAR of resting cells and ECAR after 2-DG injection; and non-glycolytic acidification which is determined after 2-DG injection.

3.8 Protein Quantification

OCR and ECAR readings were normalized to total protein levels in each well with BioRad DC Potein Assay -Microplate Assay Protocol, a colorimetric assay that allows the determination of protein concentration based on the formation of a complex between copper and peptide bonds under alkaline conditions and subsequent reduction of Follin reagent. Hundred microliters of Lysis Buffer were added to each well of XF24 Cell Culture Microplate (Seahorse Bioscience) and cells were subjected to freeze-thaw cycles. Cells were transferred to microcentrifuge tubes, the cell suspensions were centrifuged for 5 min at 14000 g and the supernatant was collected. Protein content was determined according to the manufacturer's instructions. In parallel, a standard curve was prepared using known BSA concentrations. The plate was incubated for 15 minutes in the dark at room temperature and the absorbance was measured at 750 nm in a microplate spectrophotometer (SpectraMax Plus 384, Molecular Devices).

3.9 Chemotaxis and Cell Trajectory Analysis

Cell migration experiments were performed using the µ-Slide Chemotaxis (Ibidi) as described in Suraneni *et al*. (2012)[150] (**Fig. 7**). Twenty-four hours before the experiment, µ-Slide Chemotaxis (Ibidi), plugs and cell growth media were placed in the incubator at 37°C and 5% CO_2 in a sterile 10 cm Petri dish with a wet tissue around the slide, for gas equilibration. Seventy-two hours after transfection, cells were detached from 12-well plates by incubation with dissociation medium for 5 min at 37°C, resuspended and counted. Afterwards, $1.8x10^4$ cells in a final volume of 10 µl were applied onto filling port A in µ-Slide Chemotaxis (Ibidi) plate (**Fig. 7**), using a 20 µL pipett and 10 µl of air were aspirated from the opposite filling port B, while the C, D, E and F ports were closed with plugs. Cells were allowed to adhere to the slide for 2 hours in an incubator at 37 °C and 5% CO_2. Subsequently, all plugs were gently removed from the filling ports and 65 µL of chemoattractant-free medium were applied onto filling port E, and 65 µl of air were aspirated from the filling port F. In the remaining port C, 65 µl of media with the chemoattractant EGF (Peprotech) at 10 ng/ml and 65 µL of air were aspirated from the filling port D. All plugs were then removed and replaced with a slide lid. Thereafter, cell migration was recorded by placing the µ-Slide under a microscope with a Plan-Apocromat 20x/0.8 air objective and CCD digital camera (AxiocamHRm), equipped with a 37°C incubator and 5% CO_2. The movies for the trajectory analysis were obtained by observing the cells for a period of 14 h with photographs taken every 5 minutes. Multidimensional image tiles were acquired in the chemotaxis assay and the trajectory of each cell was determined using the Image J software (v. 1.48, Wayne Rasband, NIH, USA) with the Cell Tracking plugin.

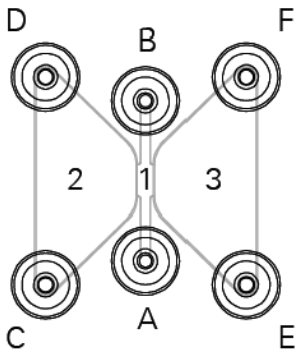

Figure. 7 Representative scheme of u-Slide Chemotaxis (Ibidi). The u-Slide Chemotaxis is composed of the observation area where the cells are plated (1), two reservoirs (2) and (3), and the filling ports A, B, C, D, E and F.

Trajectories were analysed using the Chemotaxis and Migration tool from Ibidi, where single cell trajectory was tracked by selecting the center of mass through all the time

points. Afterwards, the centre of mass, forward migration index, cell velocity and directness were obtained. The center of mass, a strong parameter for evaluating chemotaxis, represents the spatial averaged point of all cell endpoints (**Fig. 8**) and was calculated according to equation 1. Forward migration index parallel to the gradient (FMI^{II}) represents the efficiency of the forward migration when a parallel direction relative to the gradient was defined. The mean cell velocity was calculated by the displacement from the initial to the end point of the total trajectory time. Directness (**Fig. 9**) was calculated using equation 2. For each experimental condition, images were acquired in four different locations and a minimum of 20 cells were tracked. Experiments were independently repeated twice.

$$M_{end} = \frac{1}{n}\sum_{i=1}^{n}\left(X_{i,end}, Y_{i,end}\right) \quad \text{(Equation 1)}$$

where M_{end} is the cell center of mass; n is the number of cells; $X_{i,end}$ and $Y_{i,end}$ are the cells positions.

$$D = \frac{1}{n}\sum_{i=1}^{n}\frac{di.euclid}{di.accum} \quad \text{(Equation 2)}$$

where D is the cells' directness; n is the number of cells; di.euclid and di.accum are Euclidean distance and accumulated distance respectively

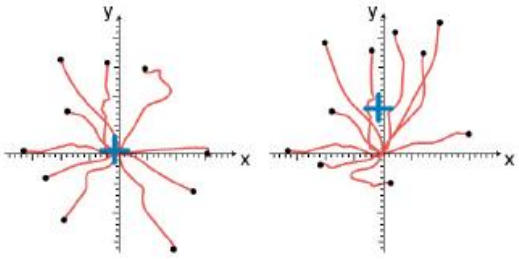

Figure 8. Schematic diagram of center of mass determination. The center of mass, indicated by a blue cross is displaced by the existence of a strong chemotaxis effect (right), when in comparison with the one representing no chemotaxis effect (left). Adapted from Ibidi

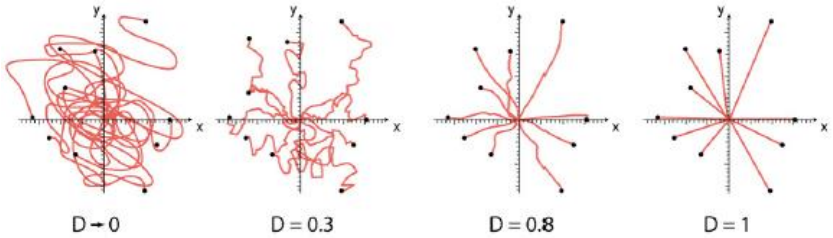

Figure 9. Schematic diagram of directness determination. Directness is defined as the ratio of the distance between the point of origin and the endpoint and the distance travelled by the cell between these two points. Adapted from Ibidi

3.10 Cell Density Evaluation

Cell density was evaluated by measuring the cellular protein content using the colorimetric sulforhodamine B (SRB) assay which is based on the ability of SRB, an anionic dye, to bind to basic amino acid residues of proteins, through electrostatic interactions, forming complex under moderately acid conditions. The SRB bound to protein will be proportional to the amount of protein and, consequently, to the total number of cells present in the well[151]. Twenty-four hours after transfection and 48 h following drug treatment, cells plated in 96-well plates were fixed by adding 200µL of a solution of 1% acetic acid in methanol, and stored at -80°C. After at least 1 hour of freezing, the solution was removed and the cells left drying for 20 min at 37°C, followed by incubation with 200 µL 0.5% SRB solution containing 1% acetic acid in water for 1 h at 37°C. Afterwards, cells were washed, at least 3 times, with a solution of 1% acetic acid in water, in order to remove all the surplus SRB dye, and dried at 37°C for 20 min. Lastly, 200 µL of 10 Mm Tris base (pH=10) were added to solubilize the protein-bound SRB. After 2 hours of incubation under mild agitation, the absorbance (Abs) of the resulting solution was read at 510 nm in a microplate reader (SpectraMax Plus 384, Molecular Devices). Cell density was expressed as percentage of control cells (non-treated), according to equation 3:

$$Cell\ Density\ (\%\ of\ control) = \frac{Abs_{treated\ cells}}{Abs_{control\ cells}} \times 100 \quad \text{(Equation 3)}$$

3.11 Cell Cycle Analysis

Cell cycle analysis was performed using flow cytometry. The distribution of the cell population through the cell cycle phases was determined by quantifying cell DNA content using propidium iodide for DNA labelling. Cells in G2/M phase which present the double of DNA copies in comparison with cells in G1 phase, display approximately the double of fluorescence intensity. Cells in the S phase, during DNA synthesis, present fluorescence values between those displayed by cells in G1 and cells in G2/M phases. Seventy-hours hours after transfection and 48 h following the drug treatment, cells plated in 12-well plates were incubated with dissociation medium for 5 min at 37°C. Afterwards, cells were resuspended and washed twice in ice-cold PBS by centrifugation at 600 g, at 4°C for 5 min. Subsequently, the supernatant was removed and the cells were fixed by slowly adding 200 µL of 70% ethanol under vortex followed by incubation at 4 °C for 3 hours. Cells were washed with 2 mL of 2% BSA in PBS and centrifuged 5 min at 600 g at 4 °C for 5 min The resulting pellet was resuspended in 300 µL of propidium iodide solution (PI/RNase,

Immunostep, Salamanca, Spain). After a 15 min incubation period at room temperature in the dark, cells were analysed in a FACS Calibur Flow Cytometer (BD, Biosciences). The data were analysed with Multi Cycle AV for Mac software and afterwards with ModFit software and presented as percentages for the different phases of the cell cycle.

3.12 Statistical Analysis

All data are presented as mean ± standard deviation (SD) of at least three independent experiments performed in duplicate, unless stated otherwise. One-way analysis of variance (ANOVA) combined with the Tukey posthoc test was used for multiple comparisons (unless stated otherwise) and considered significant when $p<0.05$. Statistical differences are presented at probability levels of $p<0.05$, $p<0.01$, $p<0.001$ and $p<0.0001$. Calculations were performed using standard statistical software (Prism 6, GraphPad, San Diego, CA, USA).

4 RESULTS

4.1. Comparative analysis of hsa-miRs expression in GBM cells and normal human astrocytes

The levels of six hsa-miRs, previously shown to be involved in GBM malignant phenotype, and predicted by bioinformatics data bases to target mRNAs of proteins involved in energy metabolism processes were quantified in U87 and DBTRG cells and compared with normal human astrocytes (HA)[152–156]. As shown in **Figure 10**, hsa-miR-19a, hsa-miR-183, hsa-miR-155, hsa-miR-200c and hsa-miR-144 were shown to be downregulated in both GBM cell lines as compared with HA. Expression of hsa-miR-144 was not detected in the DBTRG cells and was extremely low in U87 cells. Regarding hsa-miR-155 levels, U87 cells showed a small decrease with respect to normal astrocytes, whereas DBTRG cells presented almost complete ablation of this miRNA. On the other hand, hsa-miR-23a was shown to be significantly upregulated in both U87 and DBTRG cell lines. Based on these findings, hsa-miR-144 and hsa-miR-200c, which were those whose differential expression between normal HA and GBM cells was the most notorious, were selected for subsequent functional studies and evaluation of their potential as molecular targets for therapeutic intervention.

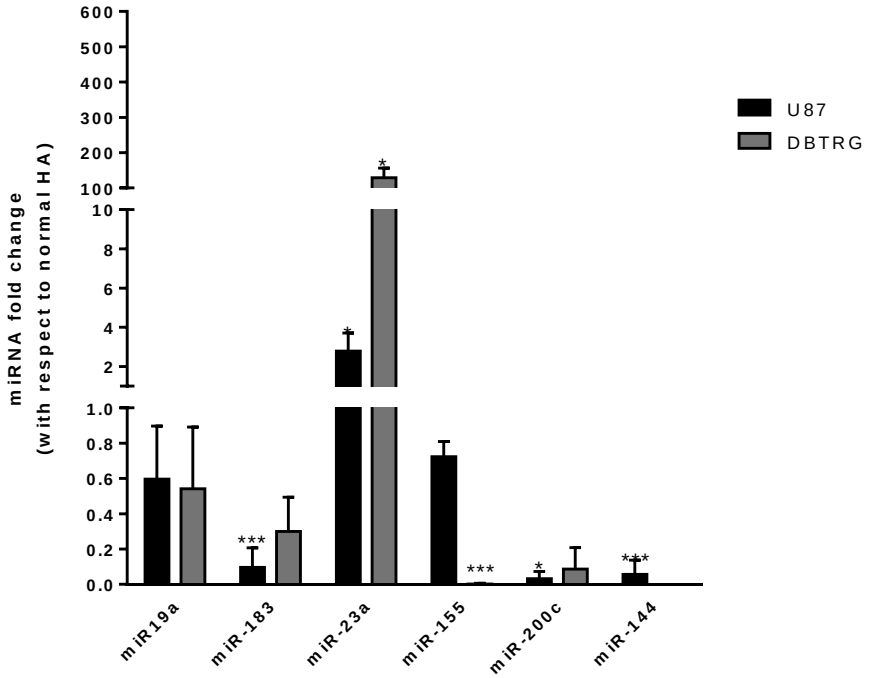

Figure 10. Hsa-miR expression levels in U87 and DBTRG cell lines, with respect to normal human astrocytes. Cells were maintained in culture conditions, as described in Material and Methods. RNA extracted from normal HA, U87 and DBTRG cells was transcribed and qRT-PCR was performed to determine miRNA expression. The Pfaffl method was used to evaluate hsa-miRs expression levels, which were normalized to the reference U6 and are presented as relative expression values with respect to normal HA. Data are presented as mean ± SD of at least three independent experiments. Pairwise comparisons were performed between the levels of each miRNA determined in U87 or DBTRG cells and those presented by normal HA (*$p<0.05$, ***$p<0.001$).

4.2. Quantification of key genes involved in the metabolism of GBM cells

The expression profile of genes whose mRNAs predicted to be targeted by hsa-miR-144-3p and hsa-miR-200c-3p, and that are known to be related with the metabolism in GBM, was assessed in U87 and DBTRG cells in comparison to normal HA. In particular, the levels of *IDH1*, *IDH2*, and *PDHA1,* genes associated with mitochondrial respiration, and *TIGAR* and *PDK1*, genes favouring both glycolysis and pentose phosphate pathway (PPP) in cancer cells, were evaluated. As shown in **Figure 11**, almost all genes showed a trend to increased expression in U87 and DBTRG cells, with exception of *IDH2*, which was found to be downregulated in both cell lines, when comparing with HA. This may indicate that the decreased levels of hsa-miR-144-3p, which predictably targets IDH2, do not impact IDH2 expression. The most significant difference was observed for *PDK1* levels in DBTRG cells, which presented a 4-fold increase in the levels of this mRNA with respect to HA, whereas in U87 cells only a slight increase in the expression of this gene was detected.

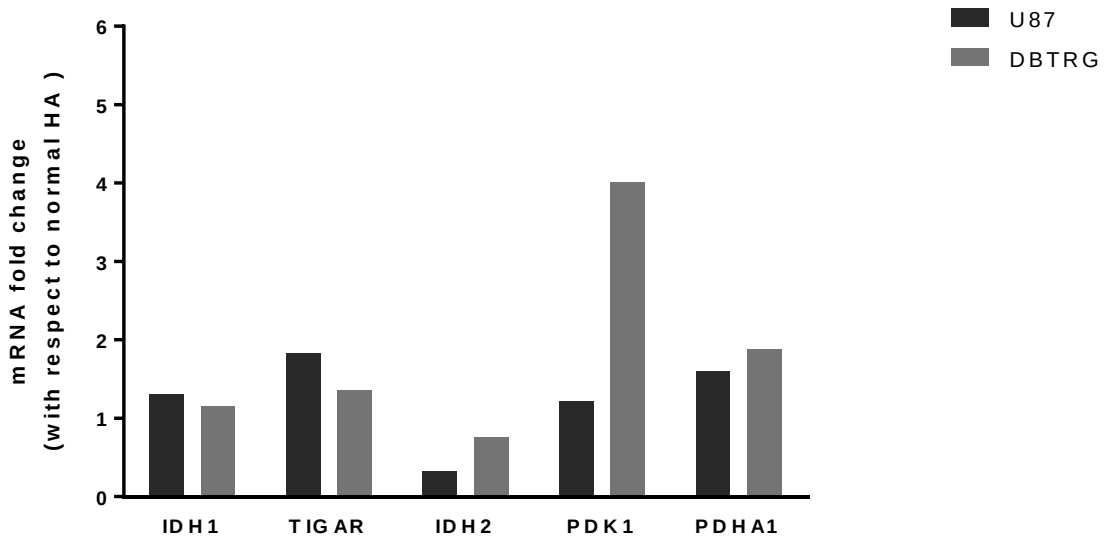

Figure 11. Gene expression profile of U87 and DBTRG cell lines in comparison with normal HA. Relative quantification of key genes involved in the metabolism of both U87 and DBTRG cells with respect to normal HA, as evaluated by qRT-PCR. The Pfaffl method was used to calculate mRNA expression levels, which were normalized to the reference HPRT1 gene and are presented as relative expression values with respect to normal HA. Data presented corresponds to one or two experiments.

4.3. Effect of miRNA modulation on the mRNA levels of their target genes

To determine the functional consequences of hsa-miR-200c-3p and hsa-miR-144-3p modulation, DBTRG cells were transfected with miRCURYLNA™ hsa-miR-200c-3p and hsa-miR-144-3p mimics. Transfection of DBTRG cells with hsa-miR-200c-3or hsa-miR-144-3p

(**Fig. 12A** and **12B**) resulted in increased hsa-miR expression levels. Due to the absence of hsa-miR-144-3p expression in DBTRG cells, we chose to present miRNA levels with respect to the levels of SNORD44, a miRNA which showed high and consistent expression across all samples, thus being a suitable control for miRNA level determination. DBTRG cell transfection with either miRNA mimics resulted in a decrease in the mRNA expression levels of the respective target genes.

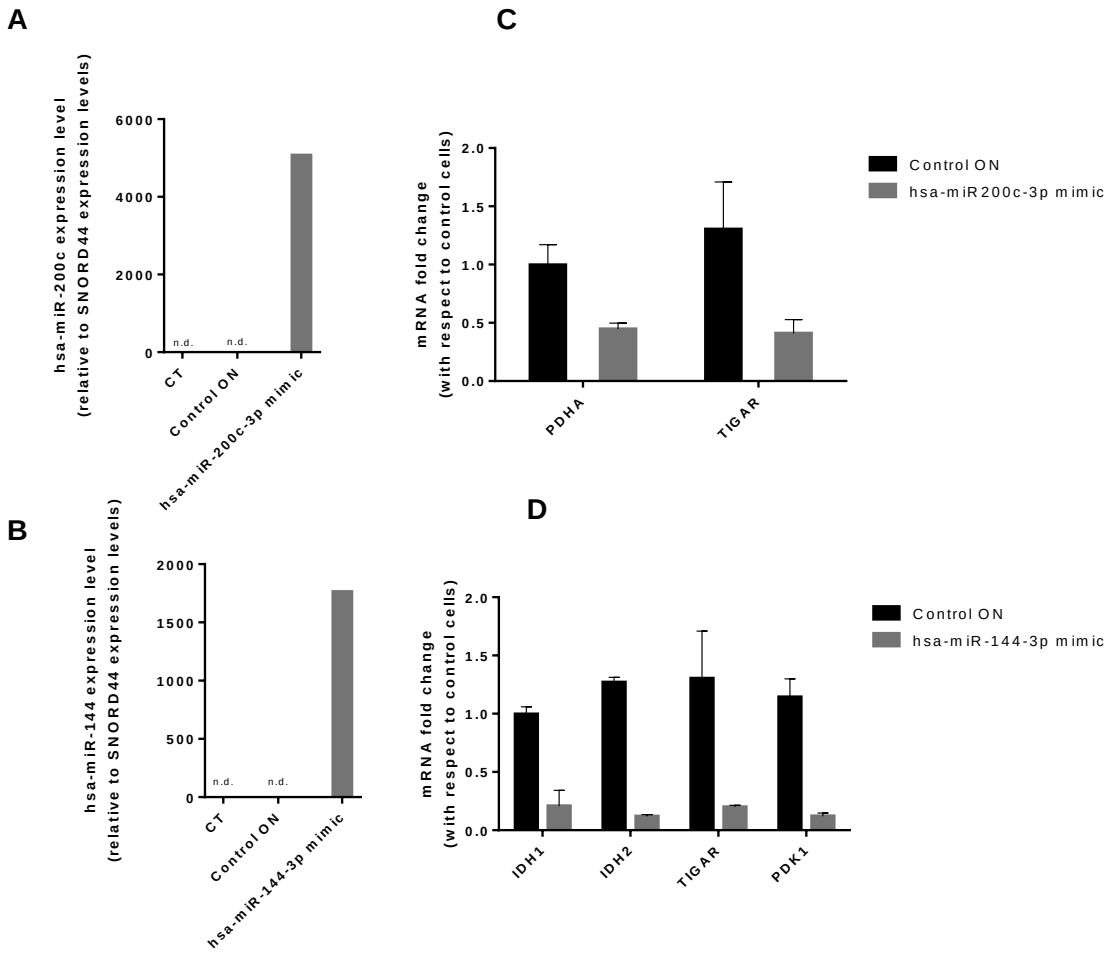

Figure 12. Levels of expression of hsa-miR-200c-3p (A) and hsa-miR-144-3p (B), and of hsa-miR-200c-3p target genes *TIGAR and PDHA 1*(C)and hsa-miR-144-3p target genes *IDH1*, *IDH2*, *TIGAR* and *PDK1*(D) in DBTRG cells after transfection with hsa-miR-200c-3p (A and C) and hsa-miR-144-3p mimics (B and D). Cells were plated onto 12-well plates at a density of $6x10^4$ cells/well. Twenty-four hours after plating, cells were transfected during 4 hours using DLS as a delivery vehicle for either hsa-miR-200c-3p or hsa-miR-144-3p mimics or the control ON. Fold changes in hsa-miR-200c-3p and hsa-miR-144-3p were estimated with respect to Snord44 expression levels by qRT-PCR. Presented data corresponding to a single experiment. The Pfaffl method was used to determine the expression levels of miRNA target genes, as compared to non-transfected cells (CT), normalized to the reference gene HPRT1, being presented as mean ± SD of two independent experiments.

In DBTRG cells transfected with hsa-miR-200c-3p, PDHA1 and TIGAR mRNA expression levels were substantially decreased, when compared with cells transfected with a non-targeting negative control ON (**Fig. 12C**). Similarly, cell transfection with hsa-miR-144-3p mimic, was reflected decreased mRNA expression levels of its target genes *IDH1*, *IDH2*, *TIGAR* and *PDK1* (**Fig. 12D**). Thus, the modulation of hsa-miR-144-3p and hsa-miR-200c-3p shows potential to regulate the levels of mRNA of enzymes involved in energy metabolism.

4.4. Effect of miRNA modulation on GBM cell metabolism

To evaluate the effects of hsa-miR-200c-3p and hsa-miR-144-3p modulation on GBM cell metabolism, the cellular oxygen consumption rate (OCR) and extracellular acidification rate (ECAR) were measured in U87 and DBTRG cells, 72 hours after miRNA modulation, using a XF24 Extracellular Flux Analyzer. As observed in **Figure 13A** and **13B**, no alterations in the non-mitochondrial and mitochondrial basal respiration were detected in U87 cells after miRNA modulation, as deduced by considering the OCR levels after rotenone injection (for non-mitochondrial respiration) and the difference between OCR of resting cells and OCR after rotenone injection (for mitochondrial basal respiration). Furthermore, miRNA modulation did not promote alterations in the FCCP-activated OCR capacity of U87 cells, obtained after FCCP-induced dissipation of the proton gradient across the inner mitochondrial membrane (**Fig. 13B**). In addition, miRNA modulation did not induce alterations in the ATP-coupled respiration, deduced from the difference between OCR of resting cells (cultured in a medium containing glucose) and OCR after oligomycin injection, which inhibits ATP synthesis at complex V. Apparently, the permeability of the inner mitochondrial membrane to protons (proton leak), was not affected by miRNA mimics, since the difference between OCR after oligomycin injection and OCR after rotenone injection was not changed (**Fig. 13A** and **13C**). The basal glycolysis, determined by the difference between ECAR of resting cells (cultured in a medium containing glucose) and ECAR after 2-DG injection, which is an inhibitor of glycolysis, showed to be significantly reduced in U87 cells upon transfection with hsa-miR-200c-3p and hsa-miR-144-3p (**Fig. 14A** and **14B**), as compared with both non-transfected cells and U87 cells transfected with control ON. No alterations, however, were observed in the glycolytic reserve, glycolytic capacity and non-glycolytic acidification upon miRNA modulation, which were calculated as referred in the Materials and Methods. Altogether, these observations did not result in differences on the OCR/ECAR ratio of U87 cells, determined in resting conditions (**Fig. 14C**).

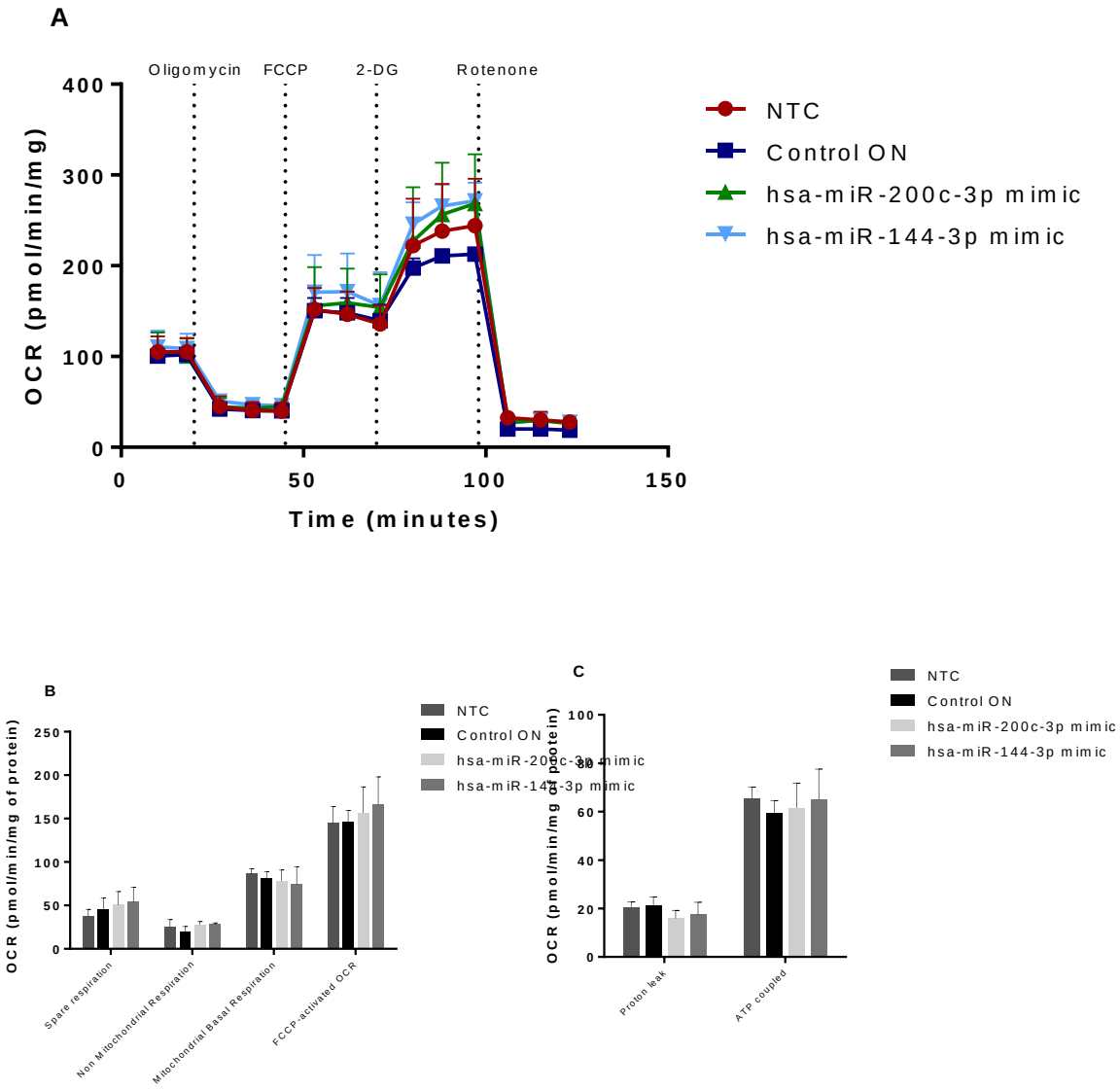

Figure 13. Effect of U87 cell transfection with hsa-miR-200c and hsa-miR-144 on oxygen consumption rate (OCR). U87 cells were plated at a density of 6x10^{3}in an XF24 plate. Twenty-four hours after plating, cells were transfected during 4 hours with hsa-miR-200c-3p, hsa-miR-144-3p or control ON, at a final concentration of 50 nM per well, using DLS as a delivery vehicle. Cells were allowed to grow for 72 hours, and 1h before the assay, the media were replaced with XF24 Assay Media. Oligomycin, FCCP, 2-DG and rotenone were diluted into XF24 media and loaded into the cartridge to achieve final concentrations of 1µM, 0.3 µM, 600 mM and 1µM respectively. (A) OCR profile of U87 cells. (B) Spare respiration, non-mitochondrial respiration, mitochondria basal respiration and FCCP-activated OCR in U87 cells. (C) Proton leak and ATP-coupled respiration in U87 cells. Oxygen consumption rate was monitored using a Seahorse Bioscience XF24 Extracellular Flux Analyzer, and data were normalized to total protein content of each well. Data is presented as mean ± SD of three independent experiments.

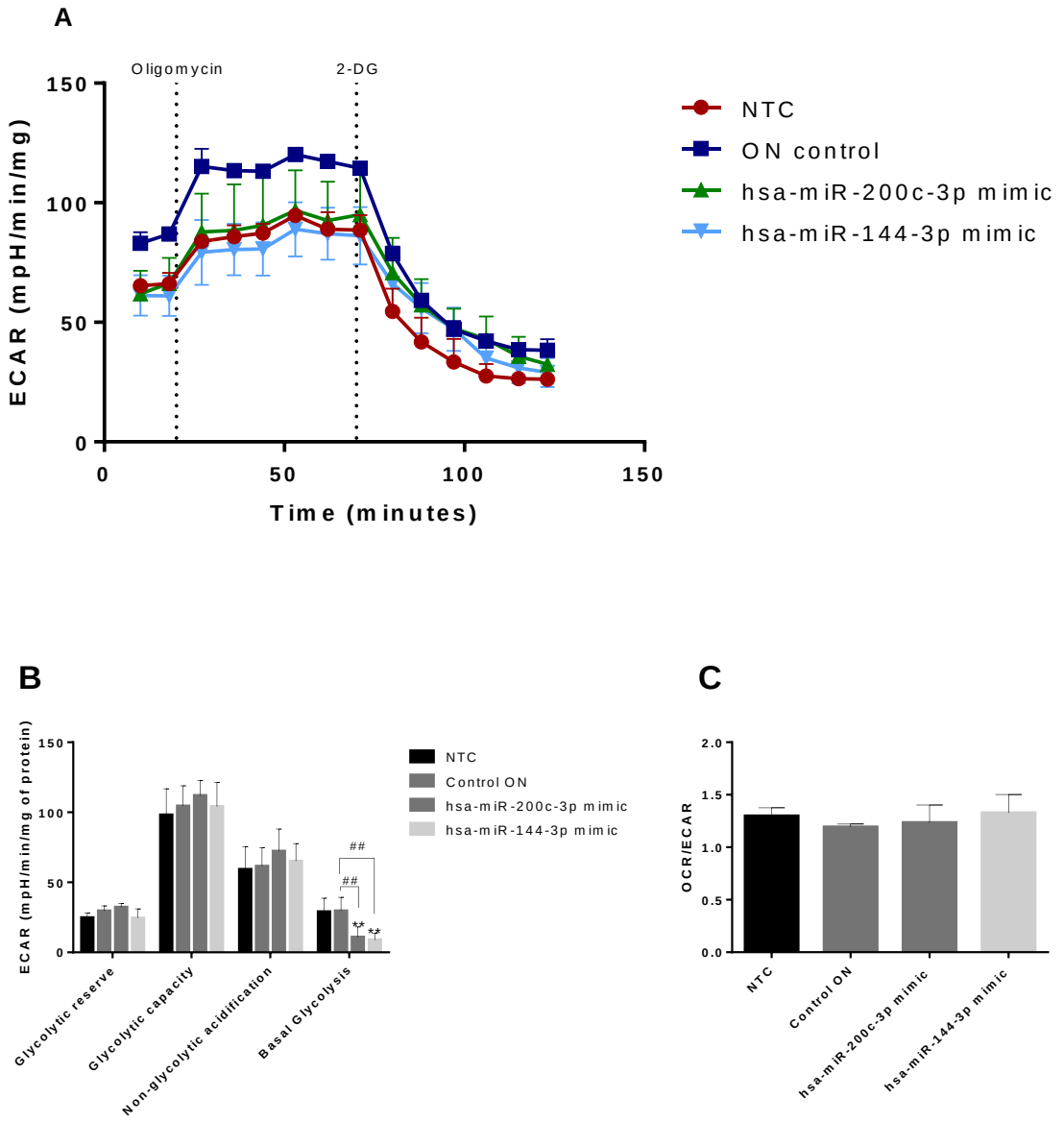

Figure 14. Effect of U87 cell transfection with hsa-miR-200c and hsa-miR-144 on extracellular acidification rate (ECAR). U87 cells were plated at a density of 6x10^{3}in an XF24 plate. Twenty-four hours after plating, cells were transfected during 4 hours with hsa-miR-200c-3p, hsa-miR-144-3p or control ON, at a final concentration of 50 nM per well, using DLS as a delivery vehicle. Cells were allowed to grow for 72 hours, and 1h before the assay, the media were replaced withXF24 Assay Media. Oligomycin, FCCP, 2-DG and Rotenone were diluted into XF24 media and loaded into the cartridge to achieve final concentrations of 1µM, 0.3 µM, 600 mM and 1µM respectively. (A) ECAR profile of U87 cells. (B) Glycolytic reserve, glycolytic capacity, non-glycolytic acidification and basal glycolysis in U87 cells. (C) OCR/ECAR ratio in U87 cells. Extracellular acidification rate was monitored using a Seahorse Bioscience XF24 Extracellular Flux Analyzer, and data were normalized to total protein content of each well. Data is presented as mean ± SD of three independent experiments. Pairwise data comparisons were performed for each parameter between cells transfected with each miRNA mimic and the respective untransfected control (**p<0.001), and between cells transfected with each miRNA mimic and control ON (##p<0.01).

In DBTRG cells, hsa-miR-144-3p and hsa-miR-200c-3p modulation resulted in decreased mitochondrial basal respiration in comparison with non-transfected cells (**Fig. 15A** and **15B),** with consequent decrease of ATP-coupled OCR and proton leak (**Fig. 15C**). Additionally, cell transfection with hsa-miR-200c-3p resulted in a statistical significant decrease in FCCP-activated OCR, in comparison with both non-transfected cells and cells transfected with control ON (**Fig. 15A** and **15B**). MiRNA modulation was accompanied with increased non-mitochondrial respiration, with the modulation of hsa-miR-200c-3p resulting in a more pronounced effect.

Concerning the measurement of ECAR in DBTRG cells (**Fig. 16A** and **16B**), only the modulation of hsa-miR-200c-3p resulted in a slight reduction in basal glycolysis and a statistical significant decrease in both glycolytic reserve and glycolytic capacity (**Fig. 16A** and **16B**), reflecting a small effect on resting cells, but a significant decrease of their ability to use glycolysis under stress conditions, such as those resulting from the inhibition of mitochondrial respiration. In comparison with U87 cells, DBTRG cells exhibited a higher proportion of energy obtained from OXPHOS as deduced by the OCR/ECAR ratios (**Fig. 14C** and **16C).** In these cells the modulation of hsa-miR-144-3p contributes to a decrease in OXPHOS activity (**Fig. 15B**), whereas that of hsa-miR-200c-3p decreases not only OXPHOS (**Fig. 15B** and **15C**) but also the glycolytic capacity (**Fig. 16B**), no significant alterations being observed in OCR/ECAR ratio upon cell transfection with both miRNAs (**Fig. 16C**).

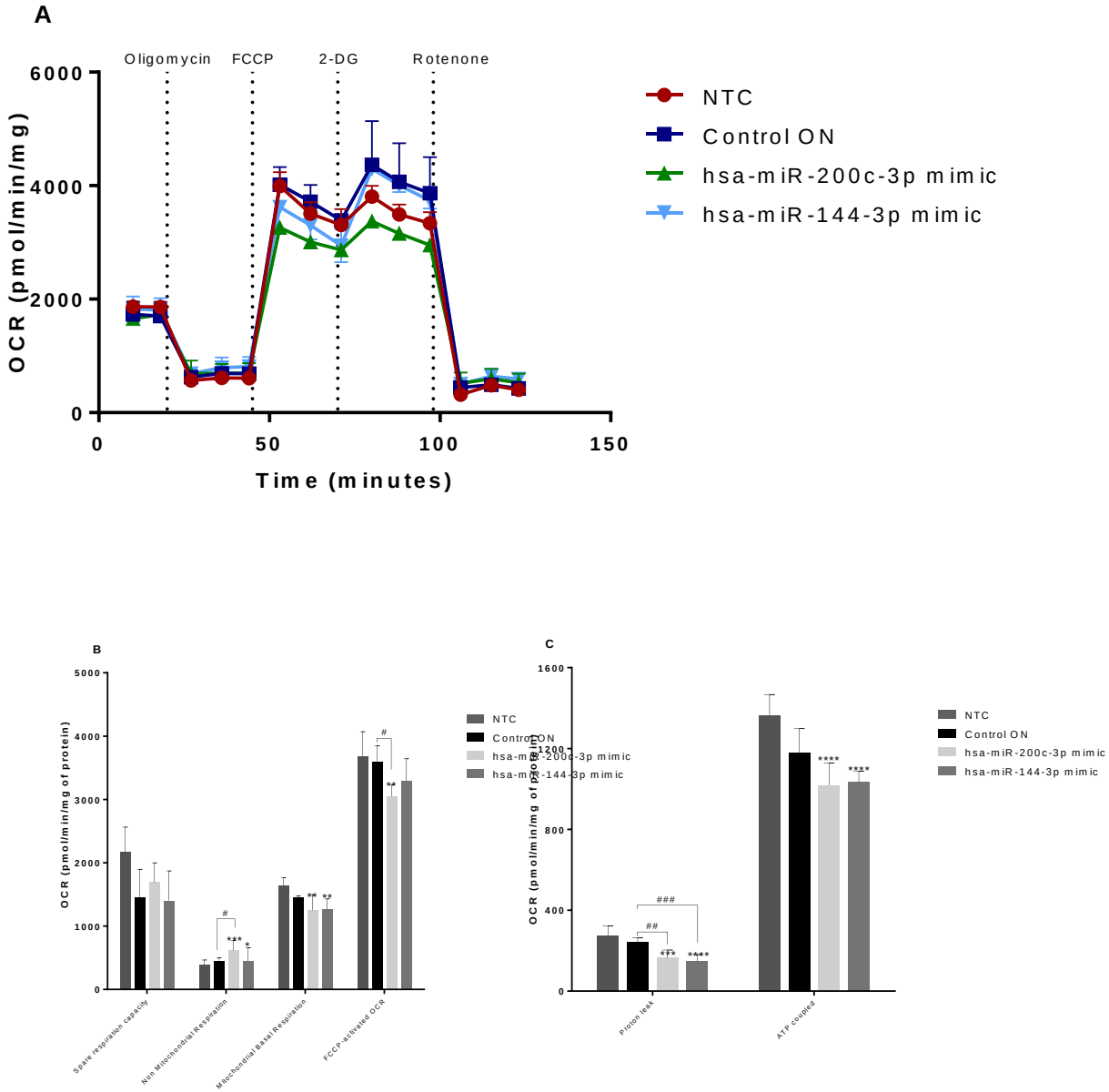

Figure 15. Effect of DBTRG cell transfection with hsa-miR-200c and hsa-miR-144 on oxygen consumption rate (OCR). DBTRG cells were plated at a density of $5x10^3$ in an XF24 plate. Twenty-four hours after plating, cells were transfected during 4 hours with hsa-miR-200c-3p, hsa-miR-144-3p or control ON, at a final concentration of 50 nM per well, using DLS as a delivery vehicle. Cells were allowed to grow for 72 hours, and 1h before the assay, the media were replaced with XF24 Assay Media. Oligomycin, FCCP, 2-DG and Rotenone were diluted into XF24 media and loaded into the cartridge to achieve final concentrations of 1µM, 0.3 µM, 600 mM and 1µM respectively. (A) OCR profile of DBTRG cells. (B) Spare respiration, non-mitochondrial respiration, mitochondria basal respiration and FCCP-activated OCR in DBTRG cells. (C) Proton leak and ATP-coupled respiration in DBTRG cells. Oxygen consumption rate was monitored using a Seahorse Bioscience XF24 Extracellular Flux Analyzer, and data were normalized to total protein content of each well. Data is presented as mean ± SD of three independent experiments. Pairwise comparisons were performed between transfection with each miRNA mimic and the respective untransfected control (*p<0.05, **p<0.01 ***p<0.001, ****p<0.0001), between transfection with each miRNA mimic and ON control (#p<0.01, ##p<0.001, ###p<0.0001).

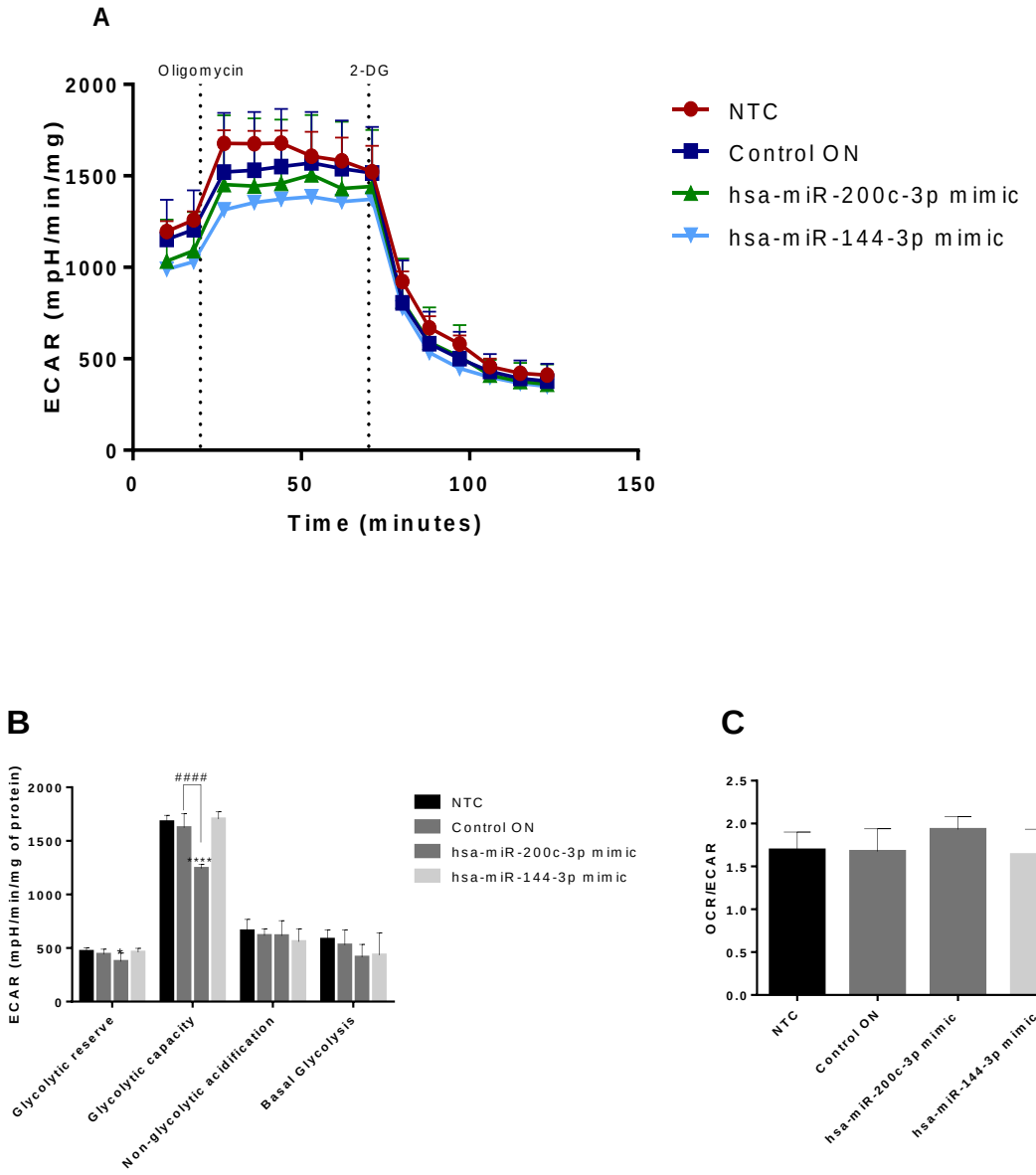

Figure 16. Effect of DBTRG cell transfection with hsa-miR-200c and hsa-miR-144 on extracellular acidification rate (ECAR). DBTRG cells were plated at a density of $5x10^3$ in an XF24 plate. Twenty-four hours after plating, cells were transfected during 4 hours with hsa-miR-200c-3p, hsa-miR-144-3p or control ON, at a final concentration of 50 nM per well, using DLS as a delivery vehicle. Cells were allowed to grow for 72 hours, and 1h before the assay, the media were replaced with XF24 Assay Media. Oligomycin, FCCP, 2-DG and Rotenone were diluted into XF24 media and loaded into the cartridge to achieve final concentrations of 1µM, 0.3 µM, 600 mM and 1µM respectively. (A) ECAR profile of DBTRG cells. (B) Glycolytic reserve, glycolytic capacity, non-glycolytic acidification and basal glycolysis in DBTRG cells. (C) OCR/ECAR ratio in DBTRG cells. Extracellular acidification rate was monitored using a Seahorse Bioscience XF24 Extracellular Flux Analyzer, and data were normalized to total protein content of each well. Data is presented as mean ± SD of three independent experiments. Pairwise comparisons were performed between transfection with each miRNA mimic and the respective untransfected control (*p<0.05, ****p<0.0001), between transfection with each miRNA mimic and ON control (####p<0.0001).

The metabolic activity of DBTRG cells (Fig.8) showed to be significantly higher than that of U87 cells, regarding either mitochondrial respiration (as deduced from the OCR in resting cells) or glycolysis (as deduced from the ECAR in resting cells) (**Fig. 17**).

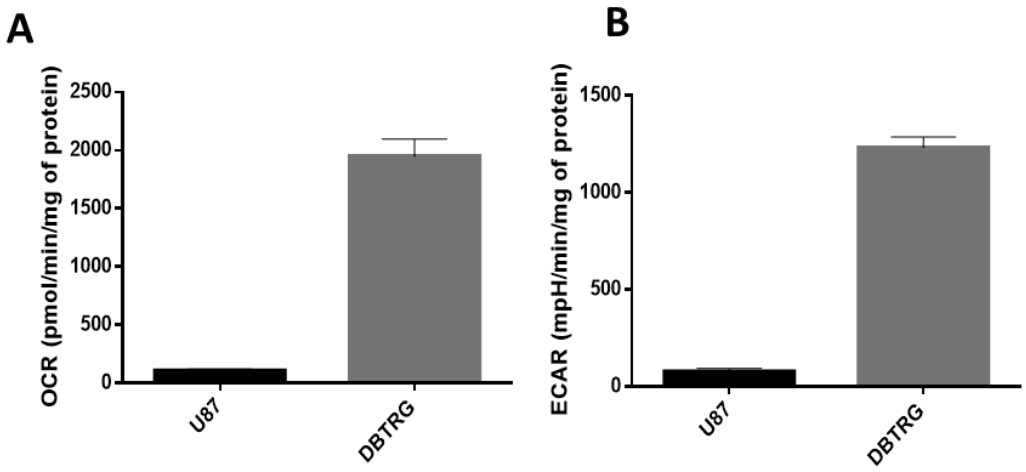

Figure 17. Metabolic activity of U87 and DBTRG cells in terms of (A) oxygen consumption rate (OCR) and (B) extracellular acidification rate (ECAR). U87 and DBTRG cells were plated at a density of $6x10^3$ and $5x10^3$ in an XF24 plate. Twenty-four hours after plating, cells were transfected during 4 hours with hsa-miR-200c-3p, hsa-miR-144-3p or the control ON at a final concentration of 50 nM per well, using DLS as a delivery vehicle. Cells were allowed to grow for 72 hours, and 1h before the assay, the media were exchanged for XF24 Assay Media. Oxygen consumption and extracellular acidification rates were monitored using a Seahorse Bioscience XF24 Extracellular Flux Analyzer, and data were normalized to total protein content of each well. Data is presented as mean ± SD of three independent experiments. OCR and ECAR values correspond to the baseline oxygen consumption and extracellular acidification of cells in resting state.

4.5. Effect of miRNA modulation on GBM cells migration

In order to determine the outcome of miRNA modulation in GBM cell migration capacity, DBTRG cells were transfected with control oligonucleotide (ON), hsa-miR-144-3p and hsa-miR-200c-3p mimics and their migratory phenotype assessed using the chemotaxis assay. Forty-eight hours after transfection, DBTRG cells were harvested and plated onto a u-Slide Chemotaxis plates (Ibidi) in the presence of a gradient of EGF as chemoattractant. DBTRG migratory capacity was evaluated over a 14 hours period with photographs taken every 5 minutes. Cell trajectory was determined using appropriate software and center of mass, FMI^{II}, cell velocity and directness are displayed in **Figure 18**. The center of mass (**Fig.18A**) is a strong parameter for chemotaxis evaluation and represents the spatial averaged endpoint of cells. DBTRG control cells (non-transfected cells), showed a tendency for migrating towards the EGF highest concentration, which corresponds to the negative values of the displacement of the center of mass. Cell transfection with the control ON did not alter the ability of cells to migrate. On the contrary, transfection of DBTRG cells with hsa-miR-144-3p mimic resulted in an average endpoint value close to zero, indicating decreased cell migration capacity. However, no significant difference in cell center of mass was observed in DBTRG cells transfected with hsa-miR-200c-3p mimic. The forward migration index parallel to the gradient, FMI^{II}, represents the efficiency of the forward migration of cells, a strong chemotactic effect corresponding to a large FMI^{II} index (**Fig. 18B**). This effect was not observed upon transfection with the ON control, but transfection with hsa-miR-200c-3p mimic resulted in FMI^{II} values significantly closer to zero, indicating a lower capacity for cell migration. Regarding the directness parameter, which characterizes the straightness of migration, being therefore an indirect parameter for chemotaxis analysis, no significant differences were detected among the experimental conditions assayed (**Fig.18C**). Significant differences in DBTRG cell migration velocity were found after transfection with both miRNA mimics, as compared with control cells as well as with cells transfected with ON control (**Fig.18D**). The migration data point to a small effect of miRNA transfection on the chemotaxis parameters, and to a significant impairment of the mobility of cells, as indicated by their slowest migration towards EGF.

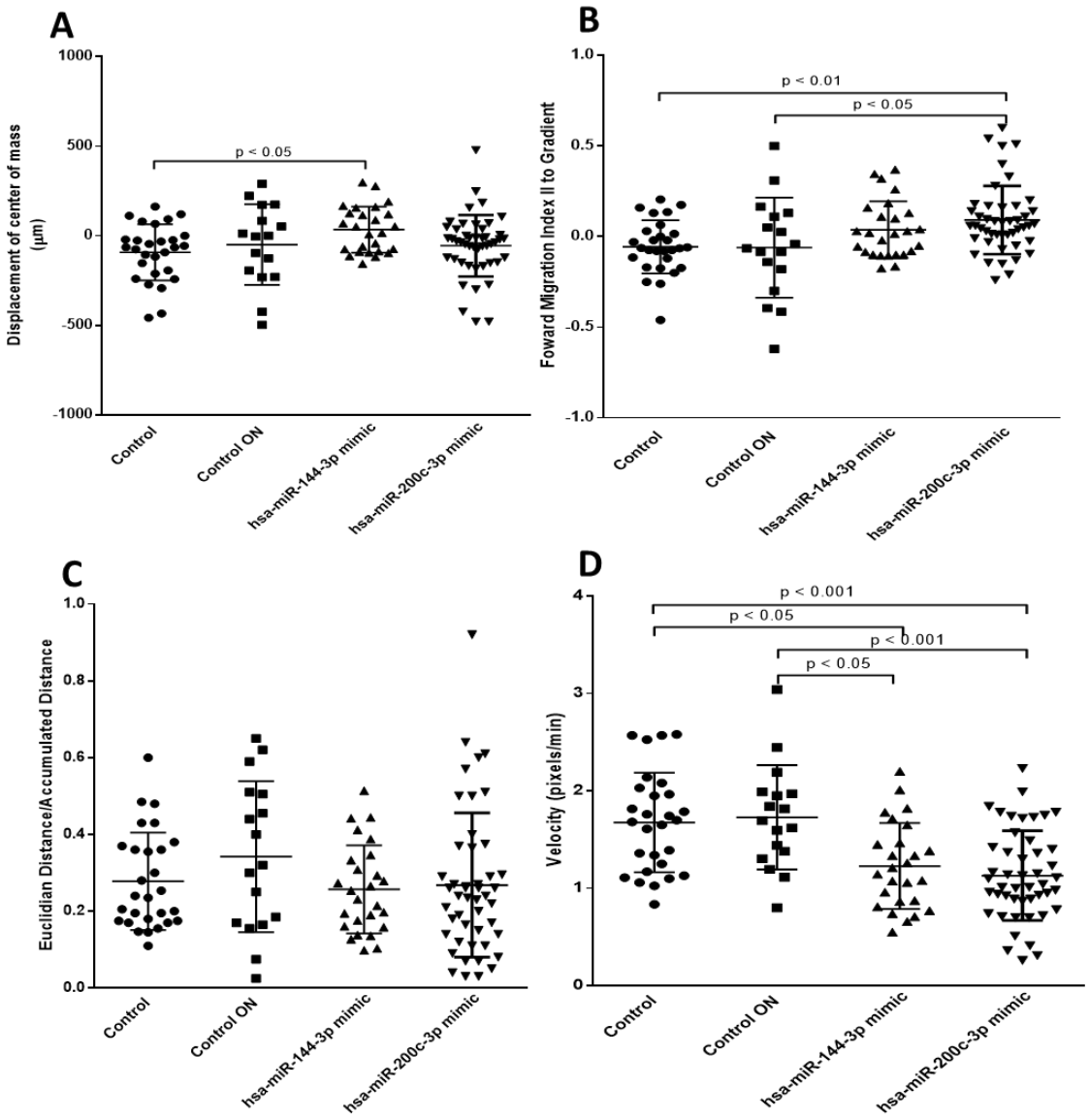

Figure 18. Effect of hsa-miR-200c-3p and hsa-miR-144-3p transfection on DBTRG cell line migration. Twenty-four hours after plating in 12-well plates, DBTRG cells were transfected either with hsa-miR-200c-3p, hsa-miR-144-3p mimics or the ON control. Forty-eight hours after transfection cells were transferred to a u-Slide Chemotaxis (Ibidi) for migratory capacity assessment and exposed to an EGF gradient for 14hwith photographs taken every 5 minutes, using aCarl Zeiss Axio Observer Z1 microscope with a Plan-Apocromat 20x/0.8 air objective and CCD digital camera (AxiocamHRm), equipped with an incubator at 37°C and 5% CO_2. The displacement of center of mass (A), the forward migration index parallel to the gradient (FMI II) (B), cell directionality (C) and cell velocity (D) were analysed using Image J and the Chemotaxis and Migration tool from Ibidi.

4.6. Determination of DCA cytotoxic profile

To fulfil our goal of designing an efficient therapeutic approach combining miRNA modulation and chemotherapy, DCA cytotoxicity was evaluated. In order to infer the concentration at which DCA reduces cell density by 20%, allowing a more reliable detection of the drug effects *per se* or in combination with miRNA modulation in subsequent studies, U87 and DBTRG cells were exposed to different drug concentrations for 24, 48 or 72 hours, and cell density was evaluated using the SRB assay. Thereafter, dose-response curves were plotted for each incubation period and the DCA concentrations of 20 mM and 40 mM were selected for the subsequent studies in U87 and DBTRG, respectively (**Fig. 19**), since incubation with these concentrations resulted in a decrease in cell density of approximately 20% at 48 h post-treatment. A concentration of 400 µM of TMZ was previously found in our laboratory to reduce cell density by 20%, being therefore used in the present study.

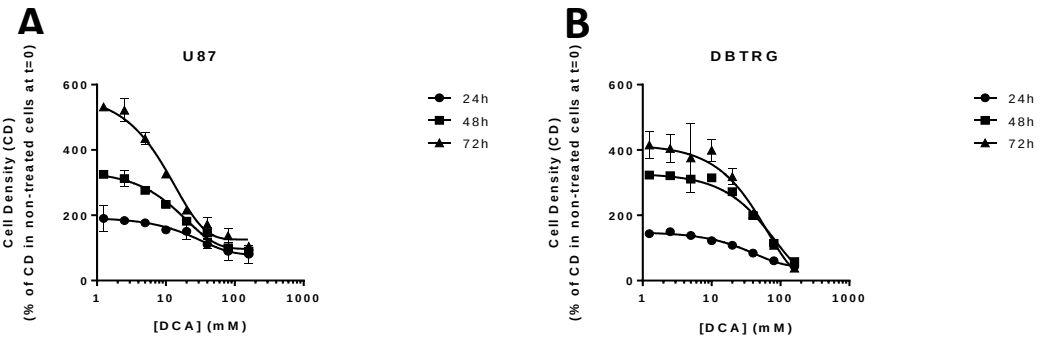

Figure 19. Effect of DCA on U87 (A) and DBTRG (B) cell density. Forty-four hours after plating on 96-well plates, U87 and DBTRG cells were exposed to increasing concentrations of DCA for 24, 48 and 72 hours, after which cells were fixed with 1% acetic acid in methanol and stored at -80 ºC after which the SRB assay was performed. The results are presented as a percentage of the control, non-treated cells at the timepoint t=0 taken as 100%, corresponding to the moment immediately before cell incubation with DCA, treated for 24h ( ). 48h ( ) and 72h ( )and represent the mean ± SD from three independent experiments.

4.7. Effect of the miRNA modulation combined with chemotherapy on GBM cell density

The effects on cell modulation of modulation of each miRNA, incubation with TMZ or DCA, or the combined treatment consisting of miRNA modulation followed by cell incubation with each of the drugs were evaluated using the SRB assay (**Fig.20**). In U87 cells, transfection with hsa-miR-200c-3p or hsa-miR-144-3p did not result in significant decrease of cell density, when comparing with cells transfected with non-targeting control ON and

non-transfected cells. As expected, both DCA and TMZ at the selected concentrations, decreased U87 cell density in 20%. Transfection with either miRNA mimic combined with DCA or TMZ did not result in any further decrease in cell density in these cells (**Fig.20A**). Regarding DBTRG cells, a significant decrease in cell density was achieved upon transfection with hsa-miR-200c-3p or hsa-miR-144-3p mimics, in contrast with what was observed in cells incubated with the control ON. Additionally, cell transfection with hsa-miR-144-3p mimic combined with DCA treatment resulted in a significant decrease of cell density, in comparison with DCA treatment and miRNA modulation *per se* (**Fig. 20B**).

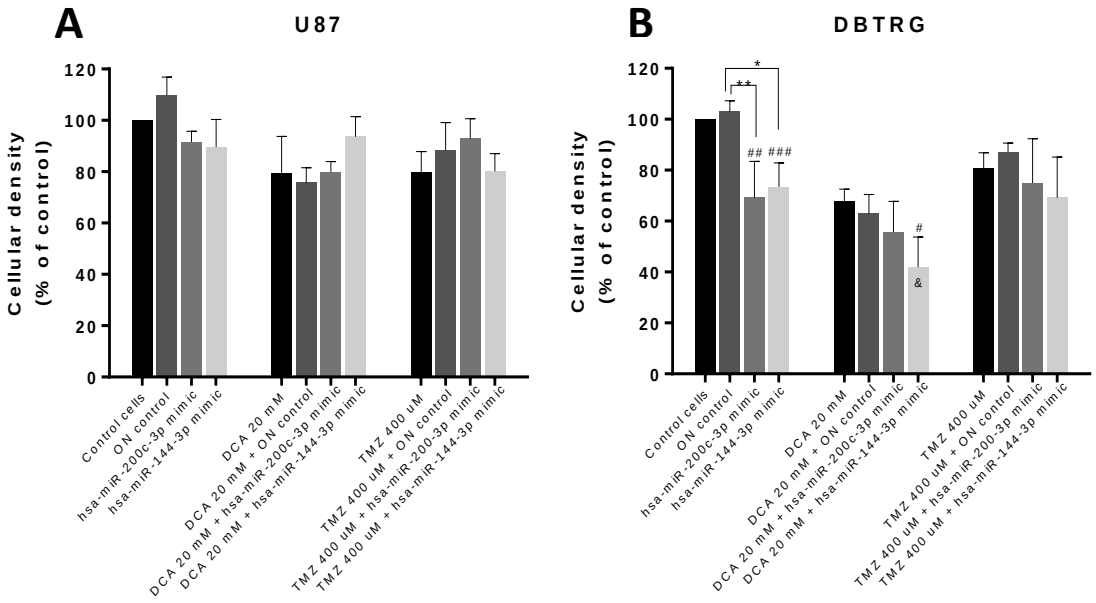

Figure 20. Effect of DCA and TMZ, either per se or in combination with transfection withhsa-miR-200c-3p, hsa-miR-144-3p or non-targeting ON control on U87 (a) and DBTRG (b)determined for the combined effects on cell density of hsa-miR-144-3p and ON control transfection plus treatment with DCA. Cells were seededonto 96-well plates at a density of $5x10^3$ cells/well. Twenty-four hours after plating, cells were transfected during 4 hours using DLS as a delivery vehicle for hsa-miR-200c-3p, hsa-miR-144-3p and ON control. Twenty-hours after transfection, cells were exposed to TMZ or DCA for 48 h. Subsequently, cellswere fixed with 1% acetic acid in methanol and stored at -80ºC, after which the SRB assay was performed. Pairwise comparisons were performed between density of cells transfected with each miRNA mimic and the ON control (*p<0.05, **p<0.01), with each miRNA mimic and the respective untransfected control (## p<0.01, ### p<0.001) and between the combined treatment and the miRNA modulation *per se*(&p<0.05).

4.8. Effect of miRNA modulation combined with chemotherapeutic on GBM cell cycle

To evaluate whether the decrease in cell density would associated with alterations in the cell cycle progression, U87 and DBTRG cells, submitted to the different treatments, were analysed by flow cytometry in terms of cell cycle. Approximately 60% of U87 cells and 70 % of DBTRG cells were in G0/G1 phase under control conditions. The remaining percentage of U87 cells were distributed evenly between S and G2/M phases (**Fig. 21A**), whereas the remaining DBTRG cells were mostly in the S phase (25%), with only a residual fraction of the cells in the G2/M phase (**Fig 21B**). As observed in the quantitative analysis, no significant alterations were observed in U87 or DBTRG cells transfected with the control ON, as compared with non-transfected cells (**Fig. 21A** and **21B**). Cell transfection with hsa-miR-144-3p mimics did not result in alteration in U87 cell cycle (**Fig. 21A**) but increased the percentage of DBTRG cells in the G2/M phase (**Fig. 21B**). On the other hand, upon transfection with hsa-miR-200c-3p mimics, the percentage of both U87 and DBTRG cells in G0/G1 phase diminished, being this decrease accompanied with an increased percentage of cells in S phase for DBTRG cells (**Fig. 21A** and **21B**). Regarding the action of the chemotherapeutics *per se*, TMZ resulted in U87 cell cycle arrest in G2/M phase at the expense of cells in G0/G1 phase (**Fig. 22A**), and in DBTRG cell cycle arrest in S phase with concomitant decrease of the percentage of cells in G0/G1 phase (**Fig. 22B**). On the other hand, DCA decreased the percentage of cells in S phase in both cell lines, while increasing G0/G1 in U87 and G0/G1 and G2/M in DBTRG cells (**Fig. 23A** and **23B**). In cells treated both with miRNA mimics and chemotherapeutic agents, the modulation of hsa-miR-144 did not reinforce TMZ or DCA effect on the cycle progression of either cell line (**Fig. 22** and **23**). Interestingly, transfection of U87 cells with hsa-miR-200c-3p mimics, combined with DCA treatment, promoted a shift from G0/G1 phase to G2/M phase with respect to drug treatment *per se* (**Fig.23A**). A strong combinatory effect was found for DBTRG cells transfected with hsa-miR-200c mimics and incubated with TMZ, being observed a reinforced effect of the drug *per se* in arresting the cells in the S phase, with complete ablation of progression to G2/M phase (**Fig.21B**). Despite the significant effects of miRNA modulation and drug incubation observed on cell cycle progression, such effects do not fully explain cell density alterations (**Fig. 20A** and **20B**).

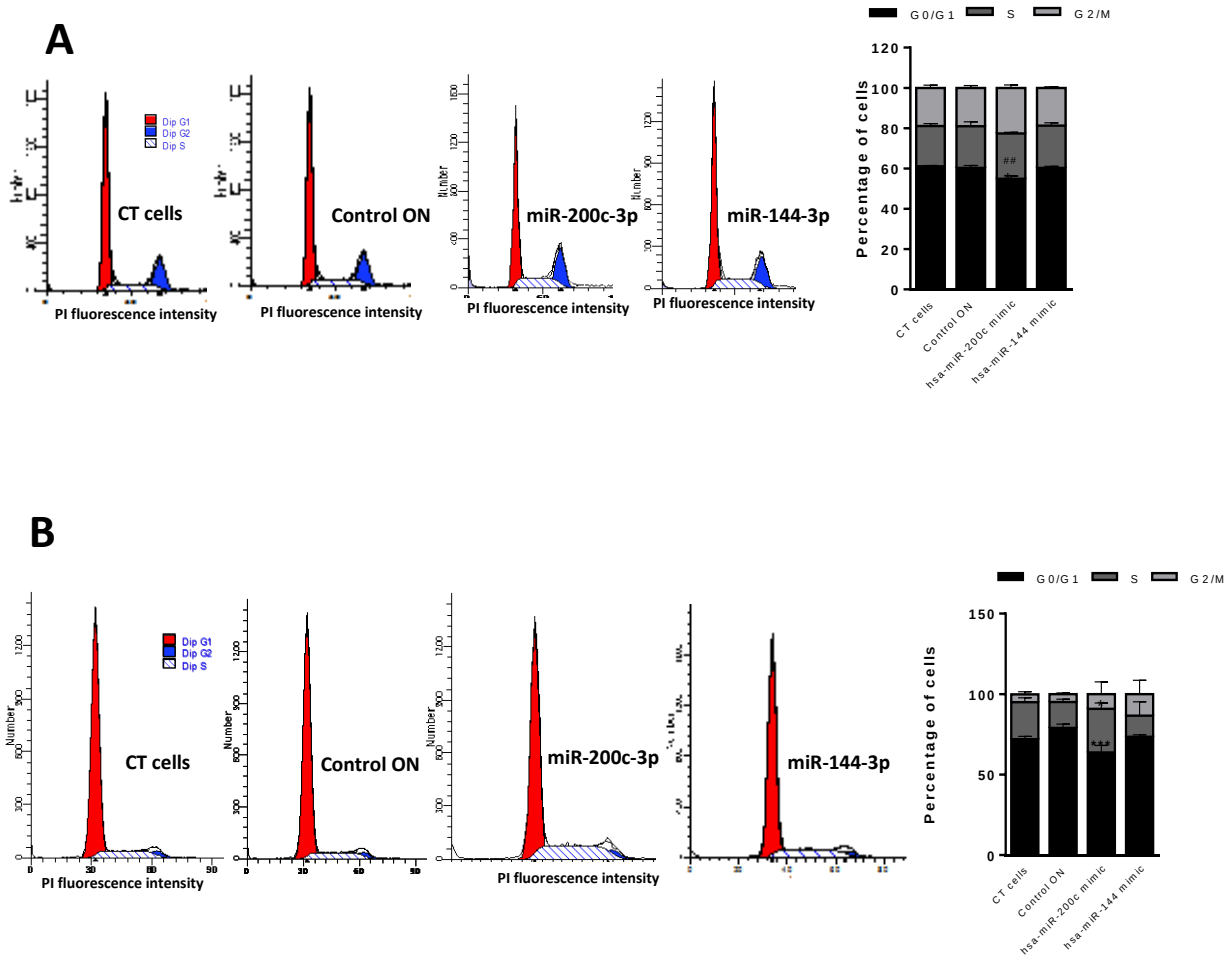

Figure 21. Effect of transfection with hsa-miR-200c-3p or hsa-miR-144-3p on cell cycle. The quantitative analyses and percentage of cells in G0/G1, S and G2/M phases of U87 and DBTRG are displayed in (A) and (B) respectively. Twenty-four hours after U87 and DBTRG cell transfection with hsa-miR-200c-3p, hsa-miR-144-3p or ON control at a final concentration of 50 nM per well using DLS, as vehicle. Cells were fixed and permeabilized with ethanol 70% and thereafter incubated with PI/RNase solution for 15 minutes. Pairwise comparisons were performed for the percentage of cells in each phase of the cell cycle between cells transfected with each miRNA mimic and the respective untransfected control (#p<0.05, ##p<0.01 ###p<0.001, ####p<0.0001), between cells transfected with each miRNA mimic and the ON control (*p<0.05, ***p<0.001, ****p<0.0001).

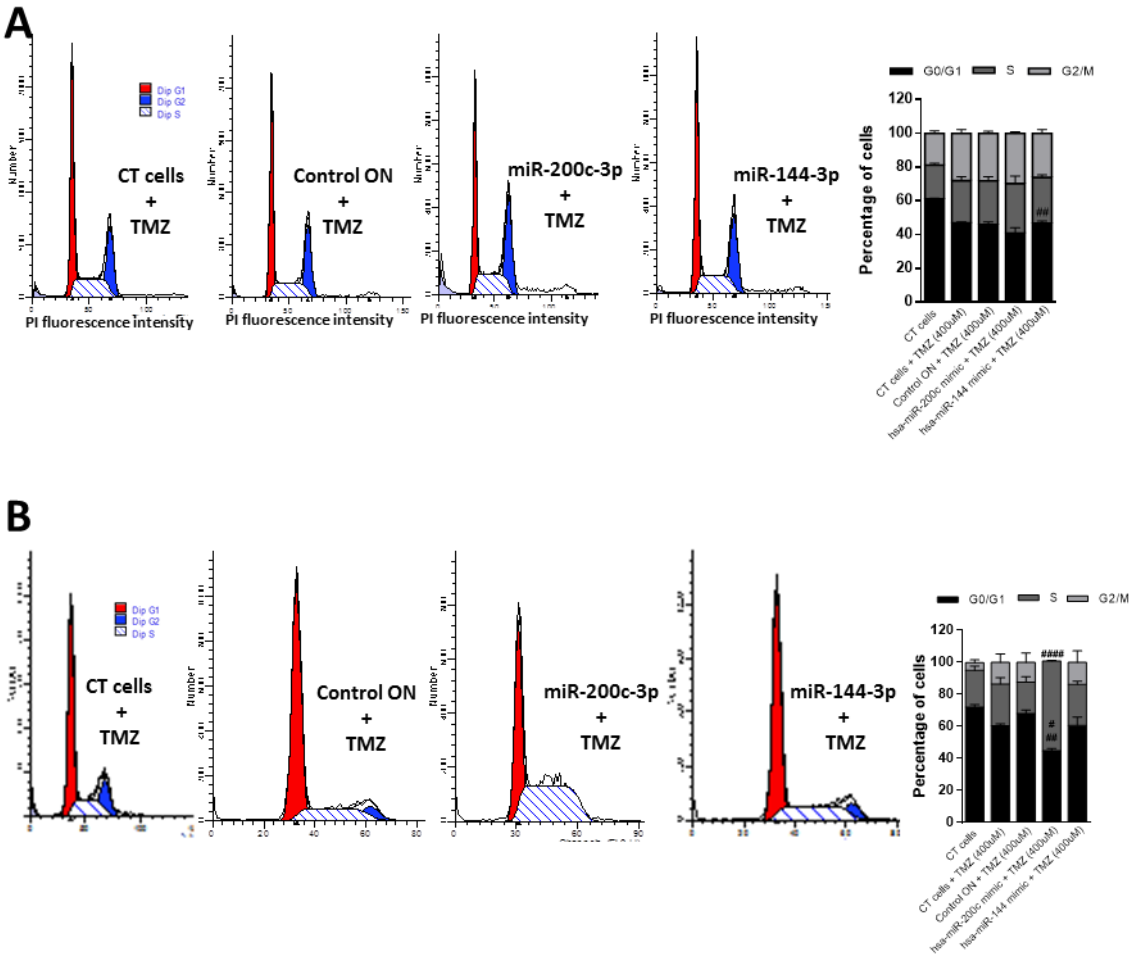

Figure 22. Effect of transfection with hsa-miR-200c-3p or hsa-miR-144-3p, and incubation with the chemotherapeutic TMZ on cell cycle. The quantitative analyses and percentage of cells in G0/G1, S and G2/M phases of U87 and DBTRG are displayed in (A) and (B) respectively. Twenty-four hours after U87 and DBTRG cell transfection with hsa-miR-200c-3p, hsa-miR-144-3p or ON control at a final concentration of 50 nM per well using DLS, as vehicle. Cells were incubated with 400 μM TMZ (U87 and DBTRG cells) for 48 hours. Cells were fixed and permeabilized with ethanol 70% and thereafter incubated with PI/RNase solution for 15 minutes. Pairwise comparisons were performed for the percentage of cells in each phase of the cell cycle between cells transfected with each miRNA mimic and the respective untransfected control (#p<0.05, ##p<0.01 ###p<0.001, ####p<0.0001), between cells transfected with each miRNA mimic and the ON control (*p<0.05, ***p<0.001, ****p<0.0001) and between cells subjected to the combined treatment and the treatment with each chemotherapeutic *per se*(§§p<0.01).

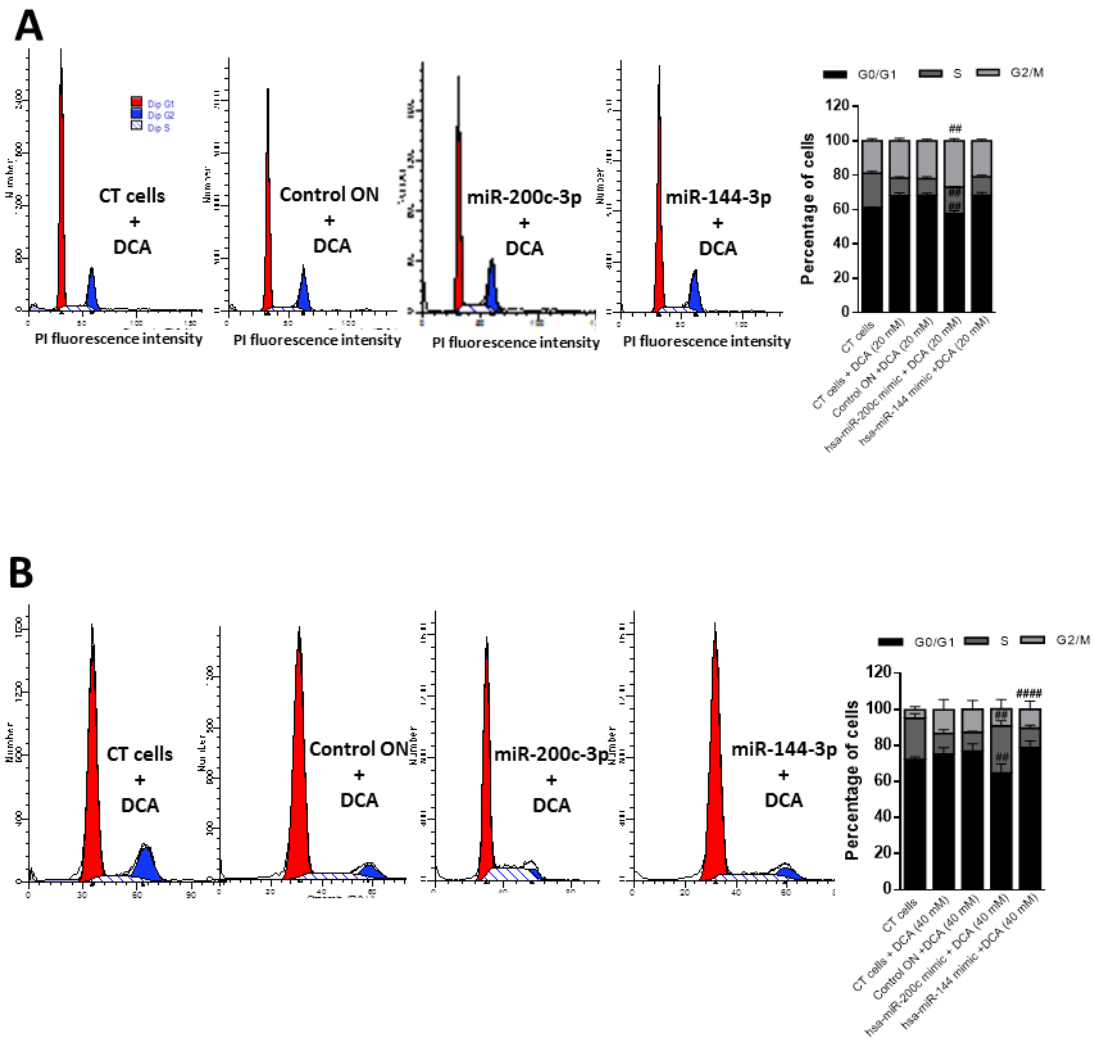

Figure 23. Effect of transfection with hsa-miR-200c-3p or hsa-miR-144-3p, and incubation with the chemotherapeutic DCA on cell cycle. The quantitative analyses and percentage of cells in G0/G1, S and G2/M phases of U87 and DBTRG are displayed in (A) and (B) respectively. Twenty-four hours after U87 and DBTRG cell transfection with hsa-miR-200c-3p, hsa-miR-144-3p or ON control at a final concentration of 50 nM per well using DLS, as vehicle. Cells were incubated with 20 mM (U87) and 40 mM (DBTRG) DCA (for 48 hours. Cells were fixed and permeabilized with ethanol 70% and thereafter incubated with PI/RNase solution for 15 minutes. Pairwise comparisons were performed for the percentage of cells in each phase of the cell cycle between cells transfected with each miRNA mimic and the respective untransfected control (#p<0.05, ##p<0.01 ###p<0.001, ####p<0.0001), between cells transfected with each miRNA mimic and the ON control (*p<0.05, ***p<0.001, ****p<0.0001) and between cells subjected to the combined treatment and the treatment with each chemotherapeutic *per se*(§§p<0.01).

5 Discussion

The major therapeutic challenge of GBM relies on its particular location, which renders this type of tumours extremely difficult to remove without causing severe damage to the patient. The infiltrative nature of GBM cells further enhances this difficulty, due to the formation of a peritumoural region which comprises both tumour and normal brain cells. In parallel, the extremely fast growth rate of GBM cells and almost certain relapse after tumour excision are features that contribute to the extremely low survival rate after GBM diagnosis[15]. All these characteristics should be accounted for in the design of a suitable therapeutic approach to tackle GBM. One of the hallmarks of cancer that can be targeted as a means to achieve an overall decrease in all cancer cell functions is the energy metabolism. In fact, metabolic profiles of cancer cells have long been described as abnormal, and GBM cells are no exception[28,157]. Several studies have shown that GBM cells rely extensively on glycolysis, rather than on OXPHOS, for energy production, and that this metabolic shift can contribute to the fostering of anabolic pathways required for cell division and proliferation. On the other hand, the glycolytic pathway leading to the production of lactate favours an acidification of the extracellular environment, which contributes to the degradation of the extracellular matrix and facilitates tumour cell migration and invasion into the adjacent healthy tissues[158,159].

Due to the heterogeneity of tumour cells and complexity of tumoral processes, a therapeutic approach based on a single target can be less than efficient. In fact, targeting more than one molecule or process can result in a therapeutic benefit larger than the mere sum of the individual effects, due to the interconnection of cellular pathways. In this sense, miRNAs are extremely versatile regulatory elements, each miRNA having hundreds of different possible molecular targets in each cell type. The potential of miRNA modulation to induce alterations in multiple hallmarks of cancer configures an advantage, which this work aimed to combine with GBM cell exposure to chemotherapeutic drugs, in order to achieve a favourable therapeutic outcome.

A number of studies have characterized GBM tumours in terms of their dysregulated miRNAs[90]. However, due to the molecular heterogeneity of GBM cells, these profiles can vary depending on the tumour of origin. Thus, a confirmation that the miRNAs under study were differentially expressed in the GBM cell lines used herein was conducted with respect to astrocytes. The miRNAs selected for this screening were those that fulfilled two requirements: 1) to be described as dysregulated in GBM tumour cells and 2) to be predicted to target key enzymes of the energy metabolism of cells.

Regarding the evaluation of miRNA expression levels in two GBM cell lines, U87 and DBTRG, hsa-miR-23a was found to be overexpressed, whereas hsa-miR-200c and hsa-miR-144 were found to be underexpressed with respect to human astrocytes (**Fig. 10**), which is

consistent with the literature [152–156]. On the other hand, although according to previous studies[152,156] hsa-miR-155, hsa-miR-19a and hsa-miR-183 were expected to be upregulated, they were found to be expressed in lower levels in U87 and DBTRG cells than in normal astrocytes (**Fig. 10**). In this regard, it is important to refer that the previous studies involving the quantification of these miRNAs were performed in tumour tissue as compared with normal brain tissue, which contains several different types of cells, including neurons, olygodendrocytes and microglia, thus masking the astrocyte miRNA expression pattern. On the other hand, HA in culture may acquire a different miRNA expression pattern than that presented in their physiological milieu. Two miRNAs whose expression was almost completely ablated in the tested GBM cells, hsa-miR-200c and hsa-miR-144, were selected to perform the miRNA modulation studies, since the increase of their levels would be expected to produce the most relevant results.

Hsa-miR-200c was already identified, in *in vitro* studies, as an intervenient in migration and invasion processes, not only in GBM, but also in non-small cell lung cancer[160] and breast cancer[161]. Although this miRNA is predicted to target a series of metabolic enzymes (HK2, IDH1, TIGAR, PDHA1, LDHA, PFKP), to the best of our knowledge its role in cell metabolism was not yet established. In contrast, hsa-miR-144 has been reported to mediate a metabolic shift in ovarian cancer cells, by directly targeting GLUT1[162]. In addition, PDK1, ALDOB, PGAM1, TIGAR, IDH1 and IDH2 are among the predicted targets of hsa-miR-144-3p. This miRNA has been shown to inhibit cell proliferation by targeting EZH2 and mTOR in bladder cancer and renal cell carcinoma[163,164], and to inhibit proliferation and enhance apoptosis and autophagy of lung cancer cells[165].

The mRNA levels of the predicted targets of hsa-miR-200c and hsa-miR-144 from the bioenergetics pathways were also evaluated in both GBM cell lines and compared with the normal astrocyte levels. In particular, the levels of mRNA of *TIGAR*, *PDK1, IDH1*, *IDH2*, and *PDHA1* were evaluated in those GBM cell lines and compared with HA. Both GBM cell lines showed to be enriched in mRNA of *TIGAR, PDHA1* and *PDK1*, the latter being more overexpressed in DBTRG than in U87 cells (**Fig. 11**). The higher levels of expression of PDK1 observed in DBTRG as compared with U87 cells could be related with the fact that DBTRG cells were obtained from a patient who had been submitted to cycles of chemo- and radiotherapy and, thus, this cell type is expected to display higher prevalence of resistance mechanisms, including control of ROS production. Lactate, resulting from glycolytic activity, has been described as a scavenger of ROS[166], and its ability to neutralize the effects of ionizing radiation, administered with the purpose of inducing tumour cells' DNA/RNA damage, was attributed to these antioxidant properties[167]. Furthermore, even though the levels of IDH2 in GBM cells were found to be lower than those in HA, a differential

expression between DBTRG and U87 cells could also be observed (**Fig. 11**). In fact, IDH2 expression in DBTRG cells was ca. twice as high as that in U87, which could be related with the pivotal role played by IDH2 in NADPH production, necessary for NADPH-dependent antioxidant enzymes. Thus, DBTRG cells would be able to maintain a more balanced mitochondrial redox status than U87cells, which could prevent oxidative stress-induced cell injury[168]. Thus, the higher glycolytic activity of DBTRG as compared with U87 cells (**Fig. 17**), would result in the production of higher amount of ROS scavengers, which could counteract the extensive production of ROS associated with higher mitochondrial activity (reviewed in Adam-Vizi V. et al Chinopoulos)[169].

Due to the significant contribution of metabolic reprogramming to GBM therapy resistance, as well as to proliferation and migration ability, modulation of metabolic activity appears as a promising strategy to address GBM treatment. Thus, U87 and DBTRG cells were transfected with mimics of two miRNAs whose target mRNAs include enzymes involved in that activity. GBM cell transfection with hsa-miR-200c and hsa-miR-144 mimics resulted in alterations of the mRNAs of their target enzymes without significant unspecific effects (**Fig. 12**). Thus, although no conventional validation method was used to assess whether each of the mRNAs was a direct target of the miRNAs, it is interesting to observe that miRNA and mRNA levels are inversely correlated.

GBM cell transfection with the purpose of increasing the levels of hsa-miR-144 and hsa-miR-200c resulted in larger alterations of the mitochondrial metabolic profile of DBTRG cells, as compared to that of U87 cells. In fact, no differences were found in U87 mitochondrial activity after transfection with miR-144 or miR-200c mimics, with respect to control cells, as reflected by OCR measurements and calculated respiratory parameters (**Fig. 13A-C**), while DBTRG cells were susceptible to OCR alterations upon transfection with either miRNA. Thus, increased levels of hsa-miR-144 in DBTRG cells led to decreased mitochondrial basal respiration, which resulted from a decrease of both ATP-coupled respiration and proton leak (**Fig. 15A-C**). The slower rate of mitochondrial electron transport chain observed after cell transfection with hsa-miR-144 could be a consequence of the dowregulation of IDH2, which is responsible for α-ketoglutarate production, accompanied by NADH generation, which is necessary for OXPHOS. In fact, Shin and collaborators demonstrated that IDH2 inactivation resulted in increased production of ROS and, consequently, in major alterations in mitochondrial membrane integrity and in oxidative DNA damage[168]. Furthermore, hsa-miR-144 overexpression was previously found to affect the cellular response to oxidative stress through its target nuclear factor erytroid 2-related factor 2 (NRF2), which is necessary for glutathione regeneration[170].

Overexpression of hsa-miR-200c resulted in an even more extensive alteration of OCR in DBTRG cells. Besides decreasing mitochondrial basal respiration, similarly to hsa-miR-144, overexpression of hsa-miR-200c also reduced FCCP-activated OCR. PDHA1 enzyme emerges as the most likely hsa-miR-200c target that contributes to the observed effects, due to its role as a linker between glycolysis and TCA. Disturbance of the conversion of pyruvate to acetyl-CoA through the modulation of the levels of this key enzyme decreases the fuelling of the TCA cycle, and, consequently, of the mitochondrial electron transport chain.

In parallel to OCR, ECAR evaluation also showed different sensitivity to miRNA modulation in U87 and DBTRG cells. Decrease in the basal glycolysis observed after miRNA transfection in U87 cells (**Fig. 14A** and **14B**) suggests that both miRNAs could have a negative effect on the ability of these cells to use glycolysis as the main source of cellular energy. This effect could be attributed to the hsa-miR-144 target GLUT1, whose decreased expression would prevent the uptake of glucose, and thus block the glycolytic pathway[162]. The similar effect observed in U87 cells transfected with hsa-miR-200c mimic could result from the targeting of HK2 by this miRNA, since mRNA expression levels of this glycolytic enzyme were found to be significantly increased in GBM in comparison with low-grade gliomas and normal brain tissue[171]. In DBTRG cells, the increase of hsa-miR-144 levels did not result in decreased glycolytic activity (**Fig. 16A** and **16B**), indicating that these cells may rely on other glucose transporters, thus overcoming the inhibition of GLUT1. This subject should be further explored in order to clarify the mechanisms underlying the different response of U87 and DBTRG cells to the modulation of this miRNA. The increase of hsa-miR-200c-3p levels resulted in decreased glycolytic capacity, which measures the maximum rate of conversion of glucose into pyruvate or lactate, when mitochondrial respiration is inhibited by olygomicin, thus indicating a decrease of glycolysis activation under stress conditions. Recent *in vitro* and *in vivo* studies have reported that the attenuation of expression of genes coding for the glycolytic enzymes PFKP, PGAM1, HK2 and ALDOB was capable of decreasing GBM cell proliferation and tumour growth and increasing mice survival[144]. The fact that miRNA modulation has induced a decrease of the basal glycolysis in U87 cells, in contrast to DBTRG cells, suggests that the latter cells are less sensitive than the former to molecular alterations that lead to glycolysis impairment. In this regard, radio-resistance, such as that presented by DBTRG cells, was previously associated with elevated glycolysis, which contributes to the activation of DNA repair mechanisms, namely non-homologous end joining and homologous recombination[172]. Therefore, we propose a strategy that combines the fine regulation promoted by miRNA modulation with

chemotherapeutics, in order to overcome the enforced glycolytic phenotype developed upon radiation exposure.

To test our hypothesis that miRNA modulation could improve drug action, the effect of the increase of hsa-miR-144 and hsa-miR-200c levels on GBM cell sensitivity to the chemotherapeutics TMZ and DCA was investigated. In this regard, U87 cells transfected with both miRNAs, which showed no alteration in mitochondrial respiration but decreased basal glycolysis, did not present alterations in cell viability with respect to control cells, either upon transfection *per se* or in combination with chemotherapeutics. In contrast, the increased levels of these miRNAs resulted in significant viability decrease in DBTRG cells. In addition, transfection with hsa-miR-144 mimic combined with DCA treatment resulted in a significant decrease of cell viability, in comparison with DCA treatment or miRNA modulation *per se,* which corresponded to an additive effect, according to Bliss Interaction Index analysis. However, this additive effect was not observed with TMZ, indicating that it may be advantageous to concomitantly use two therapeutic options that act on the same molecular target, rather than through different mechanisms, in order to exhaust cell ability to compensate for the damage. Interestingly, DBTRG cells showed to be more affected by the combined treatment than U87 cells, an unpredictable outcome, taking into account that the DBTRG cell line was established from a recurrent GBM. Therefore, DBTRG cells, more than U87 cells, appear to rely on the glycolytic activity as a survival mechanism under stress conditions, thus justifying the more pronounced loss of viability as compared to U87 cells (**Fig. 20B**).

To investigate whether the decrease of GBM cell viability would be associated with alterations in the cell cycle, the distribution of U87 and DBTRG cells trough the different cell cycle phases was analysed upon transfection with miRNA mimics in the absence or presence of DCA and TMZ. U87 cells transfected with either miRNA did not present relevant alteration of cell cycle progression (**Fig. 21A**), which is consistent with the cell density determined for the same experimental conditions (**Fig. 20A**). In these cells, the hsa-miR-200c potentiates the effect of the drug. Thus, hsa-miR-200c modulation effect on the cell cycle control system only gained visible consequences when cells were challenged with a secondary insult (DCA incubation). In DBTRG cells, the increased levels of hsa-miR-200c-3p resulted in increased percentage of cells arrested in S phase, accompanied by a decreased percentage of cells in G0/G1 phase, whereas cell transfection with hsa-miR-144 promotes cell cycle arrest in G2/M, with decrease of the percentage of cells in the S phase (**Fig. 21B**). In addition, DBTRG cell transfection with hsa-miR-144 did not further enhance the cell cycle arrest mediated by TMZ or DCA (**Fig. 21B**, **Fig. 22B** and **Fig. 23B**). In contrast, cell transfection with hsa-miR-200c enhanced the effect of both drugs on the cell cycle. DBTRG cell transfection with hsa-

miR-200c-3p mimics combined with TMZ treatment was by far the strategy that resulted in more cells arrested in the S phase, which is consistent with TMZ ability to activate intra-S-phase checkpoint, by inducing higher DNA damage[173]. However, this did not result in a decrease of cell density, at least for the time point considered (**Fig. 20B**). Evaluation of cell density over a longer period of time could indicate if the S phase cell cycle arrest observed would eventually result in a decrease of cell proliferation.

Knowing the link between cell cycle regulation and metabolism, we cannot exclude the possibility that the results obtained are derived from alterations in the expression of metabolic enzymes, which indirectly interact with some of the major elements of cell cycle control system. A practical example is described by Hu and co-workers in 2014, who observed that the knockdown of HK2, target of hsa-miR-200c-3p, resulted in cell cycle checkpoint deactivation and culminated in G1 phase arrest of cancer associated fibroblast[174]. Additionally, another target of hsa-miR-200c-3p, TIGAR, besides having a functional role in glycolysis, was also shown to promote p21-independent, p53-mediated cell cycle arrest in G1 phase, and to be an expression regulator of a series of proteins involved in cell cycle control[175].

The ability of GBM cells to infiltrate adjacent healthy tissue is an important feature of this type of tumour, which can be concomitantly targeted by hsa-miR-200c and hsa-miR-144, whose targets include mRNAs of proteins involved in cell migration. In this regard, the capacity of DBTRG cells to migrate towards a chemoattractant was evaluated. A significant alteration of migratory ability of cells transfected with both miRNA mimics was observed, the increase of hsa-miR-200c-3p and hsa-miR-144 levels resulting in the decrease of DBTRG cells migratory capacity (**Fig. 18A-D**). This effect was in agreement with what has been previously described in the literature for hsa-miR-200c[159,176]. However, to the best of our knowledge, this is the first time that hsa-miR-144-3p is being described as a regulator of GBM cell migration. Hsa-miR-200c was shown to indirectly modulate E-cadherin levels, through regulation of zinc-finger E-box binding homeobox (ZEB) family of transcription factors, which are direct targets of the miR-200 family of miRNAs, and are inhibitors of E-cadherin expression[177]. Thus, absence of hsa-miR-200c-3p results in decreased E-cadherin, which contributes to epithelial-mesenchymal transition (EMT)[177]. This biological process allows a polarized epithelial cell to acquire cell motility and resistance to genotoxic agents, which translates into a more aggressive tumour phenotype[178]. Additionally, the results observed can be related with EGFR increased expression in GBM, since EGFR is a predictable target of both hsa-miR-200c-3p and hsa-miR-144-3p and has been implicated in GBM cell invasion mechanisms, by activation of PI3K/AKT and Wnt pathways. Activated EGFR phosphorylates PI3K triggering AKT activation and ultimately glycogen synthase kinase 3

beta (GSK3β) phosphorylation by AKT, which results in β-catenin stabilization and nuclear accumulation. Through the Wnt pathway, EGFR activation disrupts the association of α-catenin and β-catenin, allowing their transactivation and translocation to the nucleus and consequent interaction with T-cell factor (TCF)/lymphoid enhancer factor (LEF), transcription factors that regulate metallopeptidase (MMP) gene expression[176,179].

Overall, our observations indicate that the modulation of hsa-miR-200c-3p and hsa-miR-144-3p, miRNAs known to be downregulated in GBM and predicted to have as targets mRNAs of crucial enzymes involved in metabolism, results in metabolic alterations and impairment of DBTRG cell migration capacity. Furthermore, miRNA modulation in combination with the chemotherapeutic agent DCA resulted in a decrease of DBTRG cell density, indicating that players of metabolic pathways can emerge as interesting targets to treat GBM, by contributing to the decrease of tumour growth and invasion ability. Cell cycle analysis of DBTRG cells points to an arrest in S phase induced by hsa-miR-200c, which is reinforced upon addition of TMZ, whereas the loss of cell density associated with cell transfection with hsa-miR-144 cannot be attributed to cell cycle arrest, but can probably be assigned to increased apoptosis and autophagy, two cell death mechanisms mediated by hsa-miR-144 in lung cancer cells[164].

6 CONCLUSIONS

CONCLUSIONS

The extremely complex nature of GBM makes this type of tumour a specially challenging target. However, the increasing amount of knowledge gathered over the years regarding the specific hallmarks displayed by these tumors, has helped unravel new promising targets to use against this disease. The metabolic profile of GBM appears as a critical knot linking a number of cancer hallmarks, including proliferative capacity, migration and invasion ability, and apoptosis regulation. Thus, targeting key enzymes of the metabolic pathways can have an important impact in several properties of cancer cells and contribute to an efficient treatment strategy. Using a versatile tool, such as miRNAs, which are able to interfere with several cellular pathways through their multiple molecular targets, to modulate the metabolic railway node, in combination with new mitochondrial-targeted chemotherapeutic drugs can result in a multidimensional efficient therapeutic approach.

7 REFERENCES

1. World Health Organization. World Cancer Report 2014.
2. Jemal, A., Bray, F. & Ferlay, J. Global Cancer Statistics. 61, 69–90 (2011).
3. Hanahan, D. Weinberg, R. The Hallmarks of Cancer. *Cell* 57–70 (2000).
4. Hanahan, D. & Weinberg, R. A. Hallmarks of cancer: the next generation. *Cell* 144, 646–74 (2011).
5. Andriy Marusyk and Kornelia Polyak. Tumor heterogeneity: causes and consequences Andriy. *Biochim Biophys Acta.* 1805, 1–28 (2011).
6. Collected, Y. D. Cbtrus 2004-2005. (2005).
7. Jhanwar-Uniyal, M., Labagnara, M., Friedman, M., Kwasnicki, A. & Murali, R. Glioblastoma: molecular pathways, stem cells and therapeutic targets. *Cancers (Basel).* 7, 538–55 (2015).
8. Louis, D. N. *et al.* The 2007 WHO classification of tumours of the central nervous system. *Acta Neuropathol.* 114, 97–109 (2007).
9. MC, R., ML, W., Imaging, B. & Journal, I. Glioblastoma multiforme: a rare manifestation of extensive liver and bone metastases. *Biomed. Imaging Interv. J.* 2–5 (2008). doi:10.2349/biij.4.1.e3
10. Adamson, C. *et al.* Glioblastoma multiforme : a review of where we have been and where we are going. 1061–1084 (2009).
11. Ohgaki, H. & Kleihues, P. The Definition of Primary and Secondary Glioblastoma. *Clin. Cancer Res.* 19, 764–773 (2013).
12. Jigisha P. Thakkar, Therese A. Dolecek, Craig Horbinski, Quinn T. Ostrom, Donita D.Lightner, Jill S. Barnholtz-Sloan, and J. L. V. & Jigisha P. Thakkar, Therese A. Dolecek, Craig Horbinski, Quinn T. Ostrom, Donita D. Lightner, Jill S. Barnholtz-Sloan, and J. L. V. Epidemiologic and Molecular Prognostic Review of Glioblastoma. *Cancer Epidemiol Biomarkers* 23, 1985–1996 (2015).
13. Kleihues, P. & Ohgaki, H. Primary and secondary glioblastomas : From concept to clinical diagnosis 1. 44–51 (1999).
14. Watanabe T, Nobusawa S, Kleihues P, and O. H., Watanabe, T., Nobusawa, S., Kleihues, P. & Ohgaki, H. IDH1 Mutations Are Early Events in the Development of Astrocytomas and Oligodendrogliomas. *Am. J. Pathol.* 174, 1149–1153 (2009).
15. Alifieris, C. & Trafalis, D. T. Glioblastoma Multiforme: Pathogenesis and Treatment. *Pharmacol. Ther.* (2015). doi:10.1016/j.pharmthera.2015.05.005
16. Verhaak, R. G. W. *et al.* An integrated genomic analysis identifies clinically relevant subtypes of glioblastoma characterized by abnormalities in PDGFRA, IDH1, EGFR and NF1. *Cancer Cell* 17, 1–25 (2011).
17. Mischel, P. S. *et al.* Identification of molecular subtypes of glioblastoma by gene expression profilin. *Oncogene* 2361–2373 (2003). doi:10.1038/sj.onc.1206344
18. Luo, J. W., Wang, X., Yang, Y. & Mao, Q. Role of micro-RNA (miRNA) in pathogenesis of glioblastoma. 1630–1639 (2015).
19. Preusser, M. *et al.* Current concepts and management of glioblastoma. *Ann. Neurol.* 70, 9–21 (2011).
20. Schwartzbaum, J. A., Fisher, J. L., Aldape, K. D. & Wrensch, M. Epidemiology and molecular pathology of glioma. *Nature* 2, 494–503 (2006).
21. Fisher, J. L., Schwartzbaum, J. a, Wrensch, M. & Wiemels, J. L. Epidemiology of brain tumors. *Neurol. Clin* (2007).
22. Hardell, L., Carlberg, M., So, F., Mild, K. H. & Morgan, L. L. Long-term use of cellular phones and brain tumours: increased risk associated with use for > 10 years. *Occup. Environ. Med.* 626–632 (2007). doi:10.1136/oem.2006.029751
23. Deberardinis, R. J. *et al.* Beyond aerobic glycolysis : Transformed cells can engage in glutamine metabolism that exceeds the requirement for protein and nucleotide synthesis. (2007).

24. Kosaka, N. *et al.* PET of Common Enhancing Malignant Brain Tumors. *Am. J. Roentgenol.* 365–369 (2008). doi:10.2214/AJR.07.2660

25. Pardo, F. S. *et al.* Correlation of FDG-PET Interpretation with Survival in a Cohort of Glioma Patients. *Anticancer Res.* 2366, 2359–2365 (2004).

26. Štolc, S., Jakubíková, L. & Kukurová, I. Body distribution of 11 C-methionine and 18 FDG in rat measured by microPET. *Interdiscip. Toxicol.* 4, 52–55 (2011).

27. Heiden, Matthew G. Vander ; Cantley, Lewis C. ; Thompson, C. B. & Heiden, Matthew G. Vander, Cantley, Lewis C. ,Thompson, C. B. Understanding the Warburg Effect: The Metabolic Requirements of Cell Proliferation. *Science.* 324, 1029–1033 (2010).

28. Warburg, O. On the origin of cancer cells. *Science (80-.).* 123, 309–314 (1956).

29. Gatenby, R. A. & Gillies, R. J. Why do cancers have high aerobic glycolysis? *Nat Rev Cancer* 4, 891–9 (2004).

30. Suganuma, K. *et al.* Energy metabolism of leukemia cells : glycolysis versus oxidative phosphorylation. *Leuk. Lymphoma* 51, 2112–2119 (2010).

31. Gaude, E. & Frezza, C. Defects in mitochondrial metabolism and cancer. *Cancer Metab.* 2, 1–9 (2014).

32. Levine, A. J. & Puzio-kuter, A. M. The Control of the Metabolic Switch. *Science (80-.).* 1340, (2012).

33. Mao, H., Lebrun, D. G., Yang, J., Zhu, V. F. & Li, M. Deregulated signaling pathways in glioblastoma multiforme: molecular mechanisms and therapeutic targets. *Cancer Invest.* 30, 48–56 (2012).

34. Fayard, E., Xue, G., Parcellier, A., Bozulic, L. & Hemmings, B. A. Protein Kinase B (PKB / Akt), a Key Mediator of the PI3K Signaling Pathway. 1, 31–56

35. Elstrom, R. L. *et al.* Akt Stimulates Aerobic Glycolysis in Cancer Cells. *Cancer Res.* 473, 3892–3899 (2004).

36. Robey, R. B. & Hay, N. Is Akt the 'Warburg kinase'?—Akt-energy metabolism interactions and oncogenesis. *Semin. Cancer Biol.* 19, 1–15 (2009).

37. Fang, M. *et al.* The ER UDPase ENTPD5 Promotes Protein N-Glycosylation , the Warburg Effect , and Proliferation in the PTEN Pathway. *Cell* 143, 711–724 (2010).

38. Khatri, S., Yepiskoposyan, H., Gallo, C. A., Tandon, P. & Plas, D. R. FOXO3a Regulates Glycolysis via Transcriptional Control of Tumor Suppressor TSC1. *J. Biol. Chem.* 285, 15960–15965 (2010).

39. Guertin, D. A. & Sabatini, D. M. Defining the Role of mTOR in Cancer. *Cancer Cell* (2007). doi:10.1016/j.ccr.2007.05.008

40. Fiorenzo, P. *et al.* HIF1-positive and HIF1-negative glioblastoma cells compete in vitro but cooperate in tumor growth in vivo. *Int. J. Oncol.* 785–791 (2010). doi:10.3892/ijo

41. Robinson, J. P., Vanbrocklin, M. W., Mckinney, A. J., Gach, H. M. & Holmen, S. L. Akt signaling is required for glioblastoma maintenance in vivo. 1, 155–167 (2011).

42. Kaptsinou, P. & Haase, V. The VHL tumor suppressor and HIF: insights from genetic studies in mice. *Cell Death Differ.* 15, 650–659 (2008).

43. Jr, W. G. K. The von Hippel – Lindau tumour suppressor protein : O 2 sensing and cancer. 8, 865–873 (2008).

44. Selak, M. A. *et al.* Succinate links TCA cycle dysfunction to oncogenesis by inhibiting HIF- ⎵ prolyl hydroxylase. 7, 77–85 (2005).

45. King, A., Selak, M. A. & Gottlieb, E. Succinate dehydrogenase and fumarate hydratase : linking mitochondrial dysfunction and cancer. 4675–4682 (2006). doi:10.1038/sj.onc.1209594

46. Semenza, G. L. HIF-1 : upstream and downstream of cancer metabolism. *Curr. Opin. Genet. Dev.* 20, 1–10 (2011).

47. Lu, C., Lin, S., Chen, K., Lai, Y. & Tsai, S. Induction of Pyruvate Dehydrogenase Kinase-3 by

Hypoxia-inducible Factor-1 Promotes Metabolic Switch and Drug Resistance * □. *J. Biol. Chem.* 283, 28106–28114 (2008).

48. Kim, J., Gao, P., Liu, Y., Semenza, G. L. & Dang, C. V. Hypoxia-Inducible Factor 1 and Dysregulated c-Myc Cooperatively Induce Vascular Endothelial Growth Factor and Metabolic Switches Hexokinase 2 and Pyruvate Dehydrogenase Kinase 1. *Mol. Cell. Biol.* 27, 7381–7393 (2007).

49. Kim, J. *et al.* Evaluation of Myc E-Box Phylogenetic Footprints in Glycolytic Genes by Chromatin Immunoprecipitation Assays †. *Mol. Cell. Biol.* 24, 5923–5936 (2004).

50. Bensaad, K. *et al.* TIGAR , a p53-Inducible Regulator of Glycolysis and Apoptosis. *Cell* 53, 107–120 (2006).

51. Mathupala, S. P., Heese, C. & Pedersen, P. L. Glucose Catabolism in Cancer Cells. *J. Biol. Chem.* 272, 22776–22780 (1997).

52. Cairns, R. A., Harris, I. S. & Mak, T. W. Regulation of cancer cell metabolism. *Nat. Rev. Cancer* 11, (2011).

53. Costoya, J. A., Ríos, M., Foretz, M., Viollet, B. & Prieto, A. AMPK Activation by Oncogenesis Is Required to Maintain Cancer Cell Proliferation in Astrocytic Tumors. *Cancer Res.* 73, 2628–2639 (2013).

54. Shackelford, D. B. & Shaw, R. J. The LKB1-AMPK pathway: metabolism and growth control in tumor suppression David. *Nat Rev Cancer* 9, 563–575 (2010).

55. Jones, R. G. *et al.* AMP-Activated Protein Kinase Induces a p53-Dependent Metabolic Checkpoint. *Mol. Cel* 18, 283–293 (2005).

56. Liu, X. *et al.* AMPK regulated metabolic programing : oncogenic or growth suppressive ? Evolving lessons from genetic and pharmacologic studies. *Cancer Metab.* 2, O23 (2014).

57. Luo, Weibo and Semenza, G. L. Emerging roles of PKM2 in cell metabolism and cancer progression. *Trends Endocrinol Metab.* 23, 560–566 (2012).

58. Wong, N., Ojo, D., Yan, J. & Tang, D. PKM2 contributes to cancer metabolism. *Cancer Lett.* 356, 184–91 (2015).

59. Mukherjee, J. *et al.* Pyruvate Kinase M2 Expression , but Not Pyruvate Kinase Activity , Is Up-Regulated in a Grade-Specific Manner in Human Glioma. *PLoS One* 8, (2013).

60. Petros, J. A. *et al.* mtDNA mutations increase tumorigenicity in prostate cancer. 102, (2014).

61. Polyak, K. *et al.* Somatic mutations of the mitochondrial genome in human colorectal tumours. *Nat. Genet.* 20, 291–293 (1998).

62. Horton, T. M. *et al.* Novel Mitochondria DNA Deletion Found in a Renal Cell Carcinoma. *Genes Chromosom. Cancer* 101, 95–101 (1996).

63. Xiao, M. *et al.* Inhibition of a -KG-dependent histone and DNA demethylases by fumarate and succinate that are accumulated in mutations of FH and SDH tumor suppressors. 1326–1338 (2012). doi:10.1101/gad.191056.112.Damato

64. Figueroa, M. E. *et al.* Article Leukemic IDH1 and IDH2 Mutations Result in a Hypermethylation Phenotype , Disrupt TET2 Function , and Impair Hematopoietic Differentiation. 553–567 doi:10.1016/j.ccr.2010.11.015

65. Izquierdo-Garcia, J. L. *et al.* IDH1 mutation induces reprogramming of pyruvate metabolism. *Cancer Res.* (2015). doi:10.1158/0008-5472.CAN-15-0840

66. Kos, I. *et al.* IDH1 and IDH2 Mutations in Gliomas. *N. Engl. J. Med.* (2009).

67. Combs, S. E. *et al.* Prognostic significance of IDH-1 and MGMT in patients with glioblastoma: one step forward, and one step back? *Radiat. Oncol.* 6, 115 (2011).

68. Martinelli, C. *et al.* SDH Mutations Establish a Hypermethylator Phenotype in Paraganglioma. *Cancer Cell* 739–752 (2013). doi:10.1016/j.ccr.2013.04.018

69. S˘edivcova, M. *et al.* Succinate Dehydrogenase (SDH) -deficient Renal A Clinicopathologic Series of 36 Tumors From 27 Patients. *Am. J. Surg. Pathol.* 38, 1588–1602 (2014).

70. Kim, S., Kim, D. H., Jung, W. & Koo, J. S. Succinate dehydrogenase expression in breast cancer. *Springerplus* (2013).

71. Castro-vega, L. J. *et al.* Germline mutations in FH confer predisposition to malignant pheochromocytomas and paragangliomas. *Hum. Mol. Genet.* 23, 2440–2446 (2014).

72. Sudarshan, S. *et al.* Reduced Expression of Fumarate Hydratase in Clear Cell Renal Cancer Mediates HIF-2 a Accumulation and Promotes Migration and Invasion. *PLoS One* 6, (2011).

73. Khalil, A. A. Biomarker discovery : A proteomic approach for brain cancer profiling. *Cancer Sci.* 98, 201–213 (2007).

74. Lee, S. *et al.* Neuronal apoptosis linked to EglN3 prolyl hydroxylase and familial pheochromocytoma genes : Developmental culling and cancer. *Cancer Cell* 8, 155–167 (2005).

75. Alam, N. A., Barwell, J., Barclay, E., Wortham, N. C. & Hunt, T. Accumulation of Krebs cycle intermediates and over-expression of HIF1 a in tumours which result from germline FH and SDH mutations. *Hum. Mol. Genet.* 14, 2231–2239 (2005).

76. Sjo, J. *et al.* Distinct expression profile in fumarate-hydratase- deficient uterine fibroids. *Hum. Mol. Genet.* 15, 97–103 (2006).

77. Pollard, P. *et al.* Evidence of increased microvessel density and activation of the hypoxia pathway in tumours from the hereditary leiomyomatosis and renal cell cancer syndrome. *Jounal Pathol.* 41–49 (2005). doi:10.1002/path.1686

78. Gross, S. *et al.* Cancer-associated metabolite 2- hydroxyglutarate accumulates in acute myelogenous leukemia with isocitrate dehydrogenase 1 and 2 mutations. *J. Exp. Med.* 207, 3–8 (2010).

79. Parsons, D. W. *et al.* An Integrated Genomic Analysis of Human Glioblastoma Multiforme. *Science (80-.).* 321, (2008).

80. Mardis, E. *et al.* Recurring Mutations Found by Sequencing an Acute Myeloid Leukemia Genome. *N. Engl. J. Med.* 361, 1058–1066 (2009).

81. Xu, X. *et al.* Structures of Human Cytosolic NADP-dependent Isocitrate Dehydrogenase Reveal a Novel Self-regulatory Mechanism of Activity. *J. Bioogical Chem.* 279, 33946–33957 (2004).

82. Zhao, S. *et al.* Glioma-Derived Mutations in IDH1 Dominantly Inhibit IDH1 Catalytic Activity and Induce HIF-1α. *Science (80-.).* 324, 261–265 (2012).

83. Kalinina, J. *et al.* Detection of 'oncometabolite' 2-hydroxyglutarate by magnetic resonance analysis as a biomarker of IDH1/2 mutations in glioma. *J. Mol. Med.* 90, 1161–1171 (2014).

84. Xu, W. *et al.* Oncometabolite 2-Hydroxyglutarate Is a Competitive Inhibitor of α-Ketoglutarate-Dependent Dioxygenases. *Cancer Cell* 19, 17–30 (2011).

85. Turcan, S. *et al.* IDH1 mutation is sufficient to establish the glioma hypermethylator phenotype. *Nature* 483, 479–483 (2012).

86. Noushmehr, H. *et al.* Identification of a CpG Island Methylator Phenotype that Defines a Distinct Subgroup of Glioma. *Cancer Cell* 17, 510–522 (2010).

87. Costa, P. M. & Pedroso de Lima, M. C. MicroRNAs as Molecular Targets for Cancer Therapy: On the Modulation of MicroRNA Expression. *Pharmaceuticals (Basel).* 6, 1195–220 (2013).

88. Carthew, R. W. & Sontheimer, E. J. Origins and Mechanisms of miRNAs and siRNAs. *Cell* 136, 642–55 (2009).

89. Winter, J., Jung, S., Keller, S., Gregory, R. I. & Diederichs, S. Many roads to maturity: microRNA biogenesis pathways and their regulation. *Nat. Cell Biol.* 11, 228–34 (2009).

90. Møller, H. G. *et al.* A systematic review of microRNA in glioblastoma multiforme: micro-modulators in the mesenchymal mode of migration and invasion. *Mol. Neurobiol.* 47, 131–44 (2013).

91. Farazi, T. A., Hoell, J. I., Morozov, P. & Tuschl, T. MicroRNA Cancer Regulation. 774, (2013).

92. Bartel, D. P., Lee, R. & Feinbaum, R. MicroRNAs : Genomics , Biogenesis , Mechanism , and Function Genomics : The miRNA Genes. 116, 281–297 (2004).

93. Dong, H. *et al.* MicroRNA : Function , Detection , and Bioanalysis. (2012).

94. Djuranovic, S., Nahvi, A. & Green, R. miRNA-mediated gene silencing by translational repression followed by mRNA deadenylation and decay. *Science (80-.).* 336, 237–240 (2014).

95. Hutvágner, G. & Zamore, P. D. A microRNA in a Multiple-Turnover RNAi Enzyme Complex. *Science (80-.).* 2056, (2012).

96. Vasudevan S, Tong Y, S. J. Switching from repression to activation: microRNAs can up-regulate translation. *Science (80-.).* 1931–4 (2007).

97. Hanahan, D. & Weinberg, R. A. The Hallmarks of Cancer Review University of California at San Francisco. 100, 57–70 (2000).

98. Zhang, Y. *et al.* Epigenetic silencing of miR-126 contributes to tumor invasion and angiogenesis in colorectal cancer. *Oncol. Rep.* 30, 1976–84 (2013).

99. Kumar, M. S., Lu, J., Mercer, K. L., Golub, T. R. & Jacks, T. Impaired microRNA processing enhances cellular transformation and tumorigenesis. *Nat. Genet.* 39, 673–7 (2007).

100. Pencheva, N. & Tavazoie, S. F. Control of metastatic progression by microRNA regulatory networks. *Nat. Publ. Gr.* 15, 546–554 (2013).

101. Calin, G. A. *et al.* Frequent deletions and down-regulation of micro- RNA genes miR15 and miR16 at 13q14 in chronic lymphocytic leukemia. *Proc. Natl. Acad. Sci. U. S. A.* 99, 15524–9 (2002).

102. Mulrane L, McGee SF, Gallagher WM, O. D. miRNA dysregulation in breast cancer. *Cancer Res.* 6554–62 (2013).

103. Pan HW, Li SC, T. K. MicroRNA dysregulation in gastric cancer. *Curr Pharm Des.* 19, 1273–84 (2013).

104. Croce, C. M. MicroRNA dysregulation in acute myeloid leukemia. *J. Clin. Oncol.* 31, 2065–6 (2013).

105. Low, S. Y. Y., Ho, Y. K., Too, H.-P., Yap, C. T. & Ng, W. H. MicroRNA as potential modulators in chemoresistant high-grade gliomas. *J. Clin. Neurosci.* 21, 395–400 (2014).

106. Ciafrè, S. a *et al.* Extensive modulation of a set of microRNAs in primary glioblastoma. *Biochem. Biophys. Res. Commun.* 334, 1351–8 (2005).

107. Chen, B. *et al.* Roles of microRNA on cancer cell metabolism. *J. Transl. Med.* 10, 228 (2012).

108. Tibiche C, W. E. MicroRNA regulatory patterns on the human metabolic network. *Open Syst Biol J* 1–8 (2008).

109. Thorens B, M. M. Glucose transporters in the 21st century. *Am J Physiol Endocrinol Metab* E141–E145 (2010).

110. Horie T, Ono K, Nishi H, Iwanaga Y, Nagao K, Kinoshita M, K. Y. & Takanabe R, Hasegawa K, K. T. MicroRNA-133 regulates the expression of GLUT4 by targeting KLF15 and is involved in metabolic control in cardiac myocytes. *Biochem Biophys Res Commun* 315–320 (2009).

111. Fei X, Qi M, Wu B, Song Y, Wang Y, L. MicroRNA-195-5p suppresses glucose uptake and proliferation of human bladder cancer T24 cells by regulating GLUT3 expression. *FEBS Lett.* 392–397 (2012).

112. Macheda ML, Rogers S, B. J. Molecular and cellular regulation of glucose transporter (GLUT) proteins in cancer. *J Cell Physiol* 654–662 (2005).

113. Koh HJ, Toyoda T, Fujii N, Jung MM, Rathod A, Middelbeek RJ, L. S. & Treebak JT, Tsuchihara K, Esumi H, et al. Sucrose nonfermenting AMPKrelated kinase (SNARK) mediates contraction-stimulated glucose transport in mouse skeletal muscle. *Proc Natl Acad Sci USA* 15541–15546 (2010).

114. Guo, C., Sah, J.F., Beard, L. Willson, J.K. Markowitz, S.D. Guda, K. Guo, C., Sah, J.F., Beard, L. Willson, J.K. Markowitz, S.D. Guda, K. The noncoding RNA, miR-126, suppresses the growth of neoplastic cells by targeting phosphatidylinositol 3- kinase signaling and is frequently lost in colon cancers. 946. *Genes Chromosom. Cancer* 47, 939– 946 (2008).

115. Feng, R., Chen, X., Yu, Y., Su, L., Yu, B., Li, J., Cai, Q., Yan, M., Liu, B., Zhu, Z. MiR-126 functions as

a tumour suppressor in human gastric cancer. *Cancer Lett.* 298, 50–63 (2010).

116. Yanaihara, N., Caplen, N., Bowman, E., Seike, M., Kumamoto, K., Yi, M., Stephens, R. M. & Okamoto, A., Yokota, J., Tanaka, T., Calin, G.A., Liu, C.G., Croce, C.M., Harris, C.C. Unique microRNA molecular profiles in lung cancer diagnosis and prognosis. *Cancer Cell* 189–198 (206AD).

117. Zhu, N., Zhang, D., Xie, H., Zhou, Z., Chen, H., Hu, T., Bai, Y., Shen, Y., Yuan, W., Jing Q., Qin, Y. Endothelial-specific intron-derived miR-126 is down-regulated in human breast cancer and targets both VEGFA and PIK3R2. *Mol. Cell Biochem.* 157–164 (2011).

118. Chan, S.Y., Loscalzo, J. MicroRNA-210: A unique and pleiotropic hypoxamir. *Cell Cycle* 1072–1083 (2010).

119. Devlin, C., Greco, S., Martelli, F., Ivan, M. miR-210: More than a silent player in hypoxia. *IUBMB Life* 94–100. (2011).

120. Corn, P. G. Hypoxic regulation of miR-210: Shrinking targets expand HIF-1's Influence. *Cancer Biol. Ther.* 7–10 (2008). doi:10.4161/cbt.7.2.5745

121. Zhang, H. *et al.* HIF-1 Inhibits Mitochondrial Biogenesis and Cellular Respiration in VHL-Deficient Renal Cell Carcinoma by Repression of C-MYC Activity. *Cancer Cell* 407–420 (2007). doi:10.1016/j.ccr.2007.04.001

122. Tomasetti, M., Santarelli, L., Neuzil, J. & Dong, L. MicroRNA regulation of cancer metabolism: role in tumour suppression. *Mitochondrion* 19 Pt A, 29–38 (2014).

123. Ghosh, A.K., Shanafelt, T.D., Cimmino, A., Taccioli, C., Volinia, S., Liu, C.G., Calin, G. A., Croce, C.M., Chan, D.A., Giaccia, A.J., Secreto, C., Wellik, L.E., Lee, Y.K., M. & D., Kay, N. E. Aberrant regulation of pVHL levels by microRNA promotes the HIF/VEGF axis in CLL B cells. *Blood* 113, 5568–5574 (2009).

124. Taguchi, A., Yanagisawa, K., Tanaka, M., Cao, K., Matsuyama, Y., Goto, H., Takahashi, T. Identification of hypoxia-inducible factor-1 alpha as a novel target for miR-17-92 microRNA cluster. *Cancer Res.* 68, 5540–5545 (2008).

125. Cha, S.T., Chen, P.S., Johansson, G., Chu, C.Y., Wang, M.Y., Jeng, Y.M., Yu, S.L., C. & J.S., Chang, K.J., Jee, S.H., Tan, C.T., Lin, M.T., Kuo, M. L. MicroRNA-519c suppresses hypoxia-inducible factor-1alpha expression and tumor angiogenesis. *Cancer Res.* 70, 2675–2685 (2010).

126. Yeh, Y.M., Chuang, C.M., Chao, K.C., Wang, L.H. MicroRNA-138 suppresses ovarian cancer cell invasion and metastasis by targeting SOX4 and HIF-1α. *Int. J. Cancer.* (2013).

127. Hatziapostolou, M., Polytarchou, C. & Iliopoulos, D. miRNAs link metabolic reprogramming to oncogenesis. *Trends Endocrinol. Metab.* 24, 361–73 (2013).

128. Chan, B., Manley, J., Lee, J. & Singh, S. R. The emerging roles of microRNAs in cancer metabolism. *Cancer Lett.* 356, 301–8 (2015).

129. Vill, S., Bala, C. & Comas, S. Radiation and concomitant chemotherapy for patients with glioblastoma multiforme. *Chin. J. Cancer* 25–31 (2010). doi:10.5732/cjc.013.10216

130. Stupp, R. *et al.* Radiotherapy plus Concomitant and Adjuvant Temozolomide for Glioblastoma. *N. Engl. J. Med.* 987–996 (2005).

131. Zhang, J., Stevens, M. F. G. & Bradshaw, T. D. Temozolomide : Mechanisms of Action , Repair and Resistance. *Curr. Mol. Pharmacol.* 102–114 (2012).

132. Stevens, M. F. G. *et al.* Ant¡tumor Activity and Pharmacokinetics in Mice of 8-Carbamoyl-3-methyl- Novel Drug with Potential as an Alternative to Dacarbazine1. *Cancer Res.* 4, 5846–5852 (1987).

133. Mojas, N., Lopes, M. & Jiricny, J. Mismatch repair-dependent processing of methylation damage gives rise to persistent single-stranded gaps in newly replicated DNA. *Genes Dev.* 3342–3355 (2007). doi:10.1101/gad.455407.enzyme

134. Stojic, L., Brun, R. & Jiricny, J. Mismatch repair and DNA damage signalling. *DNA Repair (Amst).* 3, 1091–1101 (2004).

135. Nishikawa, R. Standard Therapy for Glioblastoma — A Review of Where We Are. *Neurol. Med. Chir. (Tokyo).* (2010).

136. Bonnet, S. *et al.* A mitochondria-K+ channel axis is suppressed in cancer and its normalization promotes apoptosis and inhibits cancer growth. *Cancer Cell* 11, 37*51 (2007).

137. Michelakis, E. D. *et al.* Metabolic Modulation of Glioblastoma with Dichloroacetate. 34, 1–8 (2010).

138. Dunbar, E. M. *et al.* Phase 1 trial of dichloroacetate (DCA) in adults with recurrent malignant brain tumors. *Invest New Drugs* 32, 452–464 (2014).

139. Reardon, D. A. *et al.* Immunotherapy advances for glioblastoma. *Neuro. Oncol.* 16, 1441–1458 (2014).

140. Vauleon, E., Avril, T., Collet, B. & Mosser, J. Overview of Cellular Immunotherapy for Patients with Glioblastoma. *Clin. Dev. Immunol.* 2010, (2010).

141. Ardon, H. *et al.* Integration of autologous dendritic cell-based immunotherapy in the primary treatment for patients with newly diagnosed glioblastoma multiforme : A pilot study. *J. Neurooncol.* (2010). doi:10.1007/s11060-010-0131-y

142. Chang, C., Huang, Y., Yang, D., Kikuta, K. & Wei, K. A phase I / II clinical trial investigating the adverse and therapeutic effects of a postoperative autologous dendritic cell tumor vaccine in patients with malignant glioma. *J. Clin. Neurosci.* 18, 1048–1054 (2011).

143. Mohyeldin, A. & Chiocca, E. A. Gene and viral therapy for glioblastoma: a review of clinical trials and future directions. *Cancer J.* (2012).

144. Sanzey, M. *et al.* Comprehensive analysis of glycolytic enzymes as therapeutic targets in the treatment of glioblastoma. *PLoS One* 10, e0123544 (2015).

145. Costa, P. M. *et al.* MicroRNA-21 silencing enhances the cytotoxic effect of the antiangiogenic drug sunitinib in glioblastoma. *Hum. Mol. Genet.* 22, 904–918 (2013).

146. Liu, Z., Jiang, Z., Huang, J. & Huang, S. miR-7 inhibits glioblastoma growth by simultaneously interfering with the PI3K / ATK and Raf / MEK / ERK pathways. *Int. J. Cancer* 1571–1580 (2014). doi:10.3892/ijo.2014.2322

147. Shang, C., Hong, Y., Guo, Y. A. N., Liu, Y. U. N. H. U. I. & Xue, Y. I. X. U. E. miR-128 regulates the apoptosis and proliferation of glioma cells by targeting RhoE. *Oncol. Lett.* 904–908 (2015). doi:10.3892/ol.2015.3927

148. Trabulo, S. M., Resina, S., Simões, S., Lebleu, B. & Pedroso de Lima, M. C. A non-covalent strategy combining cationic lipids and CPPs to enhance the delivery of splice correcting oligonucleotides. *J. Control. Release* (2010). doi:10.1016/j.jconrel.2010.03.021

149. de Moura, M. B. & Van Houten, B. in *Molecular Toxicology Protocols* (2014).

150. Suraneni, P. *et al.* The Arp2/3 complex is required for lamellipodia extension and directional fibroblast cell migration. *J. Cell Biol.* 197, 239–251 (2012).

151. Vichai, V. & Kirtikara, K. Sulforhodamine B colorimetric assay for cytotoxicity screening. *Nat. Protoc.* 1, 1112–1116 (2006).

152. D'Urso, P. I. *et al.* miR-155 is up-regulated in primary and secondary glioblastoma and promotes tumour growth by inhibiting GABA receptors. *Int. J. Oncol.* 41, 228–34 (2012).

153. Jiang, L. *et al.* miR-182 as a prognostic marker for glioma progression and patient survival. *Am. J. Pathol.* 177, 29–38 (2010).

154. Rao, S. A. M., Santosh, V. & Somasundaram, K. Genome-wide expression profiling identifies deregulated miRNAs in malignant astrocytoma. *Mod. Pathol.* 23, 1404–17 (2010).

155. Teplyuk, N. M. *et al.* MicroRNAs in cerebrospinal fluid identify glioblastoma and metastatic brain cancers and reflect disease activity. *Neuro. Oncol.* 14, 689–700 (2012).

156. Jia, Z., Wang, K., Zhang, A. & Wang, G. miR-19a and miR-19b Overexpression in Gliomas. *Pathol. Oncol. Res.* (2013). doi:10.1007/s12253-013-9653-x

157. Oudard, S. *et al.* High glycolysis in gliomas despite low hexokinase transcription and activity correlated to chromosome 10 loss. *Br. J. Cancer* 46, 839–845 (1996).

158. Yamagata, M., Hasuda, K., Stamato, T. & Tannock, I. F. The contribution of lactic acid to acidification of tumours : studies of variant cells lacking lactate dehydrogenase. 77, 1726–

1731 (1998).

159. Colen, C. B. *et al.* Metabolic Targeting of Lactate Efflux by Malignant Glioma Inhibits Invasiveness and Induces Necrosis : An In Vivo Study 1. *Neoplasia* 13, 620–632 (2011).

160. Li, J. *et al.* miRNA-200c inhibits invasion and metastasis of human non-small cell lung cancer by directly targeting ubiquitin specific peptidase 25. *Mol. Cancer* 1–14 (2014).

161. Zhang, W.-H., Poh, A., Fanous, A. A. & Eastman, A. DNA damage-induced S phase arrest in human breast cancer depends on Chk1, but G2 arrest can occur independently of Chk1, Chk2 or MAPKAPK2. *Cell Cycle* (2008).

162. Lu, C.-L. *et al.* Tumor cells switch to mitochondrial oxidative phosphorylation under radiation via mTOR-mediated hexokinase II inhibition--a Warburg-reversing effect. *PLoS One* 10, e0121046 (2015).

163. Guo, Y. *et al.* miR-144 downregulation increases bladder cancer cell proliferation by targeting EZH2 and regulating Wnt signaling. *FEBS J.* 280, 4531–4538 (2013).

164. Xiang, C., Cui, S. & Ke, Y. MiR-144 Inhibits Cell Proliferation of Renal Cell Carcinoma by Targeting MTOR. *J Huazhong Univ Sci Technol.* 36, 186–192 (2016).

165. Physiology, C. *et al.* MiR-144 Inhibits Proliferation and Induces Apoptosis and Autophagy in Lung Cancer Cells by Targeting TIGAR. *Cell. Physiol. Biochem.* 997–1007 (2015). doi:10.1159/000369755

166. Groussard, C. *et al.* Free radical scavenging and antioxidant effects of lactate ion : an in vitro study. *J. Appl. Physiol.* 89, 169–175 (2000).

167. Kahlon, A. S., Alexander, M., Kahlon, A. & Wright, J. Lactate levels with glioblastoma multiforme. *Baylor Univ. Med. Cent. Proc.* 13210, 313–314 (2016).

168. Park, S. Y., Lee, S., Shin, S. W. & Park, J. Inactivation of mitochondrial NADP -dependent isocitrate dehydrogenase by hypochlorous acid. *Free Radic. Res.* 5762, (2008).

169. Adam-vizi, V. & Chinopoulos, C. Bioenergetics and the formation of mitochondrial reactive oxygen species. *Trends Pharmacol. Sci.* 27, (2006).

170. Sangokoya, C., Telen, M. J. & Chi, J.-T. microRNA miR-144 modulates oxidative stress tolerance and associates with anemia severity in sickle cell disease. *Blood* 116, 4338–4348 (2010).

171. Wolf, A. *et al.* Hexokinase 2 is a key mediator of aerobic glycolysis and promotes tumor growth in human glioblastoma multiforme. *J. Ex* 208, 313–326 (2011).

172. Bhatt, A. N. *et al.* Transient elevation of glycolysis confers radio-resistance by facilitating DNA repair in cells. *BMC Cancer* 15, 1–12 (2015).

173. Bocangel, D. B. *et al.* Multifaceted Resistance of Gliomas to Temozolomide. *Clin. Cancer Res.* 8, 2725–2734 (2002).

174. Hu, J., Sun, P., Zhang, D., Xiong, W. & Mi, J. Hexokinase 2 regulates G1/S checkpoint through CDK2 in cancer-associated fibroblasts. *Cell. Signal.* 1–7 (2014). doi:10.1016/j.cellsig.2014.04.015

175. Madan, E. *et al.* TIGAR induces p53-mediated cell-cycle arrest by regulation of RB – E2F1 complex. *2012* 107, 516–526 (2012).

176. Callaghan, R. C., Gil-benso, R., Martinetto, H., Gregori-romero, A. & Gonzalez-darder, J. Correlation between EGFR Amplification and the Expression of MicroRNA-200c in Primary Glioblastoma Multiforme. *PLoS One.* 9, (2014).

177. Park, S., Gaur, A. B., Lengyel, E. & Peter, M. E. The miR-200 family determines the epithelial phenotype of cancer cells by targeting the E-cadherin repressors ZEB1 and ZEB2. *Genes Dev.* 22, 894–907 (2008).

178. Kalluri, R. & Weinberg, R. A. The basics of epithelial-mesenchymal transition. *J. Clin. Invest.* 119, 1420–128 (2009).

179. Paw, I., Carpenter, R. C., Watabe, K. & Debinski, W. Mechanisms regulating glioma invasion. *Cancer Lett.* (2015). doi:10.1016/j.canlet.2015.03.015